Summer 2006

Performance Analysis of Recoverable Flight Control Systems Subject to Neutron-Induced Upsets Using Hybrid Dynamical Models

Hong Zhang
Old Dominion University

PERFORMANCE ANALYSIS OF RECOVERABLE FLIGHT CONTROL SYSTEMS SUBJECT TO NEUTRON-INDUCED UPSETS USING HYBRID DYNAMICAL MODELS

by

Hong Zhang
B.S., July 1997, Northeastern University, Shenyang, Liaoning, P. R. China
M.S., July 2002, Tsinghua University, Beijing, P. R. China

A Dissertation Submitted to the Faculty of
Old Dominion University in Partial Fulfillment of the
Requirement for the Degree of

DOCTOR OF PHILOSOPHY

ELECTRICAL AND COMPUTER ENGINEERING

OLD DOMINION UNIVERSITY
August 2006

Approved by:

W. Steven Gray (Director)

Celeste M. Belcastro

Oscar R. González

Alex Pothen

Min Song

ABSTRACT

PERFORMANCE ANALYSIS OF RECOVERABLE FLIGHT CONTROL SYSTEMS SUBJECT TO NEUTRON-INDUCED UPSETS USING HYBRID DYNAMICAL MODELS

Hong Zhang
Old Dominion University, 2006
Director: Dr. W. Steven Gray

It has been observed that atmospheric neutrons can produce single-event upsets in digital flight control hardware. Potentially, they can reduce system performance and introduce a safety hazard. One experimental system-level approach investigated to help mitigate the effects of these upsets is NASA Langley's Recoverable Computer System. It employs rollback error recovery using dual-lock-step processors together with new fault tolerant architectures and communication subsystems.

In this dissertation, a class of stochastic hybrid dynamical models, which consists of a jump-linear system and a stochastic finite-state automaton, is used to describe the performance of a Boeing 737 aircraft system in closed-loop with a Recoverable Computer System. The jump-linear system models the switched dynamics of the closed-loop system due to the presence of controller recoveries. Each dynamical model in the jump-linear system was obtained separately using system identification techniques and high fidelity flight simulation software. The stochastic finite-state automaton approximates the recovery logic of the Recoverable Computer System. The upsets process is modeled by either an independent, identically distributed process or a first-order Markov chain.

Mean-square stability and output tracking performance of the recoverable flight control system are analyzed theoretically via a model-equivalent Markov jump-linear system of the stochastic hybrid model. The model was validated using data from a controlled experiment at NASA Langley, where simulated neutron-induced upsets were injected into the system at a desired rate. The effects on the output tracking performance of a simulated aircraft were then directly observed and quantified. The model was then used to analyze a neutron-based experiment on the Recoverable Computer System at the Los Alamos National Laboratory. This model predicts that the experimental flight control system, when functioning as designed, will provide robust control performance in the presence of neutron-induced single-event upsets at normal atmospheric levels.

To my parents: Zhang Lutai and Zhao Runfang

ACKNOWLEDGMENTS

First, I would like to express my deepest gratitude to my advisor, Dr. W. Steven Gray, for his invaluable guidance, constant support and illuminating insights. This dissertation could not have been completed without his boundless knowledge and warm encouragement. His discipline, enthusiasm and persistence will serve as an example for my future career.

I am also greatly indebted to Dr. Oscar R. González for his constructive guidance. Every formal or informal discussion with him always broadened my perspective. My research accomplishments would not have been possible without his wisdom and efforts.

My other committee members, Dr. Celeste M. Belcastro (NASA Langley Research Center), Dr. Alex Pothen (Department of Computer Science, Old Dominion University) and Dr. Min Song (Department of Electrical and Computer Engineering, Old Dominion University), have all consistently breathed fresh air into my dissertation research.

I can also not forget the faculty and staff of the Department of Electrical and Computer Engineering at Old Dominion University for all their generous assistance and support.

Confucius said, "When three men walk together, there is always something I can learn ..." (see *Lunyu*). I would like to thank all my colleagues in the Systems Research Laboratory (SRL), who have "walked" with me for so many years: Dr. Yaqin Li, Arturo Tejada, Dr. Sudarshan Patilkulkarni, Heber Herencia-Zapana, Mark Adams, Anushka Lakdawala and others for all the "SRL philosophies" I have

learned from you.

A special thanks goes to my colleagues: Dr. Christine M. Belcastro, Daniel Koppen, and Dr. Kenneth W. Eure from the NASA Langley Research Center; Richard Hess and Kent Stange from Honeywell, Inc.; Bruce E. Takala and Dr. Stephen A. Wender from the Los Alamos Neutron Science Center; Boyd Hill from ViGYAN, Inc.; and Edward F. Hogge from the Lockheed Martin Engineering and Sciences for assisting in the design and execution of the Recoverable Computer System experiments. Their efforts to produce the experimental data made this dissertation possible.

I also wish to acknowledge the generous support from the NASA Langley Research Center under contracts NCC-1-392, NCC-1-03026 and NNL04AA03A, and from the National Science Foundation under grant CCR-0209094.

Finally, I want to thank my family: my father, Zhang Lutai; my mother, Zhao Runfang; my brother, Zhang Yun; my sister, Zhang Yuzhen; and my fiancée, Li Qinqin for their everlasting love, support and encouragement.

TABLE OF CONTENTS

LIST OF TABLES

LIST OF FIGURES

LIST OF SYMBOLS

$2^{\mathbb{X}}$	Power set of a set $\mathbb{X}$
$\otimes$	Kronecker product
$\partial\mathbb{A}$	Boundary of a set $\mathbb{A}$
$\langle\cdot,\cdot\rangle$	Inner product
$\|\cdot\|$	Norm of a vector or induced norm of a linear operator
$\|\cdot\|_1$	1-norm of a matrix
$\kappa(\cdot)$	Condition number of a matrix
$\kappa(\lambda, A)$	Condition number of the eigenvalue λ of a matrix A
$[\Pi]_{ij}$	The ij-th element of a matrix Π
σ	Root mean square gust magnitude
$\sigma_{\max}(\cdot), \sigma_{\min}(\cdot)$	Maximum and minimum singular values of a matrix
$\Sigma_{\mathrm{I}}, \Sigma_{\mathrm{S}}, \Sigma_{\mathrm{O}}$	Sets of input symbols, internal states and output symbols for $\mathfrak{A}$ or $\mathfrak{M}$
$\Sigma_{\mathrm{n}} : (A_{\mathrm{n}}, G_{\mathrm{n}}, C_{\mathrm{n}})$	State space model of the nominal mode
$\Sigma_{\mathrm{r}} : (A_{\mathrm{r}}, G_{\mathrm{r}}, C_{\mathrm{r}})$	State space model of the recovery mode
φ	Column stacking operator for an MN-tuple in $\mathbb{H}^n_{MN}$
ω	Angular frequency
$\mathfrak{A}$	Stochastic finite-state automaton
$\mathscr{A}_1$	Matrix representation of the linear operator $\mathcal{T}$
$\mathscr{A}_2$	Matrix representation of the linear operator $\mathcal{L}$
$(A_{\mathrm{c}}, B_{\mathrm{c}}, C_{\mathrm{c}}, D_{\mathrm{c}})$	Linear output feedback controller
$(A_{\mathrm{cl}}, B_{\mathrm{cl}}, C_{\mathrm{cl}})$	Nominal closed-loop model of the aircraft dynamics
$(A_{\mathrm{g}}, B_{\mathrm{g}}, C_{\mathrm{g}}, D_{\mathrm{g}})$	State space model of the Dryden wind gust shaping filter
$(A_{\mathrm{p}}, B_{\mathrm{p}}, C_{\mathrm{p}})$	State space model of the aircraft dynamics
$\mathbb{B}(\cdot)$	Borel σ-algebra of a set
$\mathbb{B}(\mathbb{H}^n_K)$	Space of all bounded linear operators on $\mathbb{H}^n_K$
$\mathrm{diag}(\cdot,\cdot,\dots)$	(Block) diagonal matrix of the elements
$E\{\cdot\}$	Mean value of a (function of) random variable
$\mathfrak{H}$	Stochastic hybrid system
$\mathbb{H}^n_K$	Space of all K-tuples of $n \times n$ real matrices
$\mathbb{H}^{n+}_K$	Set $\{V \in \mathbb{H}^n_K : V \geq 0\}$
I	Identity matrix with compatible dimension
J_0	(Mean) output energy
J_w	(Mean) output power
K_{g}	Wind gusts input matrix
L	Length scale for the gust velocity
$\mathcal{L}$	Observability Gramian operator
$\mathfrak{M}$	Finite-state machine
$\mathbb{M}(\mathbb{R}^n, \mathbb{R}^m)$	Linear space of all $m \times n$ real matrices
$\mathbb{M}(\mathbb{R}^n)$	Normed linear space of all $n \times n$ real matrices
$\mathbb{M}(\mathbb{R}^n)^+$	Subset of all symmetric positive semi-definite matrices in $\mathbb{M}(\mathbb{R}^n)$

$\mathbb{N}$	Set of all natural numbers
$\Pr\{\cdot\}$	Probability of a random variable
$\mathbb{P}(\mathbb{X})$	Family of all probability measures on a set $\mathbb{X}$
$\mathbb{Q}$	Countable set of discrete variables for $\mathfrak{H}$
$r_\sigma(\cdot)$	Spectral radius of a linear operator in $\mathbb{B}(\mathbb{H}_K^n)$
$r(k)$	Reference input signal
$\mathbb{R}^n$	The n-dimensional real vector space
$S_{\mathrm{u_g}}, S_{\mathrm{v_g}}, S_{\mathrm{w_g}}$	Spectral densities of the forward, side, and down Dryden wind and gust components
$\mathrm{tr}(\cdot)$	Trace operator of a matrix in $\mathbb{M}(\mathbb{R}^n)$
T	Sample period
$\mathcal{T}$	Controllability Gramian operator
$\mathrm{u}, \mathrm{v}, \mathrm{w}$	Forward, side, and down components in the aircraft body frame
$\mathrm{u_g}, \mathrm{v_g}, \mathrm{w_g}$	Forward, side, and down wind and gust velocity components
$u_\mathrm{p}, x_\mathrm{p}, y_\mathrm{p}$	Input, state and output vectors of the aircraft dynamics
V_0	Magnitude of the apparent wind velocity from the motion of the aircraft relative to the air mass
vec	Column stacking operator for a matrix in $\mathbb{M}(\mathbb{R}^n)$
W_o	Observability Gramian of a linear system
W_t	One-dimensional standard Wiener process
$\mathbb{X}$	Continuous state space for $\mathfrak{H}$
$\mathbb{Z}^+$	Set of all non-negative integers

Acronyms

ABFT	Algorithmic-based fault tolerance
CMOS	Complementary metal oxide semiconductor
EDAC	Error detection and correction
FAA	Federal Aviation Administration
FPGA	Field-programmable gate array
FSM	Finite-state machine
IC	Integrated circuit
LANSCE	Los Alamos Neutron Science Center
MSS	Mean-square stable/stability
NASA	National Aeronautics and Space Administration
RCS	Recoverable Computer System
SEB	Single-event burnout
SEE	Single-event effect
SEL	Single-event latchup
SET	Single-event transient
SEU	Single-event upset
SFSA	Stochastic finite-state automaton
SRAM	Static random-access memory
UAV	Uncrewed air vehicle

CHAPTER I

INTRODUCTION

This dissertation analyzes the output tracking performance of an aircraft in closed-loop with a recoverable flight control system, that is subjected to neutron-induced upsets. A mathematical model is proposed to calculate the stability boundary and output performance of the closed-loop system. The model is then validated via experimental data obtained from a simulated-neutron environment. The validated model is finally used to analyze data collected from a real neutron experiment. The main conclusion of the dissertation is that the recoverable flight control system, when functioning as designed, will provide reliable control performance in the presence of neutron-induced single-event upsets at normal atmospheric levels.

This chapter is organized as follows. Section I.1 provides the background and motivation for this dissertation. In Section I.2, a literature survey is provided. Section I.3 states the primary research goals of this dissertation. Section I.4 outlines the main mathematical notation (see also the List of Symbols on pages xiv–xv). Section I.5 outlines the basic structure of the dissertation.

I.1 BACKGROUND AND MOTIVATION

When cosmic rays collide with oxygen and nitrogen atoms in the earth's upper atmosphere, free neutrons are produced with energies varying from 1 MeV to

[1]This dissertation follows the style of the *IEEE Transactions on Automatic Control* for placement of figure titles, placement of table titles, and the format of bibliography.

1 GeV [1,2]. For altitudes less than 60,000 ft, the higher the altitude, the higher the neutron flux and energy [3]. When a neutron passes through a solid state device, it has been observed that stored electric charge can be locally redistributed, which may cause a single-event effect (SEE). SEE's can be classified into three categories according to the duration of the phenomena: single-event burnout (SEB), single-event latchup (SEL), and single-event upset (SEU) [4]. SEB's are failures which cause "permanent" damage to hardware, for example, a frozen bit in a register or random-access memory that cannot be cleared by recycling the power. SEL's are errors that can usually be corrected if the hardware is reset or refreshed in some manner. For example, a short circuit between the power supply and ground of parasitic bipolar transistors of bulk CMOS (Complementary Metal Oxide Semiconductor) technologies triggered by a local charge deposition from a traversing particle is an SEL phenomenon. SEU's are errors which are transient and nondestructive, for example, a temporary bit flip in a memory cell from a binary "one" to a "zero" or vice versa. If a sequence of such bit errors is not detected and corrected, it can cause system errors and reduce closed-loop performance. This phenomenon has been studied extensively at the component level by semiconductor manufacturers [5–7]. In this context, both analytical models and data are available to provide SEU probability estimates under a wide variety of circumstances. In contrast, at the system level, the problem has not received much attention. In [8,9], the effect of upsets on system stability was studied for a few fault tolerant architectures. However, at the present time no performance analysis studies are available.

As more commercial aircraft control systems and avionics are implemented using embedded digital hardware, SEU's have recently come to the attention of the Federal

Aviation Administration (FAA) as a potential safety hazard. In response, a program has been developed by the NASA Langley Research Center with the general goal of quantifying the nature of the risk and to produce guidelines for the aerospace industry and chip manufacturers. As part of this program, this dissertation investigates the effects of atmospheric neutrons on system-level performance of commercial aircraft with experimental flight control hardware in the loop. While a variety of different technologies were tested in the NASA program, the focus here is exclusively on an experimental Recoverable Computer System (RCS) developed by Honeywell, Inc. The error recovery system in this prototype device is implemented using dual-lock-step processors together with new fault tolerant architectures and communication subsystems [10,11]. It has most recently been used to study recoveries from transient faults introduced by high intensity electromagnetic radiation [12,13]. The error recovery technique implemented on the RCS is a variation of rollback recovery [14,15]; it has the following steps: checkpointing, fault tolerant comparison, rollback, and retry. During a checkpoint, the state of each microprocessor module is stored. When an upset is detected, rollback of both microprocessor modules to a previous checkpoint takes place, and then the system is allowed to proceed with normal execution. Fig. 1 shows the architecture of the duplex fault tolerant RCS [12,13,16]. In a digital flight control application, once the execution of the normal control program is interrupted, the execution of a different control law takes place, one that has significantly different dynamics and is on a time scale that can alter the overall closed-loop dynamics. The behavior of a recoverable system can be modeled as a two-mode switched system. If there is no upset detected, the system operates in its *nominal* mode. When the controller is executing a rollback recovery, the system is in its *recovery* mode. A

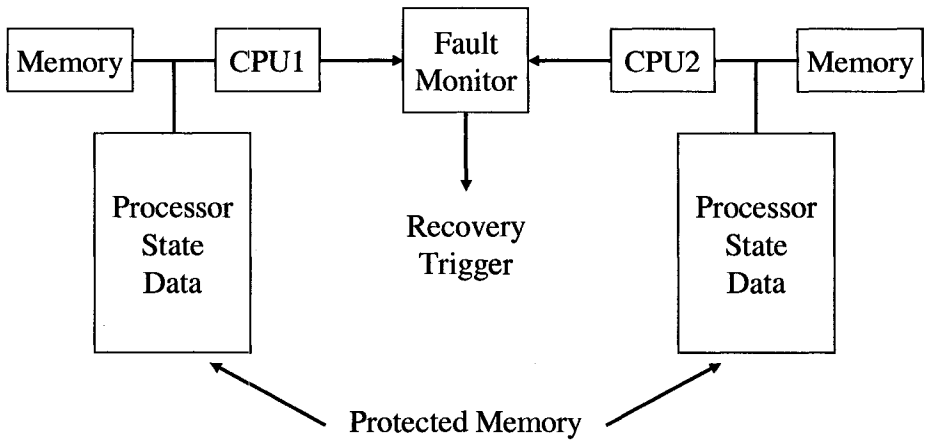

Fig. 1. Architecture of the duplex fault tolerant RCS.

conceptual diagram of the RCS in a closed-loop configuration is shown in Fig. 2.

To better understand the performance of the RCS in a radiation environment, mathematical models and performance criteria are needed. If the upset process $\boldsymbol{\nu}(k)$ is an rth-order Markov chain, where $r \in \{0, 1\}$ (see [17, 18]), and the rollback recovery process of the RCS is modeled via a *stochastic finite-state automaton* (SFSA) (formally defined in Definition II.1 on page 36), then the recoverable flight system can be modeled using the stochastic hybrid model shown in Fig. 3. Since the output process of an SFSA is not a Markov chain in general, the hybrid system may not be a Markov jump-linear system [19]. This is unfortunate since Markov jump-linear systems have been well studied in regards to their stability (see, for example, [20]) and performance (see, for example, [21]). Motivated by this fact, it will be necessary in Chapter II to identify an *equivalent* Markov jump-linear model suitable for stability and performance analysis of the hybrid system.

Throughout the dissertation, the output performance criteria, *output power* and *output energy*, are considered for the following reasons:

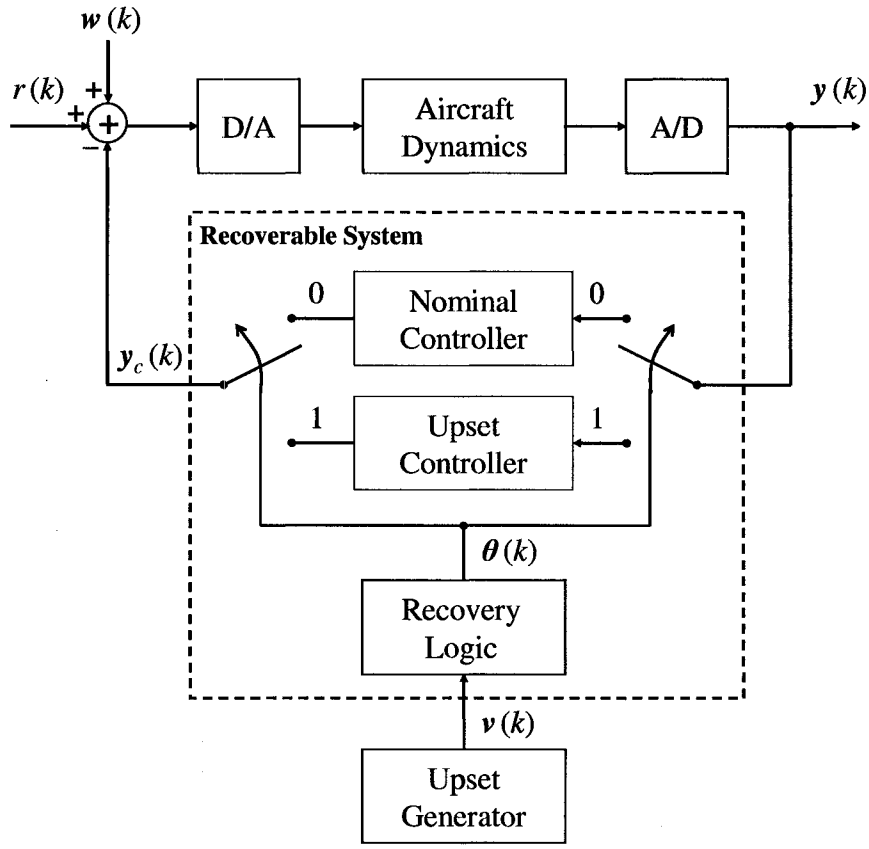

Fig. 2. A conceptual closed-loop flight control system with a recoverable flight control computer.

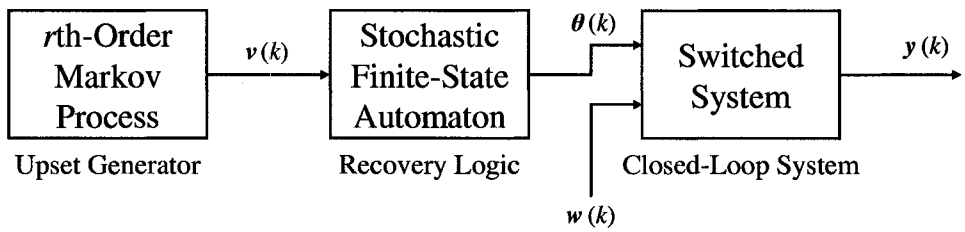

Fig. 3. The stochastic hybrid model consisting of a switched system driven by an SFSA.

(a) Output signals can be easily measured in experiments. For example, the altitude, calibrated airspeed, and tracking angle are generally available as system outputs. On the other hand, the dynamic states of a system are not always available and difficult to estimate, since the closed-loop system is nonlinear and highly coupled internally.

(b) Controller design problems are not considered in this dissertation. Instead, performance analysis is used to understand the behavior of RCS hardware with a fixed control law in an experimental setting. Therefore, it is not necessary to include the states and control signals in the performance criteria.

The basic idea behind the calculation of the output performance for a recoverable system follows from considering a simple deterministic, discrete-time linear system

$$x(k+1) = Ax(k), \quad x(0) = x_0 \tag{1a}$$

$$y(k) = Cx(k). \tag{1b}$$

Assume the system (1a) is asymptotically stable, that is, the spectral radius of A is strictly less than one. Then system (1) has a finite output energy, $J_0 := \sum_{k=0}^{\infty} \|y(k)\|^2$, which can be expressed via the observability Gramian, W_o, and initial condition, x_0, as

$$\begin{aligned}
\sum_{k=0}^{\infty} \|y(k)\|^2 &= \sum_{k=0}^{\infty} y^{\mathrm{T}}(k)y(k) \\
&= \sum_{k=0}^{\infty} \left(Cx(k)\right)^{\mathrm{T}} Cx(k) \\
&= \sum_{k=0}^{\infty} x_0^{\mathrm{T}} \left(A^{\mathrm{T}}\right)^k C^{\mathrm{T}} C A^k x_0 \\
&= x_0^{\mathrm{T}} \left(\sum_{k=0}^{\infty} \left(A^{\mathrm{T}}\right)^k C^{\mathrm{T}} C A^k \right) x_0
\end{aligned}$$

$$= \mathrm{tr}\left(X_0 W_o\right),$$

where $X_0 := x_0 x_0^{\mathrm{T}}$, and $W_o := \sum_{k=0}^{\infty} \left(A^{\mathrm{T}}\right)^k C^{\mathrm{T}} C A^k$ is the observability Gramian (see, for example, [22]). If x_0 is a second-order random variable $\boldsymbol{x}_0$, then system (1) is a stochastic system with a finite mean output energy $\tilde{J}_0 := E\left\{\sum_{k=0}^{\infty} \|\boldsymbol{y}(k)\|^2\right\} = \mathrm{tr}\left(\tilde{X}_0 W_o\right)$, where $\tilde{X}_0 := E\left\{\boldsymbol{x}_0 \boldsymbol{x}_0^{\mathrm{T}}\right\}$. By extending this idea to stochastic hybrid models, it is shown in the dissertation how to express both output energy and output power of such systems in terms of a *generalized* observability Gramian (see Chapter IV, Section IV.2). The results of this analysis are central to analyzing RCS performance in a real neutron environment.

In parallel with the theoretical studies, the performance of a simulated aircraft system in closed-loop with an RCS was evaluated experimentally in a real neutron environment. Of course, it is difficult to test any electronic device in an atmospheric neutron environment because of its low neutron intensity. Therefore, a set of high intensity (accelerated) neutron experiments was conducted at the Los Alamos Neutron Science Center (LANSCE) in Los Alamos, New Mexico. A conceptual diagram of the testbed is shown in Fig. 4. A beam of free neutrons was directed through a flux sensor at the device under test, in this case the RCS. The energy spectrum of the neutron source is shown in Fig. 5. Its shape is very similar to that produced by atmospheric neutrons, but the flux is five to six orders of magnitude higher. The RCS in this configuration ran a control program which processes outputs from a Boeing 737 flight simulation system running on a separate host computer. The RCS generated the appropriate control signals to the aircraft simulation model for maintaining straight and level flight at a cruising altitude of 34,000 ft. This interconnection between

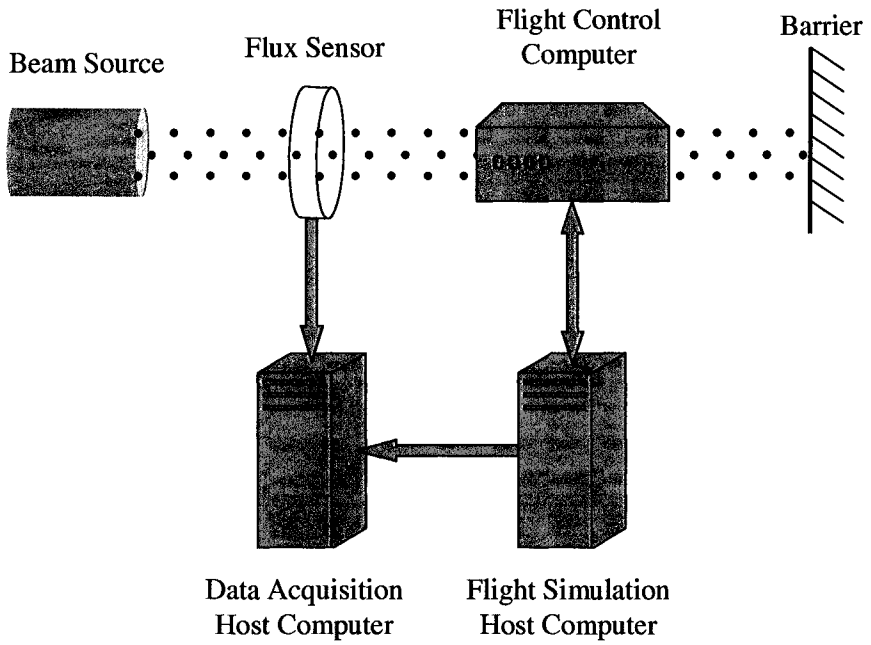

Fig. 4. The testbed for the LANSCE experiments.

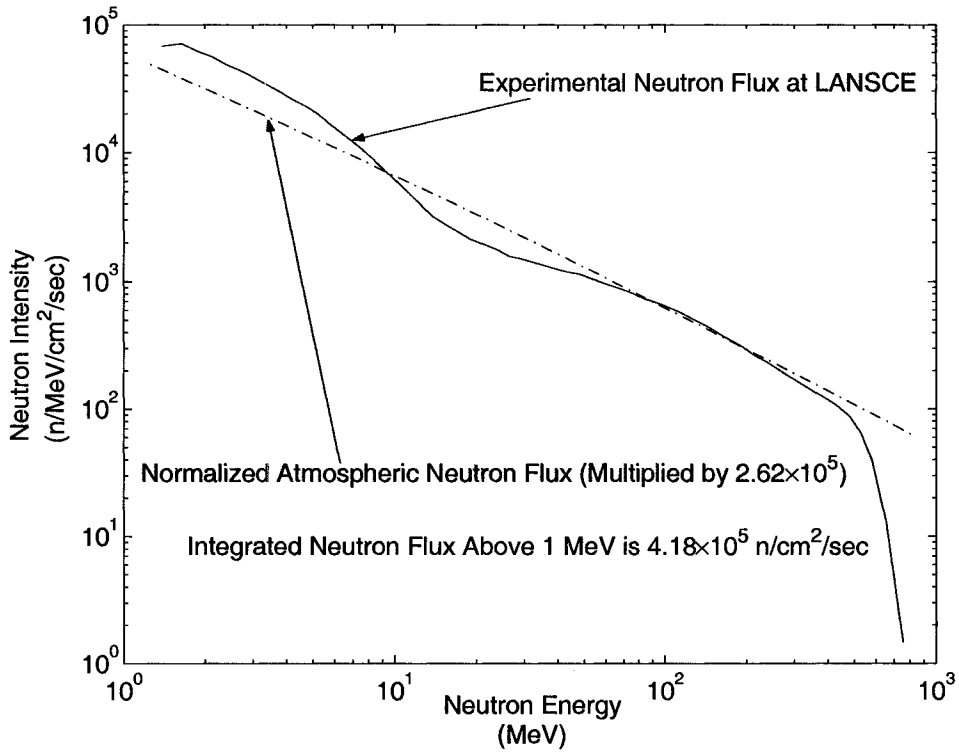

Fig. 5. The neutron energy spectrum at LANSCE in December, 2002.

the RCS and the flight simulation host computer constitutes a closed-loop feedback control system, which was the unique feature of these experiments. Under nominal conditions, i.e., no neutrons, this system regulates the aircraft heading and orientation very well, even under 1 ft/sec (light) winds and gusts which can be introduced into the simulation model. The data acquisition system was maintained on a third computer system. It collected the flight data from the simulation as well as the measurements from the flux sensor for off-line analysis. Should the aircraft deviate from the nominal flight path at any time, it was possible to determine the total radiation dose the RCS received up to that instant. When neutrons collide with the RCS, the specific effects of any disturbance will depend on the particular internal hardware affected and how effective the rollback recovery mechanism functions in this environment. Since this was an accelerated neutron experiment, the upset rate was expected to be much higher than that observed in an atmospheric neutron environment. Correspondingly, the output tracking power of the flight system in closed-loop with an RCS should also be much higher than that from the atmospheric neutron environment. In order to predict the output tracking performance under atmospheric conditions, the mathematical performance models were used to extrapolate the Los Alamos data (a conceptual example is shown in Fig. 6). This is viewed as the central contribution of the dissertation.

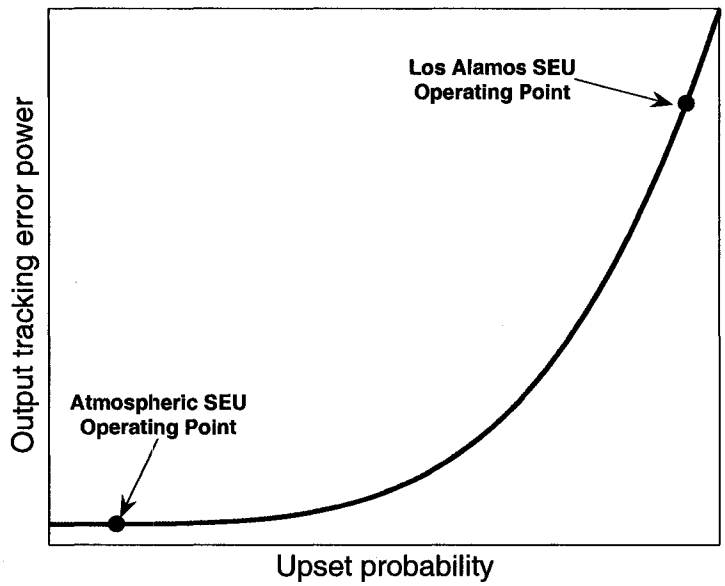

Fig. 6. Output tracking power as a function of upset probability for both atmospheric and accelerated neutron conditions.

I.2 LITERATURE SURVEY

I.2.1 Single-Event Upsets: Fault Detection and Correction

Although SEU's are soft faults and nondestructive to digital devices, they can degrade the performance of a system. For digital systems with high reliability and safety requirements, such as flight control systems, the SEU phenomenon is a potential threat. SEU's mainly occur in space applications due to the abundance of cosmic rays, trapped protons, and solar event particles [23, 24]. However, in an environment with high energy thermal neutrons and α-particles, even some ground level applications, such as devices comprised of large digital memories, like bank servers and communication servers can experience SEU's [24, 25]. Most studies on fault tolerance and SEU phenomena are focused at the component-level, especially for static

random-access memories (SRAM's), field-programmable gate arrays (FPGA's), and integrated circuits (IC's). See, for example, [26–29] and the references therein. The existing fault tolerant techniques include memory scrubbing, triple modular redundancy, crossparity checks, error detection and correction (EDAC), etc.

As described in [30], a component-level approach may not always compensate the system properly, because it does not take into account the fact that:

1. upsets can be multiplied within individual devices;

2. upsets can propagate between interconnected devices;

3. the performance of various software sets may not take into account fault tolerant routines.

Therefore, it is necessary to perform system-level compensation, analysis and testing. There are many system-level fault tolerant techniques described in the literature. In [31], an algorithmic-based fault tolerance (ABFT) is proposed which has a low level of hardware and time redundancy. In [32,33], both duplex and triplex fault tolerant architectures are presented. In [34], system-level recovery approaches are categorized as recovery via re-initialization, recovery via temporary storage and recovery via a dedicated data link. A detailed performance evaluation of each rollback recovery technique is given in [15]. In this dissertation, the prototype experimental system, the RCS, is implemented using a duplex fault tolerant system with rollback recovery techniques via temporary storage.

I.2.2 Markov Jump Systems: Applications, Stability and Performance

As discussed in [35], hybrid dynamical models usually include two components: one component embodies the system dynamics and the other executes the decision making-process. The system dynamics can be either continuous-time or discrete-time or a mixture of both. The decision-making process might be realized by a discrete-event system such as a finite-state machine (FSM) or a Markov chain, which can affect the trajectory of the system dynamics. On the other hand, the system dynamics may or may not affect the decision making. Hybrid dynamical models find wide usage, for example, in disk drive and stepper motor applications [36,37]. If the system dynamics and/or the decision-making process is stochastic, then the hybrid system is called a stochastic hybrid system. A formal mathematical definition is given below:

Definition I.1. [38, 39] A stochastic hybrid system is a collection $\mathfrak{H} = (\mathbb{Q}, \mathbb{X}, \text{Dom}, \phi, \psi, \text{Init}, \mathbb{G}, R)$, where

- $\mathbb{Q} = \{q_1, q_2, \ldots\}$ is a countable set representing the discrete state space;
- $\mathbb{X} = \mathbb{R}^n$ is the continuous state space, where $\mathbb{R}^n$ is the n-dimensional real vector space;
- $\text{Dom} : \mathbb{Q} \to 2^{\mathbb{X}}$ assigns to each $q \in \mathbb{Q}$ an open subset of $\mathbb{X}$, where $2^{\mathbb{X}}$ denotes the power set (that is, set of all subsets) of $\mathbb{X}$;
- $\phi, \psi : \mathbb{Q} \times \mathbb{X} \to \mathbb{R}^n$ are vector fields, where $\phi(q, x)$ and $\psi(q, x)$ are bounded and Lipschitz continuous at $x \in \mathbb{X}$. This ensures that for any $q \in \mathbb{Q}$, the solution

of $\mathrm{d}x(t) = \phi\big(q, x(t)\big)\,\mathrm{d}t + \psi\big(q, x(t)\big)\,\mathrm{d}W_t$ exists and is unique when W_t is a one-dimensional standard Wiener process;

- Init : $\mathbb{B}(\mathbb{Q}\times\mathbb{X}) \to [0,1]$ is an initial probability measure on $\big(\mathbb{Q}\times\mathbb{X}, \mathbb{B}(\mathbb{Q}\times\mathbb{X})\big)$ concentrated on $\bigcup_{q\in\mathbb{Q}} \big\{\{q\}\times \mathrm{Dom}(q)\big\}$, where $\mathbb{B}(\mathbb{Q}\times\mathbb{X})$ is the Borel σ-algebra of $\mathbb{Q}\times\mathbb{X}$;

- $\mathbb{G} : \mathbb{Q}\times\mathbb{Q} \to 2^{\mathbb{X}}$ assigns to each $(q,\tilde{q}) \in \mathbb{Q}\times\mathbb{Q}$ a guard $\mathbb{G}(q,\tilde{q}) \subset \mathbb{X}$ such that

  - For each $(q,\tilde{q}) \in \mathbb{Q}\times\mathbb{Q}$, $\mathbb{G}(q,\tilde{q})$ is a measurable subset of $\partial\,\mathrm{Dom}(q)$ (possibly empty), where $\partial\,\mathrm{Dom}(q)$ denotes the boundary of $\mathrm{Dom}(q)$ in $\mathbb{X}$;

  - For each $q \in \mathbb{Q}$, the family $\{\mathbb{G}(q,\tilde{q}) \mid \tilde{q} \in \mathbb{Q}\}$ is a disjoint partition of $\partial\,\mathrm{Dom}(q)$;

- $R : \mathbb{Q}\times\mathbb{Q}\times\mathbb{X} \to \mathbb{P}(\mathbb{X})$ assigns to each $(q,\tilde{q}) \in \mathbb{Q}\times\mathbb{Q}$ and $x \in \mathbb{G}(q,\tilde{q})$ a reset probability kernel on $\mathbb{X}$ concentrated on $\mathrm{Dom}(\tilde{q})$. Here $\mathbb{P}(\mathbb{X})$ denotes the family of all probability measures on $\mathbb{X}$. Furthermore, for any measurable set $\mathbb{A} \subset \mathrm{Dom}(\tilde{q})$, $R(q,\tilde{q},x)(\mathbb{A})$ is a measurable function in x.

One special class of stochastic hybrid systems is the Markov jump-linear system. In this case, the system dynamics are produced by a linear system, and the decision-making process is realized by a Markov chain. The well-known properties of Markov chains often make it is easier to analyze the stochastic stability and performance of a Markov jump-linear system. Thus, considerable research has been conducted on many system theoretical problems: stability and stabilization, H_2 and/or H_∞ control, controllability and observability, estimation and identification, etc. Many of these references are provided in [40]. In this dissertation, only the stochastic stability and

output performance of Markov jump-linear systems are relevant. In [20,41–46], stability of a Markov jump-linear has been studied extensively for both the continuous- and discrete-time cases. The main method employed in this body of work is a stochastic version of Lyapunov's second method, i.e., a set of coupled Lyapunov equations. For Markov jump-linear system, both sufficient and necessary stability conditions have been obtained. Most performance criteria are given in the context of controller design (see, for example, [46–49]). One exception is [50–52], where networked control systems with Markovian dropouts are studied. In these papers, an output performance, the *power semi-norm* of the output signals, is used to describe how to relate system performance to the data dropout rate through the autocorrelation of the output signals. A generalized version of this output performance criteria will be considered in this dissertation.

Markov jump-linear systems have been applied to a variety of applications. For example, air-launched uncrewed air vehicles (UAV's) are studied in [53]. For clear and safe separation, UAV's are often released with their wings folded. However, as they begin a significant glide slope maneuver, the wings are deployed. The "folded" and the "deployed" modes have much different dynamics and form a switched process, which can be modeled as a Markov jump-linear system. In [54], a solar energy plant is used to heat the water in a boiler. The water flow is regulated according to the atmospheric conditions, i.e., whether it is a sunny or a cloudy day. The atmospheric conditions can therefore be modeled as a two-state Markov chain: "sunny" and "cloudy". In [55], a Markov jump-linear system is used to model a macroeconomic policy problem. Specifically, in a time-variant macroeconomic model, certain model parameters are allowed to fluctuate according to a Markov chain. One simplified

case involves three modes: "bad", "neutral", and "good". Each mode represents a measurable state of the economy. Simultaneously, a second Markov chain is used to model the policy modes used by policy makers: "neutral", "Keynesian", and "classic" with a fixed probability transition matrix.

A particularly relevant application to this dissertation is described in [56]. Here a Markov jump-linear system is used to analyze the effects of random interruptions in feedback due to a non-ideal communication system network. The system has two modes: one in which the packet from the sensor is received with a probability π_0, and the other in which the packet is lost with a probability $\pi_1 = 1-\pi_0$. In this application, the switching signal is actually an independent, identically distributed (i.i.d.) process. For the communication system in [57], a Markov jump-linear system is used to model a network of single-integrator agents where the communication/sensing topology is subject to Markovian fluctuation.

I.2.3 Stochastic Finite-State Automata

In this dissertation, an SFSA is used to model the rollback recovery processes of the RCS. SFSA's are a type of probabilistic finite-state machine. A detailed review of their properties appears in [58]. Stochastic automata have been applied in a variety of areas. In [59], a stochastic automaton is used to model a quantized system, where each state of the automaton models an event produced by a quantizer, and the input symbols of the automaton are used to represent a discrete input signal for the injector. This automaton is called an abstraction of the quantized system. In [60], an SFSA is used as a simplified model of a linear time-invariant system, and its robustness with respect to the error of such approximation is analyzed. With slight

modifications to the definition, SFSA's are also widely used in modeling language behavior and machine translation [61, 62]. In [63], two algorithms are presented which check properties written in a simple probabilistic real-time logic against a given stochastic automaton. A special type of SFSA's is an FSM. In this case, the transition from the current state to the next state is deterministic if the current state and current input to the automaton are given.

In general, when the input process of an FSM is a Markov chain, neither its state nor output process is a Markov chain [19, 64]. However, it is known that the input–state cross product process is Markov when the input process is Markov [19, 64, 65]. This is relevant to the research presented in this dissertation because this proposition can be extended to an SFSA. Thereafter, the stochastic hybrid model can be made *model-equivalent* (formally defined in Definition II.9 on page 53) to a Markov jump-linear system. A collection of well-established stability and performance analysis tools for Markov jump-linear systems can then be used to analyze the flight control system in closed-loop with an RCS. In Chapter II, these properties will be extended nontrivially to a general SFSA.

I.3 PROBLEM STATEMENT

The main objectives of this dissertation are to solve the following problems:

1. To synthesize appropriate mathematical models for a Boeing 737 in closed-loop with a digital controller implemented with an RCS. This involves modeling the aircraft system with and without active rollback recovery processes, the upset generating process, and the external wind disturbances.

2. To build a class of stochastic hybrid models via the mathematical models obtained in item 1 which can be used to analyze the output tracking error.

3. To develop stability and output performance theory for these stochastic hybrid models.

4. To apply these theoretical results to predict the tracking performance of the Boeing 737 in closed-loop with the RCS subject to neutron-induced SEU's.

5. To validate these predictions with experimental data obtained from a simulated neutron environment at NASA Langley Research Center.

6. To process performance data derived from real (*accelerated*) neutron tests conducted at LANSCE.

7. To estimate the performance effects of SEU's on the aircraft's control system when it is implemented in an RCS under normal atmospheric conditions using the theory developed in item 4.

I.4 MATHEMATICAL NOTATION

The mathematical notation used throughout this dissertation is largely consistent with [66, 67]. Random variables are denoted in bold italic fonts. The symbol $\mathbb{Z}^+$ denotes the set of all non-negative integers. $\mathbb{N}$ is the set of all natural numbers. $\mathbb{M}(\mathbb{R}^n, \mathbb{R}^m)$ denotes the linear space of all $m \times n$ real matrices. $\mathbb{M}(\mathbb{R}^n)$ is the normed linear space of all $n \times n$ real matrices. The subset of all symmetric positive semi-definite matrices is $\mathbb{M}(\mathbb{R}^n)^+$. $\mathbb{H}_K^n = \{V = (V_1, V_2, \ldots, V_K) : V_i \in \mathbb{M}(\mathbb{R}^n)\}$ will be used to denote the space of all K-tuples of $n \times n$ real matrices. If every V_i of a given V

in $\mathbb{H}_K^n$ is positive definite or positive semi-definite, this is indicated, respectively, by $V > 0$ and $V \geq 0$. $\mathbb{H}_K^{n+}$ denotes the set $\{V \in \mathbb{H}_K^n : V \geq 0\}$. For $U = (U_1, U_2, \ldots, U_K)$ and $V = (V_1, V_2, \ldots, V_K)$ in $\mathbb{H}_K^{n+}$, the notation $U \leq V$ $(U < V)$ denotes that $U_i \leq V_i$ $(U_i < V_i)$ for every $i = 1, \ldots, N$. Given $U, V \in \mathbb{H}_K^n$, the inner product on $\mathbb{H}_K^n$ is defined by

$$\langle U, V \rangle = \sum_{i=1}^{N} \operatorname{tr}\left(U_i^{\mathrm{T}} V_i\right),$$

and $\|V\|^2 = \langle V, V \rangle$ is the induced norm squared of V. ($\|\cdot\|$ will also be used for representing the standard norm on $\mathbb{R}^n$.) $\mathbb{B}(\mathbb{H}_K^n)$ is the space of all bounded linear operators on $\mathbb{H}_K^n$ under the induced operator norm

$$\|\mathcal{L}\| = \sup_{V \neq 0} \frac{\|\mathcal{L}(V)\|}{\|V\|},$$

where $\mathcal{L} \in \mathbb{B}(\mathbb{H}_K^n)$. $r_\sigma(\mathcal{L})$ is used to denote the spectral radius of $\mathcal{L}$, specifically, $r_\sigma(\mathcal{L}) = \lim_{k \to \infty} \left\|\mathcal{L}^k\right\|^{\frac{1}{k}}$ for $k \in \mathbb{N}$. A summary of the symbols used in this dissertation appears on pages xiv–xv.

I.5 DISSERTATION OUTLINE

This dissertation is organized as follows. In Chapter II, the methodology for modeling a recoverable flight control system is presented in detail. There are three basic modules to consider: the aircraft dynamics, the Dryden wind gust filters, and the rollback recovery logic. The models for the aircraft system with the Dryden wind gust filters and control system (normal and upset) will be identified using a high fidelity flight simulation system. The rollback recovery process will be approximated by an SFSA. The final stochastic hybrid model is built by cascading these models as shown in Fig. 2. Because the input–output cross product process of an SFSA can

be proven to be a Markov chain, when the input process is also a Markov chain, a model equivalence theory and the theory of Markov jump-linear systems will be used to analyze the recoverable system.

In Chapter III, the mean-square stability of a hybrid system is analyzed by studying that of an equivalent Markov jump-linear system. A variety of definitions of stochastic stability are considered. Under certain assumptions, it can be shown that some of these definitions are equivalent. The main empirical task in this chapter is to apply the analytical tools to determine the stability region of the hybrid system modeling the recoverable aircraft system.

In Chapter IV, the output performance criteria, mean output power and mean output energy, are considered. The main theory needed for the calculation of the two criteria is presented in detail. Using these results, a prediction of the mean output tracking error power due to the presence of SEU's in the aircraft system is calculated.

In Chapter V, two experiments are described. One experiment was conducted at the NASA Langley Research Center under a simulated neutron environment. The SEU's were triggered using predetermined Markov chains. This experiment was used to validate the hybrid model and the stability and performance prediction tools. The second experiment involved the real neutron environment at Los Alamos. The output performance data from this experiment is used to produce output performance predictions for normal atmospheric conditions.

In Chapter VI, main conclusions are summarized, and future research topics are given.

CHAPTER II

MODELING RECOVERABLE DIGITAL FLIGHT CONTROL SYSTEMS

In order to analytically evaluate the stability and performance of the recoverable digital flight control system described in Chapter I, a mathematical model is needed to describe these experiments. The system under consideration consists of three main subsystems: the linear (open-loop) aircraft dynamics $(A_{\mathrm{p}}, B_{\mathrm{p}}, C_{\mathrm{p}})$, a set of Dryden wind gust shaping filters, and the digital control system, which is assumed to be implemented with an RCS. A simplified view of the system structure is shown in Fig. 7. The actual system is complex, highly interconnected and nonlinear. Therefore, a major task here is to *synthesize* a simplified, linear representation of the recoverable flight system [68, 69].

This chapter is organized as follows. First, a conceptual model for each of the three subsystems is presented in Section II.1. It serves as guide for the practical model that needs to be synthesized. In Section II.2, it is shown that these models are not in some instances directly available nor simple enough for the stability and output performance analyses to be presented in Chapters III and IV. Thus, some central modeling approximations are proposed which will lead to the primary mathematical model for the recoverable closed-loop system. In the subsequent three sections, this model is developed. Specifically, in Section II.3, linear models for both the nominal and the recovery modes are obtained via system identification. Section II.4 describes

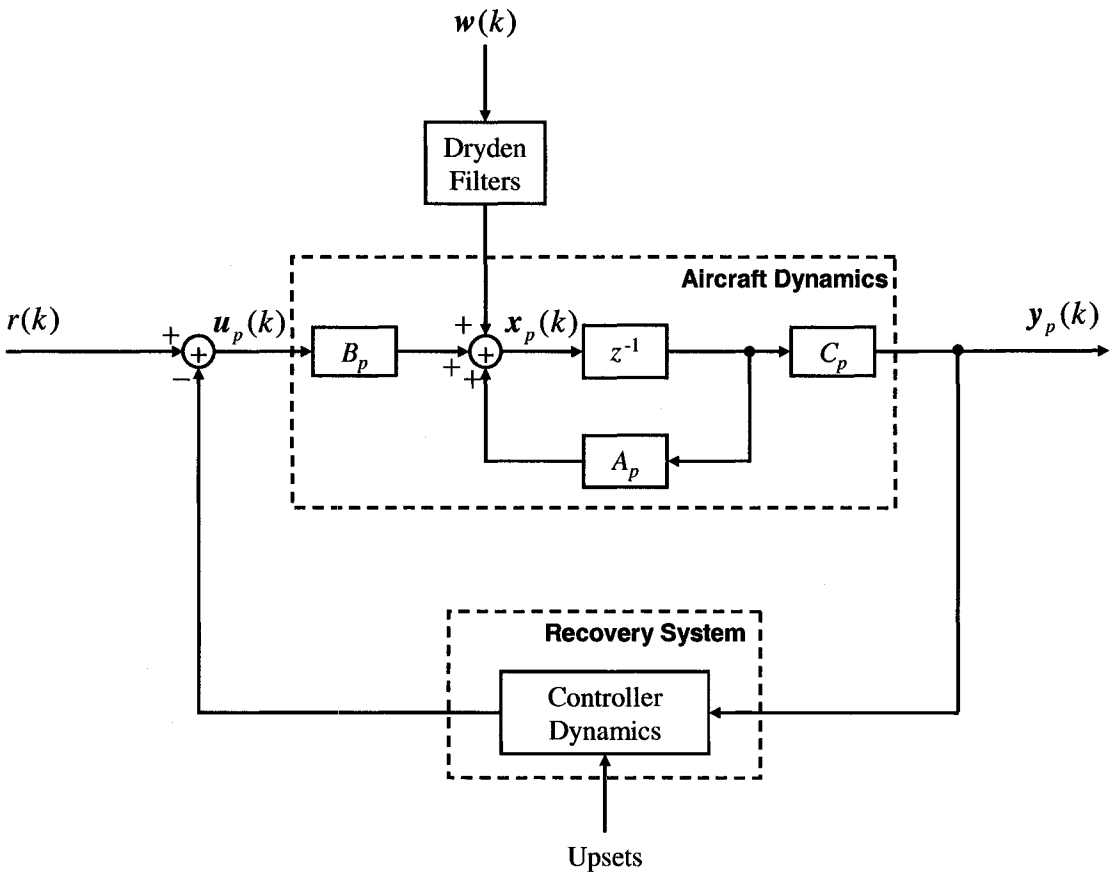

Fig. 7. A simplified view of the Boeing 737 in closed-loop with an RCS.

the modeling of the rollback recovery process using SFSA's. Section II.5 describes how to integrate the models obtained from the previous two sections to produce a stochastic hybrid system. Some Markov characterizations of the input and output processes of SFSA's and model-equivalent Markov jump-linear systems of the hybrid system are also discussed in this section. Finally, the chapter is summarized in Section II.6.

II.1 A CONCEPTUAL MODEL OF THE RECOVERABLE BOEING 737 CONTROL SYSTEM

In this section, the three subsystems in the recoverable Boeing 737 control system shown in Fig. 7 are characterized with mathematical models that are more conceptual than practical. But these models are important as they guided most of the real model development.

II.1.1 The Aircraft Dynamics of a Boeing 737

The Boeing 737 aircraft control system under consideration maintains straight and level flight at a cruising altitude of 34,000 ft and at a speed of 0.78 Mach. The aircraft's discretized linear state space model is the deterministic system

$$x_{\mathrm{p}}(k+1) = A_{\mathrm{p}}x_{\mathrm{p}}(k) + B_{\mathrm{p}}u_{\mathrm{p}}(k)$$

$$y_{\mathrm{p}}(k) = C_{\mathrm{p}}x_{\mathrm{p}}(k),$$

where the input $u_{\mathrm{p}}(k)$ is a vector of seven control signals: engine thrust (lb); stabilator position (pilot units); aileron, elevator, and rudder deflections (deg); and left/right spoiler deflections (deg). $x_{\mathrm{p}}(k)$ is the plant's state vector, which contains states defined in either the aircraft body reference frame or the earth inertial reference frame. In the body frame, ten states are defined: forward, side, and down velocities (ft/sec); roll, pitch, and yaw angles relative to the inertial frame (rad); roll, pitch, and yaw angular velocities (rad/sec); and altitude above mean sea level (ft). In the inertial frame, eight states are specified: latitude and longitude (deg); velocities to the north, east, and downward (ft/sec); and accelerations to the north, east, and downward (ft/sec^2). $y_{\mathrm{p}}(k)$ is the output vector of the aircraft model, which in this

dissertation is taken to be the altitude of the aircraft (ft), the track angle (deg) and the calibrated airspeed (kt).

The controller in principle can be modeled under the given flight conditions by a linear output feedback control law with state space description (A_c, B_c, C_c, D_c). Letting $\tilde{A}_p := A_p - B_p D_c C_p$ and $r(k) \equiv 0$, the nominal closed-loop plant (A_{cl}, B_{cl}, C_{cl}) has the form

$$A_{cl} = \begin{bmatrix} \tilde{A}_p & -B_p C_c \\ B_c C_p & A_c \end{bmatrix}, \quad B_{cl} = \begin{bmatrix} I \\ 0 \end{bmatrix}, \quad C_{cl} = \begin{bmatrix} C_p & 0 \end{bmatrix}, \tag{2}$$

where I is an identity matrix. But as will be discussed in the next section, the control law was not directly available. Thus, a system identification procedure was employed with the help of a high fidelity Boeing 737 Simulink model [70].

II.1.2 The Dryden Wind Gust Model

Winds and gusts in this application are typically modeled by white noise, $\boldsymbol{w}(k)$, passed through Dryden shaping filters to produce random processes having the spectral densities:

$$\begin{aligned} S_{u_g}(\omega) &= \sigma_u^2 \frac{L_u}{\pi V_0} \frac{1}{1 + (L_u \omega / V_0)^2} \\ S_{v_g}(\omega) &= \sigma_v^2 \frac{L_v}{2\pi V_0} \frac{1 + 3(L_v \omega / V_0)^2}{[1 + (L_v \omega / V_0)^2]^2} \\ S_{w_g}(\omega) &= \sigma_w^2 \frac{L_w}{2\pi V_0} \frac{1 + 3(L_w \omega / V_0)^2}{[1 + (L_w \omega / V_0)^2]^2}, \end{aligned}$$

where the subscripts "u", "v" and "w" represent the forward, side, and down components in the aircraft body frame, respectively, and u_g, v_g and w_g represent the corresponding wind and gust velocity components [70]. ω is the angular frequency (rad/sec); σ is the root mean square gust magnitude (ft/sec); L is the length

scale for the gust velocity (ft); V_0 is the magnitude of the apparent wind velocity from the motion of the aircraft relative to the air mass (ft/sec). Let $\gamma \in \{\mathrm{u}, \mathrm{v}, \mathrm{w}\}$ and $\delta \in \{\mathrm{v}, \mathrm{w}\}$. Define the parameters:

$$\beta_\gamma = \frac{V_0}{L_\gamma}, \qquad \alpha_\gamma = \frac{1}{\sqrt{3}}\beta_\gamma, \qquad d_\gamma = \exp(-\beta_\gamma T)$$
$$a_\gamma = \frac{1}{\beta_\gamma}\left[1 - \frac{1}{T\beta_\gamma}(1 - d_\gamma)\right], \qquad b_\gamma = -a_\gamma + \frac{1}{\beta_\gamma}(1 - d_\gamma)$$
$$i_\delta = \frac{1}{\sqrt{3}} + \left(\frac{1 - 1/\sqrt{3}}{\beta_\delta T}\right)(1 - d_\delta), \qquad j_\delta = -i_\delta + \frac{1}{\sqrt{3}}(1 - d_\delta),$$

where T is the sample period. Then the corresponding discrete-time transfer functions for the shaping filters can be expressed as

$$\frac{Y_{\mathrm{u_g}}(z)}{W_{\mathrm{u}}(z)} = \sigma_{\mathrm{u}}\sqrt{\frac{2}{T}\beta_{\mathrm{u}}} \cdot \frac{a_{\mathrm{u}} + b_{\mathrm{u}}z^{-1}}{1 - d_{\mathrm{u}}z^{-1}}$$
$$\frac{Y_{\mathrm{v_g}}(z)}{W_{\mathrm{v}}(z)} = \sigma_{\mathrm{v}}\sqrt{\frac{3}{T}\beta_{\mathrm{v}}} \cdot \frac{a_{\mathrm{v}} + b_{\mathrm{v}}z^{-1}}{1 - d_{\mathrm{v}}z^{-1}} \cdot \frac{i_{\mathrm{v}} + j_{\mathrm{v}}z^{-1}}{1 - d_{\mathrm{v}}z^{-1}}$$
$$\frac{Y_{\mathrm{w_g}}(z)}{W_{\mathrm{w}}(z)} = \sigma_{\mathrm{w}}\sqrt{\frac{3}{T}\beta_{\mathrm{w}}} \cdot \frac{a_{\mathrm{w}} + b_{\mathrm{w}}z^{-1}}{1 - d_{\mathrm{w}}z^{-1}} \cdot \frac{i_{\mathrm{w}} + j_{\mathrm{w}}z^{-1}}{1 - d_{\mathrm{w}}z^{-1}}.$$

Their discrete-time state space representations are given by

$$\boldsymbol{x}_{\mathrm{g}}(k+1) = A_{\mathrm{g}}\boldsymbol{x}_{\mathrm{g}}(k) + B_{\mathrm{g}}\boldsymbol{w}(k) \tag{3a}$$

$$\boldsymbol{y}_{\mathrm{g}}(k) = C_{\mathrm{g}}\boldsymbol{x}_{\mathrm{g}}(k) + D_{\mathrm{g}}\boldsymbol{w}(k), \tag{3b}$$

with $A_{\mathrm{g}} = \mathrm{diag}(A_{\mathrm{u_g}}, A_{\mathrm{v_g}}, A_{\mathrm{w_g}})$, $B_{\mathrm{g}} = \mathrm{diag}(B_{\mathrm{u_g}}, B_{\mathrm{v_g}}, B_{\mathrm{w_g}})$, $C_{\mathrm{g}} = \mathrm{diag}(C_{\mathrm{u_g}}, C_{\mathrm{v_g}}, C_{\mathrm{w_g}})$ and $D_{\mathrm{g}} = \mathrm{diag}(D_{\mathrm{u_g}}, D_{\mathrm{v_g}}, D_{\mathrm{w_g}})$, where for forward winds and gusts:

$$A_{\mathrm{u_g}} = \left[d_{\mathrm{u}}\right]$$
$$B_{\mathrm{u_g}} = \left[1\right]$$
$$C_{\mathrm{u_g}} = \left[\sigma_{\mathrm{u}}\sqrt{\frac{2}{T}\beta_{\mathrm{u}}}(b_{\mathrm{u}} + a_{\mathrm{u}}d_{\mathrm{u}})\right]$$
$$D_{\mathrm{u_g}} = \left[\sigma_{\mathrm{u}}\sqrt{\frac{2}{T}\beta_{\mathrm{u}}}a_{\mathrm{u}}\right],$$

and for side and down winds and gusts:

$$A_{\delta_g} = \begin{bmatrix} 2d_\delta & -d_\delta^2 \\ 1 & 0 \end{bmatrix}$$

$$B_{\delta_g} = \begin{bmatrix} 1 \\ 0 \end{bmatrix}$$

$$C_{\delta_g} = \begin{bmatrix} \sigma_\delta \sqrt{\frac{3}{T}} \beta_\delta (b_\delta i_\delta + a_\delta j_\delta + 2a_\delta d_\delta i_\delta) \\ \sigma_\delta \sqrt{\frac{3}{T}} \beta_\delta (b_\delta j_\delta - a_\delta d_\delta^2 i_\delta) \end{bmatrix}^{\mathrm{T}}$$

$$D_{\delta_g} = \left[\sigma_\delta \sqrt{\frac{3}{T}} \beta_\delta a_\delta i_\delta \right].$$

When the reference input signal $r(k) \equiv 0$, the Dryden wind gust model can be integrated with the closed-loop aircraft dynamic model, as shown in Fig. 8, using an

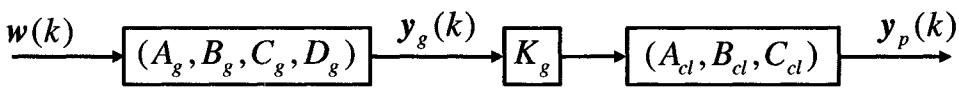

Fig. 8. The integrated Dryden wind gust model and the closed-loop system.

input matrix K_g. According to (2) and (3), the modified closed-loop system with $\boldsymbol{w}(k)$ as the input is then

$$\tilde{A}_{\mathrm{cl}} = \begin{bmatrix} \tilde{A}_{\mathrm{p}} & -B_{\mathrm{p}}C_{\mathrm{c}} & K_{\mathrm{g}}C_{\mathrm{g}} \\ B_{\mathrm{c}}C_{\mathrm{p}} & A_{\mathrm{c}} & 0 \\ 0 & 0 & A_{\mathrm{g}} \end{bmatrix}, \quad \tilde{B}_{\mathrm{cl}} = \begin{bmatrix} K_{\mathrm{g}}D_{\mathrm{g}} \\ 0 \\ B_{\mathrm{g}} \end{bmatrix}, \quad \tilde{C}_{\mathrm{cl}} = \begin{bmatrix} C_{\mathrm{p}} & 0 & 0 \end{bmatrix}.$$

II.1.3 The Recoverable Control System

In [16] (Lemma 3.2.1), a rollback interference model is given for an autonomous system. In this subsection, a variation of this approach is introduced which admits wind gust disturbances. In Fig. 2, let $\boldsymbol{\nu}(k)$ denote the state of the upset process and

$\boldsymbol{\theta}(k)$ the state of the recovery process. When $\boldsymbol{\theta}(k) = 0$, the nominal control system is engaged, and when $\boldsymbol{\theta}(k) = 1$, the recovery process is activated. Let $\boldsymbol{x}_{\mathrm{c}}(k)$ be the state of the controller. Suppose the last checkpoint occurred q sample periods ago; and $\hat{\hat{\boldsymbol{x}}}_{\mathrm{r}1}(k), \hat{\hat{\boldsymbol{x}}}_{\mathrm{r}2}(k), \ldots, \hat{\hat{\boldsymbol{x}}}_{\mathrm{r}q}(k)$ are q auxiliary vectors, then the rollback interference can be integrated into the closed-loop system model as shown below:

$$\tilde{\boldsymbol{x}}(k+1) = \tilde{A}_{\boldsymbol{\theta}(k)}\tilde{\boldsymbol{x}}(k) + \tilde{G}\boldsymbol{w}(k)$$

$$\boldsymbol{y}_{\mathrm{p}}(k) = \tilde{C}\tilde{\boldsymbol{x}}(k),$$

where

$$\tilde{\boldsymbol{x}}(k) := \left[\boldsymbol{x}_{\mathrm{p}}^{\mathrm{T}}(k) \quad \boldsymbol{x}_{\mathrm{c}}^{\mathrm{T}}(k) \quad \boldsymbol{x}_{\mathrm{g}}^{\mathrm{T}}(k) \quad \hat{\hat{\boldsymbol{x}}}_{\mathrm{r}1}^{\mathrm{T}}(k) \quad \hat{\hat{\boldsymbol{x}}}_{\mathrm{r}2}^{\mathrm{T}}(k) \quad \cdots \quad \hat{\hat{\boldsymbol{x}}}_{\mathrm{r}q}^{\mathrm{T}}(k)\right]^{\mathrm{T}}, \tag{4}$$

and

$$\tilde{A}_0 = \begin{bmatrix} \tilde{A}_{\mathrm{p}} & -B_{\mathrm{p}}C_{\mathrm{c}} & K_{\mathrm{g}}C_{\mathrm{g}} & 0 & \cdots & 0 & 0 \\ B_{\mathrm{c}}C_{\mathrm{p}} & A_{\mathrm{c}} & 0 & 0 & \cdots & 0 & 0 \\ 0 & 0 & A_{\mathrm{g}} & 0 & \cdots & 0 & 0 \\ 0 & I & 0 & 0 & \cdots & 0 & 0 \\ 0 & 0 & 0 & \bar{I} & \cdots & 0 & 0 \\ \vdots & \vdots & \vdots & \vdots & \ddots & \vdots & \vdots \\ 0 & 0 & 0 & 0 & \cdots & \bar{I} & 0 \end{bmatrix} \text{ when } \boldsymbol{\theta}(k) = 0,$$

$$\tilde{A}_1 = \begin{bmatrix} \tilde{A}_p & 0 & K_g C_g & -B_p C_c & \cdots & 0 & 0 \\ 0 & 0 & 0 & 0 & \cdots & 0 & \bar{I} \\ 0 & 0 & A_g & 0 & \cdots & 0 & 0 \\ 0 & 0 & 0 & I & \cdots & 0 & 0 \\ \vdots & \vdots & \vdots & \vdots & \ddots & \vdots & \vdots \\ 0 & 0 & 0 & 0 & \cdots & \bar{I} & 0 \\ 0 & 0 & 0 & 0 & \cdots & 0 & \bar{I} \end{bmatrix} \quad \text{when } \boldsymbol{\theta}(k) = 1,$$

$$\tilde{G} = \begin{bmatrix} (K_g D_g)^T & 0 & B_g^T & 0 & \cdots & 0 \end{bmatrix}^T$$

$$\tilde{C} = \begin{bmatrix} C_p & 0 & \cdots & 0 \end{bmatrix}.$$

Here $\bar{I}$ is a modified identity matrix with diagonal entries set to zero if the corresponding states are not stored during checkpointing. When $\bar{I} \neq I$, the recovery scheme is called *partial state rollback*. In the RCS experiments conducted at LANSCE, only the elevator and the aileron commands were implemented with rollback capability. Therefore, only the control states associated with those commands were rollback enabled. A conceptual model of the partial state rollback system is shown in Fig. 9, where $\boldsymbol{y}_{c1}(k)$ is the control vector without rollback recovery; $\boldsymbol{y}_{c2}(k)$ is the elevator and the aileron commands without rollback recovery and $\boldsymbol{y}'_{c2}(k)$ is the corresponding vector with recovery.

II.2 PRACTICAL MODELING CONSIDERATIONS AND ASSUMPTIONS

The modeling approach presented in the previous section is useful for understanding how the system works *logically*. For a simple system, such as the simplified

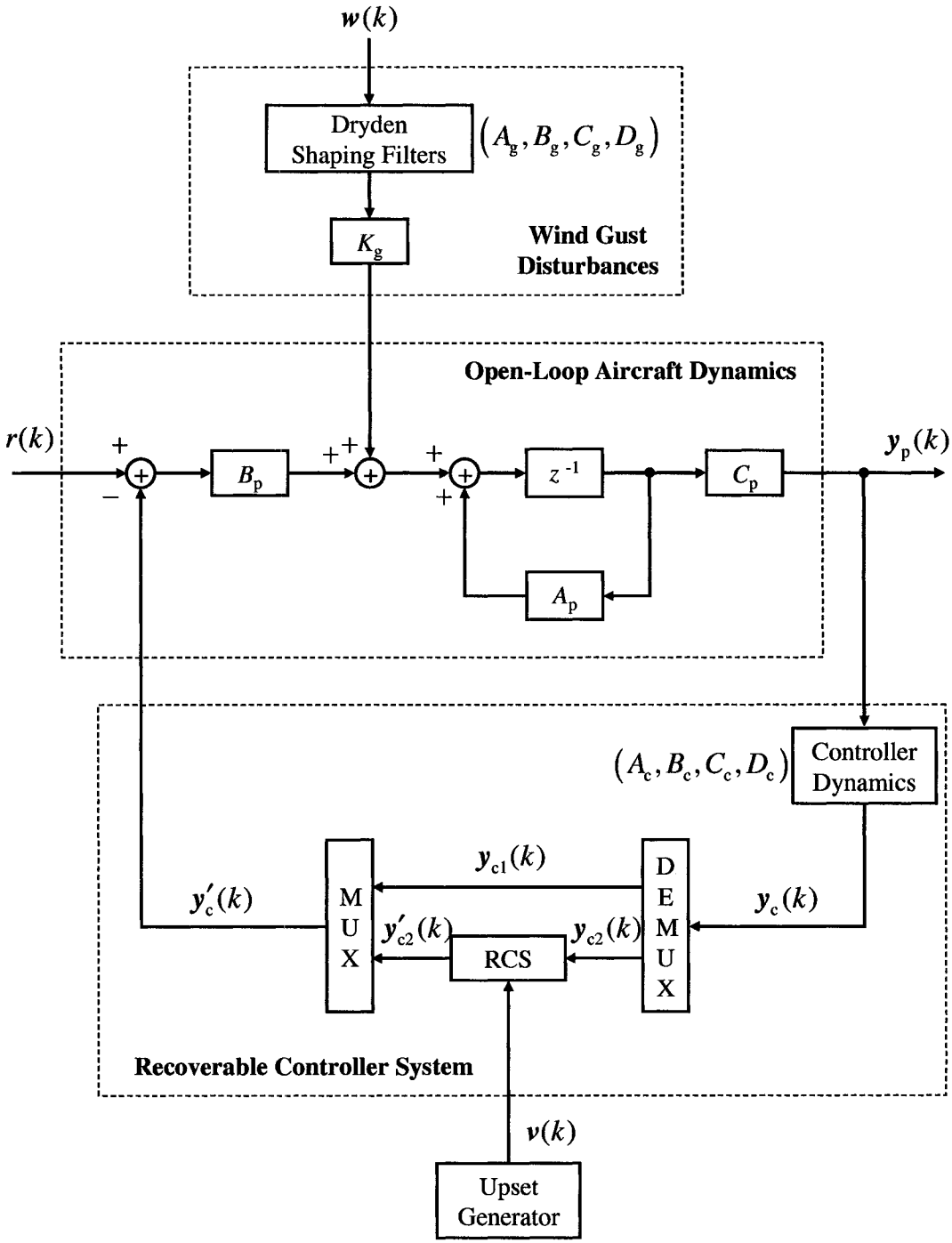

Fig. 9. A conceptual closed-loop model of the recoverable aircraft system.

longitudinal dynamics of the F-16 discussed in [9, 16], it can be fully realized to obtain a very accurate model. For example, the actual freezing of the control signals, the rolling back of the control data, the logic of the recovery process, and the delay introduced into the feedback loop were all considered in [9, 16]. However, there were significant difficulties in applying this method to the Boeing 737 flight system:

1. It is difficult to obtain the state space model (A_c, B_c, C_c, D_c), since the control system employed in the Boeing 737 Simulink model is highly complex and nonlinear. For example, there are many mode switches that can be activated by even light winds and gusts. Thus, as to be described in Section II.3, a model identification procedure was employed to characterize the closed-loop system.

2. The dimension of the recoverable control system presented in Subsection II.1.3 is too large to conduct the stability and performance analyses in the subsequent chapters. In the Boeing 737 Simulink model, the open-loop aircraft model is a ten-dimensional system. Suppose the controller system is modeled as an n_c-dimensional system. From (3), the Dryden wind gust filters can be modeled as a five-dimensional system. Then according to (4), the dimension of the state vector, $\tilde{\boldsymbol{x}}(k)$, of the recoverable flight system is $10 + 5 + n_c(q + 1)$. As will be shown in Chapters III and IV, to determine the stability and output performance of the system, one needs to calculate the spectral radius of a nonsymmetric matrix $\mathscr{A}_2$ (formally defined on page 58) and the inverse of a nonsymmetric matrix $I - \mathscr{A}_2$, each having dimension $2\big(10 + 5 + n_c(q + 1)\big)^2$. Let, for example, $n_c = 10$ and $q = 6$, then the dimension of $\mathscr{A}_2$ is 14,450, which is presently too large to reliably calculate its spectral radius and the inverse of

$I - \mathscr{A}_2$.

3. In Chapter V, it will be shown that the experimental data suggest that the delay parameter, q, described in Subsection II.1.3 should be modeled as a stochastic process, $\boldsymbol{q}(k)$. This gives rise to different models whose dimension is a function of time. Thus, a nontrivial revision of the existing theory would be required.

In addition to the issues above, the experimental data suggested that certain approximations be made. Consider, for example, the data[1] shown in Fig. 10. Observe:

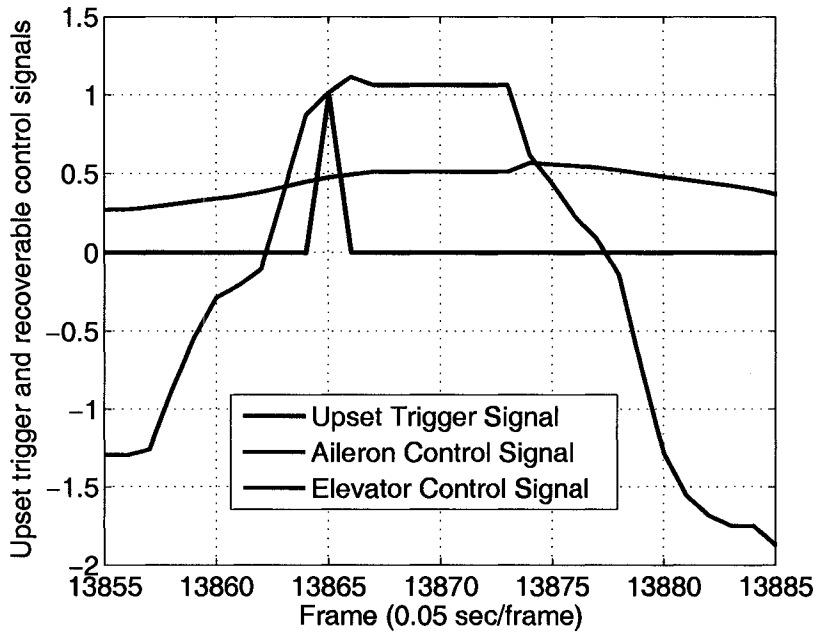

Fig. 10. The applied control signals (aileron and elevator) in response to an upset detected at Frame 13,865.

1. Fig. 10 shows the applied aileron and elevator control signals in response to an upset signal. The upset triggers a request for a rollback at Frame 13,865. After a two frame delay, i.e., at Frame 13,867, both the aileron and the elevator start

[1]This experimental data comes from file `RCS_preiid1_3.mat` (see Table XI in Appendix B.2). More details about the experiments will be presented in Chapter V.

reacting to the upset signal. Both control signals are frozen by the RCS, so their values are constants during the period from Frame 13,867 to Frame 13,873, which will be referred as the *recovery period.* The two frame delay is not modeled as it does not affect closed-loop performance. But internally, the rollback process has already been initiated within the RCS.

2. The RCS must freeze the aileron and the elevator control signals during a portion of the rollback process. In Fig. 10, the recovery period is six frames. This is typical, but in practice, the recovery period is a random variable. Thus, the closed-loop model needs to describe this type of behavior in some manner.

3. In practice, after a recovery process is finished, the states of the controller will be reinitialized to the values store at the previous check point. In this case, at Frame 13,874, the states of the aileron and the elevator were set to their previously stored values. The RCS then tried to restart the calculation from this point. This reinitialization and retry process was ignored in subsequent modeling because it is specifically the source for the large increase in the dimensionality of the model. Only the control signal delay due to rollback recoveries was explicitly modeled.

Other experiments showed that if several upset signals occurred consecutively, only the first one would have the potential to trigger a rollback recovery process. For example, the single upset signal occurring at Frame 2 in Fig. 11(a) has precisely the same effect on the RCS's rollback recovery mechanism as the three consecutive upset signals occurring at Frames 2–4 in Fig. 11(b). Therefore, in Fig. 11(b), when modeling the upset signal process, it is of no consequence to consider only the first upset and to

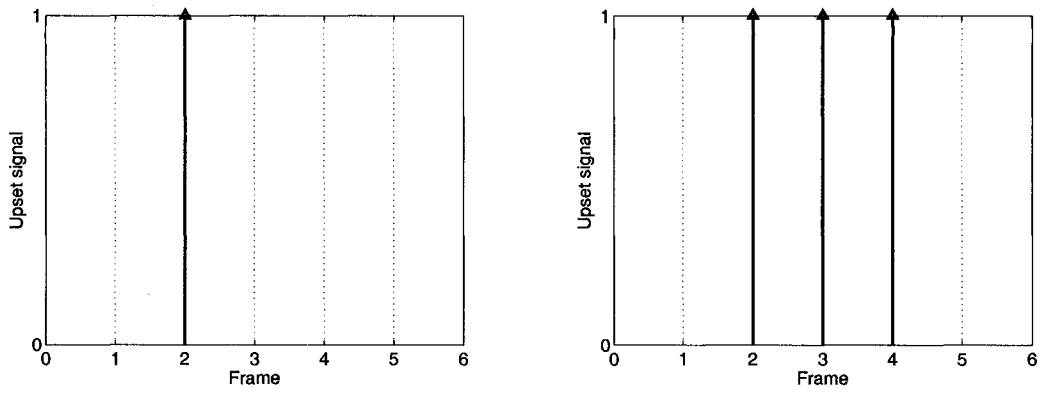

(a) One single upset signal. (b) Three consecutive upset signals.

Fig. 11. Two types of upset signals have the same effect on the RCS's rollback recovery mechanism.

ignore the other two. This observation will significantly simplify the determination of the probability transition matrix when the upset process is modeled as a first-order Markov chain (see Subsection III.3.1 for details). Of course if the upset probability is very small to begin with, then the probability of two or more consecutive upsets is very small. For example, in the RCS experiments, the probability of two or more consecutive upsets is smaller than 4×10^{-3}. In this case, the upset process can also be approximately modeled as a zeroth-order Markov chain, i.e., an i.i.d. process (see Subsection III.3.2 for details).

With these assumptions in place, the closed-loop flight control system and the recovery process of the RCS can in some sense be modeled separately. The following sections describe precisely how these approximations were utilized to produce the primary mathematical model for the recoverable aircraft system.

II.3 IDENTIFYING LINEAR MODELS FOR THE CLOSED-LOOP AIRCRAFT DYNAMICS

In light of the modeling approximations introduced in the previous section, two state space models for the Boeing 737 in closed-loop with an RCS in level flight were identified: one for the nominal mode $\Sigma_{\rm n} : (A_{\rm n}, G_{\rm n}, C_{\rm n})$ (i.e., the dynamics outside a recovery period) and one for the recovery mode $\Sigma_{\rm r} : (A_{\rm r}, G_{\rm r}, C_{\rm r})$ (i.e., the dynamics during a recovery period). Input–output data was collected for model identification using the nonlinear Boeing 737 Simulink model described in [70]. With the reference input set to zero, the only nonzero inputs in this case were the noise signals, which were used in the Simulink code to drive the Dryden wind gusts model. The output signals were taken to be the altitude of the aircraft, the calibrated airspeed, and the track angle. The model for the nominal mode was identified without any modification of the closed-loop structure of the Simulink model. However, the recovery mode was identified using the following modification: both the aileron and the elevator control signals were frozen, i.e., kept as constants after being initialized. The function `pem` from MATLAB's System Identification Toolbox was used for identifying the state space models. Seventeen sample input functions of 2,000 samples (0.05 sec/sample) each were used for building the nominal model, and another 35 sample input functions were used to validate it. The identified model for the nominal mode, $\Sigma_{\rm n}$, was an eight-dimensional system. Assuming the system operates in the recovery mode for a short period of time, a sample length of 200 samples per sample input function was used for building the recovery model. A total of 190 sample input functions were used for identification and another 35 sample input functions were used for validation.

The identified model for the recovery mode Σ_r was six-dimensional. Tables I and II summarize the system identification parameters and model validation results. The identified models are given in Appendix A.1.

TABLE I
System Identification Parameters

Inputs	Forward, side and down components of the wind
Outputs	Altitude, calibrated airspeed, and track angle
Sample period	0.05 second
Identification algorithm	`m = pem(data,'best')`

TABLE II
Modeling and Model Validation Data

	Nominal mode	Recovery mode
Data length (in samples)	2000	200
Data sets for modeling	17	190
Data sets for validation	35	35
Model dimension	8	6

Switching between Σ_n and Σ_r is only possible if their respective state spaces coordinate systems are the same. But here not even their dimensions are equivalent. To remedy the situation, Σ_r was embedded into an eight-dimensional system in such a way that the new system, $\tilde{\Sigma}_r$, had the same *controllability indices* as Σ_n, specifically, $\{3, 3, 2\}$. Therefore, each system can be transformed to the same Brunovsky

form [22], and the switching can be done (formally) by simply switching the state-space gain matrices, $\tilde{K}_{\mathrm{n}}$ and $\tilde{K}_{\mathrm{r}}$, and the input transformation matrices, $\tilde{L}_{\mathrm{n}}$ and $\tilde{L}_{\mathrm{r}}$. Specifically, Fig. 12 shows how the Brunovsky canonical form acts as a "bridge" be-

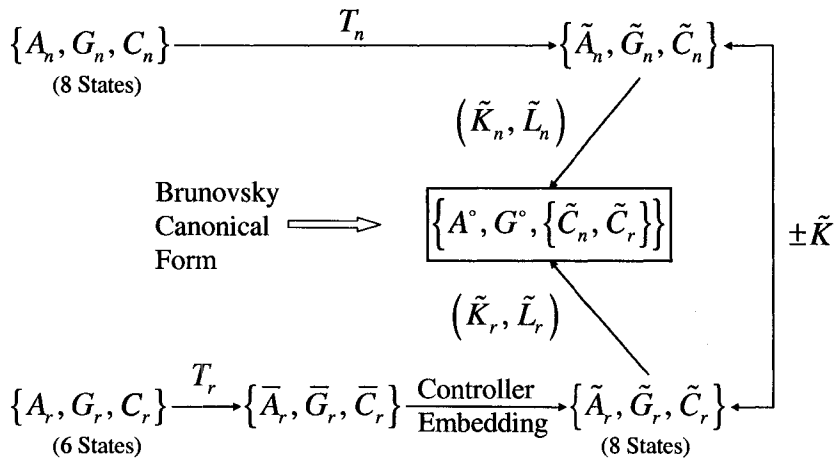

Fig. 12. The Brunovsky canonical form acts as a "bridge" between the state space models for the two system models, Σ_{n} and Σ_{r}.

tween the controller canonical forms of the two modes. Here Σ_{n} was transformed into its controller canonical form $\bar{\Sigma}_{\mathrm{n}}$ by T_{n}. Likewise, Σ_{r} was transformed into its controller canonical form $\bar{\Sigma}_{\mathrm{r}}$ by T_{r}. Then two stable states were added to $\bar{\Sigma}_{\mathrm{r}}$ to produce an eight-dimensional system $\tilde{\Sigma}_{\mathrm{r}}$. Now $\tilde{\Sigma}_{\mathrm{n}}$ and $\tilde{\Sigma}_{\mathrm{r}}$ can be transformed to the same Brunovsky canonical form (A°, G°) by $\left(\tilde{K}_{\mathrm{n}}, \tilde{L}_{\mathrm{n}}\right)$ and $\left(\tilde{K}_{\mathrm{r}}, \tilde{L}_{\mathrm{r}}\right)$, respectively, where $A^\circ = \tilde{A}_{\mathrm{n}} - \tilde{G}_{\mathrm{n}}\tilde{L}_{\mathrm{n}}\tilde{K}_{\mathrm{n}} = \tilde{A}_{\mathrm{r}} - \tilde{G}_{\mathrm{r}}\tilde{L}_{\mathrm{r}}\tilde{K}_{\mathrm{r}}$ and $G^\circ = \tilde{G}_{\mathrm{n}}\tilde{L}_{\mathrm{n}} = \tilde{G}_{\mathrm{r}}\tilde{L}_{\mathrm{r}}$. The switching between $\tilde{\Sigma}_{\mathrm{n}}$ and $\tilde{\Sigma}_{\mathrm{r}}$ can be done using $\tilde{K} := \tilde{K}_{\mathrm{n}} - \tilde{K}_{\mathrm{r}}$, $\tilde{L}_{\mathrm{n}}$ and $\tilde{L}_{\mathrm{r}}$, since $\tilde{A}_{\mathrm{n}} = \tilde{A}_{\mathrm{r}} + G^\circ\tilde{K}$ and $\tilde{G}_{\mathrm{n}} = \tilde{G}_{\mathrm{r}}\tilde{L}_{\mathrm{r}}\tilde{L}_{\mathrm{n}}^{-1}$. The linear models for switching are given in Appendix A.2.

II.4 MODELING THE RECOVERY PROCESSES OF THE RCS USING AN SFSA

As discussed in Section II.2, a simplified approach to modeling a rollback recovery process of the RCS is to only consider its rollback recovery period. Experiments, which will be presented in more detail in Chapter V, showed that approximately 80% of the recovery periods of the RCS were six frames in length and 20% were five frames. Any upset for a recovery during an active recovery process was ignored. This information was encoded into an FSM by assuming that all the recovery periods were six frames. For better accuracy, an SFSA was also designed to match the recovery length probability distribution. Some basic concepts of an SFSA/FSM and its application to modeling the rollback recovery of an RCS are discussed next.

II.4.1 Definition of an SFSA

In [71], a stochastic automaton is defined in a purely probabilistic setting. In [72, 73], it is defined in terms of graph theory. In this dissertation, an SFSA is defined from the viewpoint of systems theory, which means that it has a finite number of internal states, and receives input symbols and generates output symbols. From this perspective, an SFSA is defined as follows [59, 74–76].

Definition II.1 (SFSA). Let $(\Omega, \mathbb{F}, \Pr)$ represent the ambient probability space. A *stochastic finite-state automaton*, $\mathfrak{A}$, is a six-tuple, $(\Sigma_{\mathrm{I}}, \Sigma_{\mathrm{S}}, \Sigma_{\mathrm{O}}, [0,1], f, g)$, where $\Sigma_{\mathrm{I}} = \{\eta_1, \eta_2, \ldots, \eta_M\}$ is the set of input symbols; $\Sigma_{\mathrm{S}} = \{\zeta_1, \zeta_2, \ldots, \zeta_N\}$ denotes the set of internal states; and $\Sigma_{\mathrm{O}} = \{\xi_1, \xi_2, \ldots, \xi_P\}$ is the set of output symbols. Let $\boldsymbol{\nu}(k)$, $\boldsymbol{z}(k)$, and $\boldsymbol{\theta}(k)$ denote the input random process, the state process, and the output

process of the automaton, respectively, where $k \in \mathbb{Z}^+$. f describes the dynamics of the state transition probabilities:

$$f : (\Sigma_S, \Sigma_I, \Sigma_S) \to [0,1]$$
$$(\zeta_j, \eta_l, \zeta_i) \mapsto \Pr\left\{\boldsymbol{z}(k+1) = \zeta_j \mid \left(\boldsymbol{\nu}(k) = \eta_l, \boldsymbol{z}(k) = \zeta_i\right)\right\} := [\Pi^{\eta_l}]_{\zeta_i\zeta_j},$$

where $[\Pi^{\eta_l}]_{\zeta_i\zeta_j}$ is the $\zeta_i\zeta_j$-th component of the state transition matrix Π^{η_l} for the input symbol η_l. For fixed $i \in \{1,2,\ldots,N\}$ and $l \in \{1,2,\ldots,M\}$, $\sum_{j=1}^{N} [\Pi^{\eta_l}]_{\zeta_i\zeta_j} = 1$. It is assumed that the state transition probabilities at time i depend *solely* on the input symbol at that instant. That is, given the input sequence $\{\boldsymbol{\nu}(k) = \nu(k), \boldsymbol{\nu}(k-1) = \nu(k-1), \ldots, \boldsymbol{\nu}(0) = \nu(0)\}$ and initial condition $\{\boldsymbol{z}(0) = z(0)\}$, the following identity holds:

$$\begin{aligned}&\Pr\{\boldsymbol{z}(k) = z(k), \boldsymbol{z}(k-1) = z(k-1), \ldots, \boldsymbol{z}(1) = z(1) \mid \\ &\qquad \boldsymbol{\nu}(k) = \nu(k), \boldsymbol{\nu}(k-1) = \nu(k-1), \ldots, \boldsymbol{\nu}(0) = \nu(0), \boldsymbol{z}(0) = z(0)\} \\ &= \prod_{i=0}^{k-1} [\Pi^{\nu(i)}]_{z(i)z(i+1)}.\end{aligned}$$

The output relation g is described by

$$g : (\Sigma_O, \Sigma_I, \Sigma_S) \to [0,1]$$
$$(\xi_t, \eta_r, \zeta_s) \mapsto \Pr\left\{\boldsymbol{\theta}(k) = \xi_t \mid \left(\boldsymbol{\nu}(k) = \eta_r, \boldsymbol{z}(k) = \zeta_s\right)\right\} := [\Phi^{\eta_r}]_{\zeta_s\xi_t},$$

where for given $s \in \{1,2,\ldots,N\}$ and $r \in \{1,2,\ldots,M\}$, $0 \le \sum_{t=1}^{P} [\Phi^{\eta_r}]_{\zeta_s\xi_t} \le 1$.

Definition II.2 (FSM). Given an SFSA, if both $[\Pi^{\eta_l}]_{\zeta_i\zeta_j}$ and $[\Phi^{\eta_r}]_{\zeta_s\xi_t}$ only assume values 0 or 1 for all $\eta_l, \eta_r \in \Sigma_I$, $\zeta_i, \zeta_j, \zeta_s \in \Sigma_S$ and $\xi_t \in \Sigma_O$, then the automaton is called a *finite-state machine*, and is denoted by the six-tuple $\mathfrak{M} = (\Sigma_I, \Sigma_S, \Sigma_O, \{0,1\}, f, g)$.

Therefore, an FSM is simply a special case of an SFSA with transition probabilities only taking the value 0 or 1. In the current application, it is always assumed that the output is *isomorphic* to the state of an SFSA with probability one, that is, $P \equiv N$ and $g(\xi_t, \eta_r, \zeta_s) = \mathbf{1}_{\{s=t\}}$ for all input symbols $\eta_r \in \Sigma_{\mathrm{I}}$, where $\mathbf{1}_{\{s=t\}}$ is the Dirac measure.

II.4.2 Modeling the Recovery Processes Using an SFSA

The five or six-frame recovery period of the RCS can be modeled by either an FSM $\mathfrak{M} = (\Sigma_{\mathrm{I}}, \Sigma_{\mathrm{S}}, \Sigma_{\mathrm{O}}, \{0,1\}, f, g)$ or an SFSA $\mathfrak{A} = (\Sigma_{\mathrm{I}}, \Sigma_{\mathrm{S}}, \Sigma_{\mathrm{O}}, [0,1], f, g)$. The corresponding FSM and SFSA are shown in Figs. 13 and 14, respectively. The input

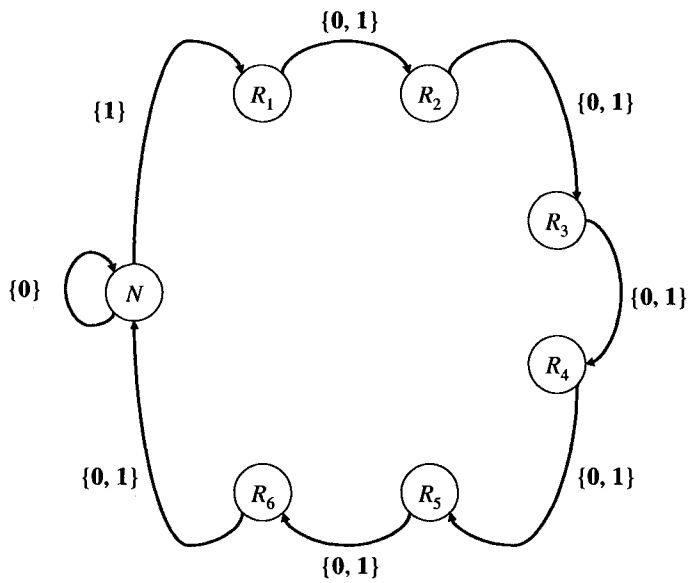

Fig. 13. The FSM used to model the rollback recovery process of the RCS.

process to the SFSA/FSM is a homogeneous, two-state, first-dimensional Markov chain. The probability transition matrix of the input Markov chain is Π_{I}. The set of states is $\Sigma_{\mathrm{I}} = \{0,1\}$, where "0" indicates that no upset was detected and "1" indicates that an upset was detected. The SFSA/FSM symbol sets are $\Sigma_{\mathrm{S}} =$

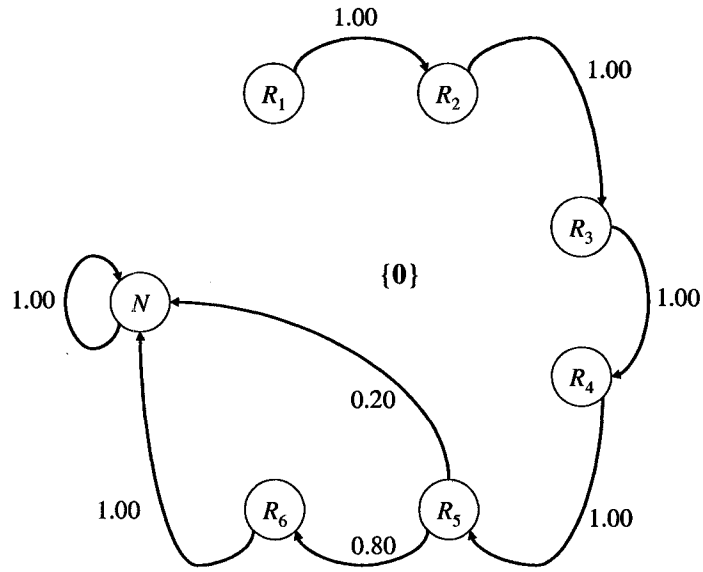

(a) The state transition diagram for input symbol "0", which specifies Π^0.

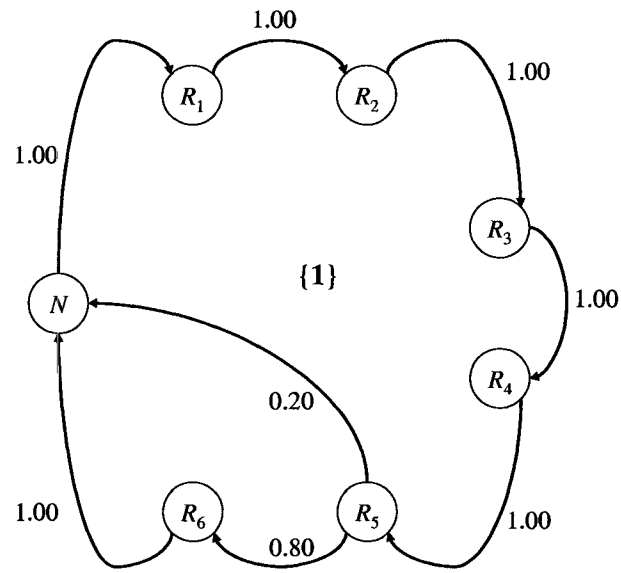

(b) The state transition diagram for input symbol "1", which specifies Π^1.

Fig. 14. The SFSA used to model the rollback recovery process of the RCS.

$\{\mathrm{N}, \mathrm{R}_1, \mathrm{R}_2, \ldots, \mathrm{R}_6\}$ and $\Sigma_O = \{\mathrm{n}, \mathrm{r}_1, \mathrm{r}_2, \ldots, \mathrm{r}_6\}$. f is described by Π^0 and Π^1, and g is a state-to-output isomorphism. The SFSA/FSM produces at its output the random signal $\boldsymbol{\theta}(k)$, which switches between the symbols "n" and "r_i", $i = 1, 2, \ldots, 6$ representing the "nominal" mode and the "recovery" modes, respectively.

When the SFSA/FSM is in the nominal state "N", and if the input symbol is "0", the SFSA/FSM will remain in the nominal state. Otherwise, it will transit to the recovery mode "R_1". If it is in one of its recovery states, "R_i" (for $i = 1, 2, \ldots, 6$), then the input is ignored, and the state will transit to the next state "R_{i+1}" for $i = 1, 2, \ldots, 4$. When the current state is "R_5", for the SFSA, then 20% of the next-step transitions go to "N" and 80% go to "R_6". For the FSM, the state "R_5" will always transit to "R_6". The state will transit without exception back to its nominal state "N" when $i = 6$ for both the SFSA and the FSM. The state transition matrices for the SFSA and the FSM are given in Appendix A.3.

II.5 STOCHASTIC HYBRID MODELS FOR THE RECOVERABLE CLOSED-LOOP SYSTEM

The main class of stochastic hybrid models used in this dissertation to model an aircraft in closed-loop with an RCS is shown in Fig. 3 (page 5). It consists of a jump-linear system driven by an SFSA with a Markov input process. Electromagnetic radiation induced upsets (see [8]) and the neutron-induced upsets [17, 18] can be modeled as a two-state rth-order Markov chain with either $r = 0, 1$. The SFSA models the rollback recovery process. The switched system models the dynamics of the closed-loop due to the presence of controller recoveries with the nominal mode

Σ_{n} and the recovery modes $\{\Sigma_{\mathrm{r}_i} = \Sigma_{\mathrm{r}}, i = 1, 2, \ldots, 6\}$. If the switching process $\boldsymbol{\theta}(k)$ is a Markov chain, then the system's mean-square stability and output performance can be analyzed using existing methods (for example, see [20,21]). However, in most cases, the output process of an SFSA is not Markovian. Therefore, the goal of this section is to describe a related process which is Markov. This is a generalization of the results given in [19, 64, 65]. In Subsection II.5.1, it is shown that in general, if the input process of an SFSA is a Markov chain, then its input–output cross product process is also a Markov chain. This result is then used in Subsection II.5.2 to construct a model-equivalent Markov jump-linear system for the stochastic hybrid model.

II.5.1 Markov Characterization of the Input and Output Processes of an SFSA

This subsection presents a main theorem which describes the Markov characteristics of an input–output *cross product* process generated by an SFSA with a Markov input. The special case for FSM's appears in [19, 64] and the references therein. A similar idea (without proof) also appears in [77] for random dynamical systems with jumps. A more general result was proved in [78] using only measure theoretical tools. The related Feller-Markov property is proved in [79] for continuous-time stochastic systems. The following three lemmas (Lemmas II.3, II.4 and II.5) are useful tools for proving the main theorem (Theorem II.6 on page 46).

Lemma II.3. *For an SFSA* $\mathfrak{A} = (\Sigma_{\mathrm{I}}, \Sigma_{\mathrm{S}}, \Sigma_{\mathrm{O}}, [0,1], f, g)$*, given integers* k *and* q *with*

$k > q$, the probability of a random event $\{\nu(k), \nu(k-1), \ldots, \nu(k-q), z(k-q)\}$ is

$$\begin{aligned}
&\Pr\{\nu(k), \nu(k-1), \ldots, \nu(k-q), z(k-q)\} \\
&= \sum_{\substack{\nu(k-q-1)\in\Sigma_{\mathrm{I}} \\ z(k-q-1)\in\Sigma_{\mathrm{S}}}} \left[\Pi^{\nu(k-q-1)}\right]_{z(k-q-1)z(k-q)} \cdot \\
&\qquad \Pr\{\nu(k), \nu(k-1), \ldots, \nu(k-q-1), z(k-q-1)\}.
\end{aligned} \tag{5}$$

Proof. For any $k \in \mathbb{Z}^+$, let, for example, $\{\nu(k)\}$ represent the event $\{\boldsymbol{\nu}(k) = \nu(k)\}$ and $\{(\nu(k), z(k))\}$ represent the event $\{(\boldsymbol{\nu}(k), \boldsymbol{z}(k)) = (\nu(k), z(k))\}$. For a random event $\{\nu(k), \nu(k-1), \ldots, \nu(k-q), z(k-q)\}$, observe that the following equality holds:

$$\begin{aligned}
&\{\nu(k), \nu(k-1), \ldots, \nu(k-q), z(k-q)\} \\
&= \bigcup_{\substack{\nu(k-q-1)\in\Sigma_{\mathrm{I}} \\ z(k-q-1)\in\Sigma_{\mathrm{S}}}} \{\nu(k), \nu(k-1), \ldots, \nu(k-q), \nu(k-q-1), z(k-q), z(k-q-1)\}.
\end{aligned}$$

Furthermore, the set of events

$$\left\{\{\nu(k), \nu(k-1), \ldots, \nu(k-q), \nu(k-q-1), z(k-q), z(k-q-1)\}\right\}_{\substack{\nu(k-q-1)\in\Sigma_{\mathrm{I}} \\ z(k-q-1)\in\Sigma_{\mathrm{S}}}}$$

is mutually exclusive. Therefore,

$$\begin{aligned}
&\Pr\{\nu(k), \nu(k-1), \ldots, \nu(k-q), z(k-q)\} \\
&= \sum_{\substack{\nu(k-q-1)\in\Sigma_{\mathrm{I}} \\ z(k-q-1)\in\Sigma_{\mathrm{S}}}} \Pr\{\nu(k), \nu(k-1), \ldots, \nu(k-q), \nu(k-q-1), z(k-q), z(k-q-1)\} \\
&= \sum_{\substack{\nu(k-q-1)\in\Sigma_{\mathrm{I}} \\ z(k-q-1)\in\Sigma_{\mathrm{S}}}} \left[\Pi^{\nu(k-q-1)}\right]_{z(k-q-1)z(k-q)} \cdot \\
&\qquad \Pr\{\nu(k), \nu(k-1), \ldots, \nu(k-q-1), z(k-q-1)\}.
\end{aligned}$$

The proof is complete. □

Lemma II.4. *For an SFSA* $\mathfrak{A} = (\Sigma_{\mathrm{I}}, \Sigma_{\mathrm{S}}, \Sigma_{\mathrm{O}}, [0,1], f, g)$, *given integers* k *and* q *with* $k > q$, *the probability of a random event* $\{\nu(k), \nu(k-1), \ldots, \nu(k-q), z(k-q)\}$ *is*

$$\begin{aligned}
&\Pr\{\nu(k), \nu(k-1), \ldots, \nu(k-q), z(k-q)\} \\
&= \sum_{\substack{\nu(0),\ldots,\nu(k-q-1)\in\Sigma_{\mathrm{I}} \\ z(0),\ldots,z(k-q-1)\in\Sigma_{\mathrm{S}}}} \prod_{i=1}^{k-q} \left[\Pi^{\nu(k-q-i)}\right]_{z(k-q-i)z(k-q-i+1)} \Pr\{\nu(k), \nu(k-1), \ldots, \nu(0), z(0)\}.
\end{aligned} \tag{6}$$

Proof. The identity is verified by applying Lemma II.3 repeatively $k-q$ times. For example, using it once, (5) can be obtained. If $k-q-1 \geq 1$, then

$$\begin{aligned}
&\Pr\{\nu(k), \nu(k-1), \ldots, \nu(k-q-1), z(k-q-1)\} \\
&= \sum_{\substack{\nu(k-q-2)\in\Sigma_{\mathrm{I}} \\ z(k-q-2)\in\Sigma_{\mathrm{S}}}} \left[\Pi^{\nu(k-q-2)}\right]_{z(k-q-2)z(k-q-1)} \cdot \\
&\qquad \Pr\{\nu(k), \nu(k-1), \ldots, \nu(k-q-2), z(k-q-2)\}.
\end{aligned}$$

Thus,

$$\begin{aligned}
&\Pr\{\nu(k), \nu(k-1), \ldots, \nu(k-q), z(k-q)\} \\
&= \sum_{\substack{\nu(k-q-1)\in\Sigma_{\mathrm{I}} \\ z(k-q-1)\in\Sigma_{\mathrm{S}}}} \Pr\{\nu(k), \nu(k-1), \ldots, \nu(k-q), \nu(k-q-1), z(k-q), z(k-q-1)\} \\
&= \sum_{\substack{\nu(k-q-1)\in\Sigma_{\mathrm{I}} \\ z(k-q-1)\in\Sigma_{\mathrm{S}}}} \left[\Pi^{\nu(k-q-1)}\right]_{z(k-q-1)z(k-q)} \cdot \\
&\qquad \Pr\{\nu(k), \nu(k-1), \ldots, \nu(k-q-1), z(k-q-1)\}, \\
&= \sum_{\substack{\nu(k-q-1)\in\Sigma_{\mathrm{I}} \\ z(k-q-1)\in\Sigma_{\mathrm{S}}}} \left[\Pi^{\nu(k-q-1)}\right]_{z(k-q-1)z(k-q)} \sum_{\substack{\nu(k-q-2)\in\Sigma_{\mathrm{I}} \\ z(k-q-2)\in\Sigma_{\mathrm{S}}}} \left[\Pi^{\nu(k-q-2)}\right]_{z(k-q-2)z(k-q-1)} \cdot \\
&\qquad \Pr\{\nu(k), \nu(k-1), \ldots, \nu(k-q-2), z(k-q-2)\} \\
&= \sum_{\substack{\nu(k-q-1)\in\Sigma_{\mathrm{I}} \\ z(k-q-1)\in\Sigma_{\mathrm{S}}}} \sum_{\substack{\nu(k-q-2)\in\Sigma_{\mathrm{I}} \\ z(k-q-2)\in\Sigma_{\mathrm{S}}}} \left[\Pi^{\nu(k-q-1)}\right]_{z(k-q-1)z(k-q)} \left[\Pi^{\nu(k-q-2)}\right]_{z(k-q-2)z(k-q-1)} \cdot
\end{aligned}$$

$$\Pr\{\nu(k), \nu(k-1), \ldots, \nu(k-q-2), z(k-q-2)\}$$

$$= \sum_{\substack{\nu(k-q-1),\nu(k-q-2)\in\Sigma_{\mathrm{I}} \\ z(k-q-1),z(k-q-2)\in\Sigma_{\mathrm{S}}}} \prod_{i=1}^{2} \left[\Pi^{\nu(k-q-i)}\right]_{z(k-q-i)z(k-q-i+1)} \cdot$$

$$\Pr\{\nu(k), \ldots, \nu(k-q-2), z(k-q-2)\}.$$

Doing this recursively for a total of $k-q$ times produces (6). □

Lemma II.5. *For an SFSA* $\mathfrak{A} = (\Sigma_{\mathrm{I}}, \Sigma_{\mathrm{S}}, \Sigma_{\mathrm{O}}, [0,1], f, g)$, *given integers* k *and* r *with* $k \geq r$, *if* $\boldsymbol{\nu}$ *is an* r*th-order Markov chain and independent of* $\boldsymbol{z}(0)$, *it follows that*

$$\Pr\{\nu(k) \mid \nu(k-1), \ldots, \nu(k-r), z(k-r)\} = \Pr\{\nu(k) \mid \nu(k-1), \ldots, \nu(k-r)\}.$$

Proof. From the assumptions,

$$\begin{aligned}
&\Pr\{\nu(k), \nu(k-1), \ldots, \nu(0), z(0)\} \\
&\quad = \Pr\{\nu(k) \mid \nu(k-1), \ldots, \nu(0), z(0)\} \Pr\{\nu(k-1), \ldots, \nu(0), z(0)\} \\
&\quad = \Pr\{\nu(k) \mid \nu(k-1), \ldots, \nu(0)\} \Pr\{\nu(k-1), \ldots, \nu(0), z(0)\} \\
&\quad = \Pr\{\nu(k) \mid \nu(k-1), \ldots, \nu(k-r)\} \Pr\{\nu(k-1), \ldots, \nu(0), z(0)\}.
\end{aligned}$$

When $k = r$, then

$$\begin{aligned}
&\Pr\{\nu(r), \nu(r-1), \ldots, \nu(0), z(0)\} \\
&\quad = \Pr\{\nu(r) \mid \nu(r-1), \ldots, \nu(0)\} \Pr\{\nu(r-1), \ldots, \nu(0), z(0)\},
\end{aligned}$$

and thus,

$$\Pr\{\nu(r) \mid \nu(r-1), \ldots, \nu(0), z(0)\} = \Pr\{\nu(r) \mid \nu(r-1), \ldots, \nu(0)\}.$$

When $k > r$, according to Lemma II.4,

$$\Pr\{\nu(k), \nu(k-1), \ldots, \nu(k-r), z(k-r)\}$$

$$= \sum_{\substack{\nu(0),\ldots,\nu(k-r-1)\in\Sigma_I \\ z(0),\ldots,z(k-r-1)\in\Sigma_S}} \prod_{i=1}^{k-r} [\Pi^{\nu(k-r-i)}]_{z(k-r-i)z(k-r-i+1)} \Pr\{\nu(k), \nu(k-1), \ldots, \nu(0), z(0)\}$$

$$= \sum_{\substack{\nu(0),\ldots,\nu(k-r-1)\in\Sigma_I \\ z(0),\ldots,z(k-r-1)\in\Sigma_S}} \prod_{i=1}^{k-r} [\Pi^{\nu(k-r-i)}]_{z(k-r-i)z(k-r-i+1)} \cdot$$

$$\Pr\{\nu(k) \mid \nu(k-1), \ldots, \nu(0), z(0)\} \Pr\{\nu(k-1), \ldots, \nu(0), z(0)\}$$

$$= \sum_{\substack{\nu(0),\ldots,\nu(k-r-1)\in\Sigma_I \\ z(0),\ldots,z(k-r-1)\in\Sigma_S}} \prod_{i=1}^{k-r} [\Pi^{\nu(k-r-i)}]_{z(k-r-i)z(k-r-i+1)} \cdot$$

$$\Pr\{\nu(k) \mid \nu(k-1), \ldots, \nu(k-r)\} \Pr\{\nu(k-1), \ldots, \nu(0), z(0)\}$$

$$= \Pr\{\nu(k) \mid \nu(k-1), \ldots, \nu(k-r)\} \cdot$$

$$\left\{ \sum_{\substack{\nu(0),\ldots,\nu(k-r-1)\in\Sigma_I \\ z(0),\ldots,z(k-r-1)\in\Sigma_S}} \prod_{i=1}^{k-r} [\Pi^{\nu(k-r-i)}]_{z(k-r-i)z(k-r-i+1)} \cdot \right.$$

$$\left. \Pr\{\nu(k-1), \nu(k-2), \ldots, \nu(0), z(0)\} \right\}$$

$$= \Pr\{\nu(k) \mid \nu(k-1), \ldots, \nu(k-r)\} \Pr\{\nu(k-1), \nu(k-2), \ldots, \nu(k-r), z(k-r)\}.$$

Therefore,

$$\Pr\{\nu(k) \mid \nu(k-1), \ldots, \nu(k-r), z(k-r)\} = \Pr\{\nu(k) \mid \nu(k-1), \ldots, \nu(k-r)\},$$

and the proof is complete. □

With these lemmas established, the following main theorem shows that, under certain conditions, the input–output cross product process of an SFSA is Markov

when its input process is Markov. Furthermore, its probability transition matrix can be calculated using the probability transition matrix of the input process and the state transition matrices of the SFSA.

Theorem II.6. *If the input process $\boldsymbol{\nu}(k)$ of an N-state SFSA, $\mathfrak{A}$, is an M-state Markov chain with probability transition matrix Π_{I}, which is independent of the initial state of the automaton, $\boldsymbol{z}(0)$, then the Cartesian product of the input and output processes of the SFSA, $\boldsymbol{\rho}(k) := \big(\boldsymbol{\nu}(k), \boldsymbol{\theta}(k)\big)$, is an MN-state Markov chain with state transition matrix*

$$\Pi_{\mathrm{I/O}} = \operatorname{diag}\left(\Pi^{\eta_1}, \Pi^{\eta_2}, \ldots, \Pi^{\eta_M}\right) \cdot \left(\Pi_{\mathrm{I}} \otimes I_N\right), \tag{7}$$

where $\otimes$ denotes the Kronecker product. (Here I_N denotes an $N \times N$ identity matrix.)

Proof. For any $k \in \mathbb{Z}^+$, consider an arbitrary event of the form

$$\mathscr{F}(k) := \left\{\big(\nu(k), z(k)\big), \big(\nu(k-1), z(k-1)\big), \ldots, \big(\nu(0), z(0)\big)\right\}.$$

When $k \geq 2$, from the assumptions that $\boldsymbol{\nu}$ is Markov and independent of $\boldsymbol{z}(0)$, it follows that

$$\begin{aligned}
&\Pr\{\mathscr{F}(k)\} \\
&\quad = \prod_{i=0}^{k-1} \left[\Pi^{\nu(i)}\right]_{z(i)z(i+1)} \Pr\{\nu(k), \nu(k-1), \ldots, \nu(0), z(0)\} \\
&\quad = \prod_{i=0}^{k-1} \left[\Pi^{\nu(i)}\right]_{z(i)z(i+1)} \Pr\{\nu(k) \mid \nu(k-1), \ldots, \nu(0)\} \Pr\{\nu(k-1), \ldots, \nu(0), z(0)\} \\
&\quad = \left[\Pi^{\nu(k-1)}\right]_{z(k-1)z(k)} \prod_{i=0}^{k-2} \left[\Pi^{\nu(i)}\right]_{z(i)z(i+1)} \Pr\{\nu(k) \mid \nu(k-1)\} \cdot \\
&\qquad \Pr\{\nu(k-1), \ldots, \nu(0), z(0)\}
\end{aligned}$$

$$= \left[\Pi^{\nu(k-1)}\right]_{z(k-1)z(k)} [\Pi_{\mathrm{I}}]_{\nu(k-1)\nu(k)} \prod_{i=0}^{k-2} \left[\Pi^{\nu(i)}\right]_{z(i)z(i+1)} \Pr\{\nu(k-1), \ldots, \nu(0), z(0)\}$$

$$= \left[\Pi^{\nu(k-1)}\right]_{z(k-1)z(k)} [\Pi_{\mathrm{I}}]_{\nu(k-1)\nu(k)} \Pr\{\mathscr{F}(k-1)\}.$$

Therefore,

$$\Pr\left\{\big(\nu(k), z(k)\big) \mid \mathscr{F}(k-1)\right\} = \left[\Pi^{\nu(k-1)}\right]_{z(k-1)z(k)} [\Pi_{\mathrm{I}}]_{\nu(k-1)\nu(k)}. \tag{8}$$

Applying Lemma II.5 (with $r = 1$) gives

$$\Pr\{\nu(k) \mid \nu(k-1), z(k-1)\} = \Pr\{\nu(k) \mid \nu(k-1)\}, \quad k \geq 1.$$

Thus,

$$\begin{aligned}
&\Pr\left\{\big(\nu(k), z(k)\big), \big(\nu(k-1), z(k-1)\big)\right\} \\
&\quad = \left[\Pi^{\nu(k-1)}\right]_{z(k-1)z(k)} \Pr\{\nu(k), \nu(k-1), z(k-1)\} \\
&\quad = \left[\Pi^{\nu(k-1)}\right]_{z(k-1)z(k)} \Pr\{\nu(k) \mid \nu(k-1), z(k-1)\} \Pr\{\nu(k-1), z(k-1)\} \\
&\quad = \left[\Pi^{\nu(k-1)}\right]_{z(k-1)z(k)} \Pr\{\nu(k) \mid \nu(k-1)\} \Pr\{\nu(k-1), z(k-1)\} \\
&\quad = \left[\Pi^{\nu(k-1)}\right]_{z(k-1)z(k)} [\Pi_{\mathrm{I}}]_{\nu(k-1)\nu(k)} \Pr\left\{\big(\nu(k-1), z(k-1)\big)\right\}.
\end{aligned}$$

Consequently,

$$\Pr\left\{\big(\nu(k), z(k)\big) \mid \big(\nu(k-1), z(k-1)\big)\right\} = \left[\Pi^{\nu(k-1)}\right]_{z(k-1)z(k)} [\Pi_{\mathrm{I}}]_{\nu(k-1)\nu(k)}. \tag{9}$$

Comparing (8) and (9), it is clear that

$$\Pr\left\{\big(\nu(k), z(k)\big) \mid \mathscr{F}(k-1)\right\} = \Pr\left\{\big(\nu(k), z(k)\big) \mid \big(\nu(k-1), z(k-1)\big)\right\},$$

which implies that the input–state cross product process $(\boldsymbol{\nu}, \boldsymbol{z})$ is Markov. From the assumption that the output process is isomorphic to the state process of the

SFSA with probability one, it is immediate that $\boldsymbol{\rho} = (\boldsymbol{\nu}, \boldsymbol{\theta})$ is also Markov with the transition probability

$$\Pr\left\{\left(\boldsymbol{\nu}(k) = \eta_t, \boldsymbol{\theta}(k) = \xi_j\right) \mid \left(\boldsymbol{\nu}(k-1) = \eta_s, \boldsymbol{\theta}(k-1) = \xi_i\right)\right\} = [\Pi_{\mathrm{I}}]_{\eta_s\eta_t} [\Pi^{\eta_s}]_{\xi_i\xi_j} .$$

The matrix of transition probabilities $[\Pi_{\mathrm{I}}]_{\eta_s\eta_t} [\Pi^{\eta_s}]_{\xi_i\xi_j}$ for $i, j = 1, 2, \ldots, N$ and $s, t = 1, 2, \ldots, M$ is

$$\Pi_{\mathrm{I/O}} = \begin{bmatrix} [\Pi_{\mathrm{I}}]_{\eta_1\eta_1} [\Pi^{\eta_1}]_{\xi_1\xi_1} & \cdots & [\Pi_{\mathrm{I}}]_{\eta_1\eta_1} [\Pi^{\eta_1}]_{\xi_1\xi_N} & \cdots \\ \vdots & & \vdots & \\ [\Pi_{\mathrm{I}}]_{\eta_1\eta_1} [\Pi^{\eta_1}]_{\xi_N\xi_1} & \cdots & [\Pi_{\mathrm{I}}]_{\eta_1\eta_1} [\Pi^{\eta_1}]_{\xi_N\xi_N} & \cdots \\ \vdots & & \vdots & \\ [\Pi_{\mathrm{I}}]_{\eta_M\eta_1} [\Pi^{\eta_M}]_{\xi_1\xi_1} & \cdots & [\Pi_{\mathrm{I}}]_{\eta_M\eta_1} [\Pi^{\eta_M}]_{\xi_1\xi_N} & \cdots \\ \vdots & & \vdots & \\ [\Pi_{\mathrm{I}}]_{\eta_M\eta_1} [\Pi^{\eta_M}]_{\xi_N\xi_1} & \cdots & [\Pi_{\mathrm{I}}]_{\eta_M\eta_1} [\Pi^{\eta_M}]_{\xi_N\xi_N} & \cdots \end{bmatrix}$$

$$\begin{bmatrix} [\Pi_{\mathrm{I}}]_{\eta_1\eta_M} [\Pi^{\eta_1}]_{\xi_1\xi_1} & \cdots & [\Pi_{\mathrm{I}}]_{\eta_1\eta_M} [\Pi^{\eta_1}]_{\xi_1\xi_N} \\ \vdots & & \vdots \\ [\Pi_{\mathrm{I}}]_{\eta_1\eta_M} [\Pi^{\eta_1}]_{\xi_N\xi_1} & \cdots & [\Pi_{\mathrm{I}}]_{\eta_1\eta_M} [\Pi^{\eta_1}]_{\xi_N\xi_N} \\ \vdots & & \vdots \\ [\Pi_{\mathrm{I}}]_{\eta_M\eta_M} [\Pi^{\eta_M}]_{\xi_1\xi_1} & \cdots & [\Pi_{\mathrm{I}}]_{\eta_M\eta_M} [\Pi^{\eta_M}]_{\xi_1\xi_N} \\ \vdots & & \vdots \\ [\Pi_{\mathrm{I}}]_{\eta_M\eta_M} [\Pi^{\eta_M}]_{\xi_N\xi_1} & \cdots & [\Pi_{\mathrm{I}}]_{\eta_M\eta_M} [\Pi^{\eta_M}]_{\xi_N\xi_N} \end{bmatrix}$$

$$= \begin{bmatrix} [\Pi_{\mathrm{I}}]_{\eta_1\eta_1} \Pi^{\eta_1} & \cdots & [\Pi_{\mathrm{I}}]_{\eta_1\eta_M} \Pi^{\eta_1} \\ \vdots & & \vdots \\ [\Pi_{\mathrm{I}}]_{\eta_M\eta_1} \Pi^{\eta_M} & \cdots & [\Pi_{\mathrm{I}}]_{\eta_M\eta_M} \Pi^{\eta_M} \end{bmatrix}$$

$$= \mathrm{diag}\left(\Pi^{\eta_1}, \Pi^{\eta_2}, \ldots, \Pi^{\eta_M}\right) \cdot \left(\Pi_{\mathrm{I}} \otimes I_N\right),$$

which concludes the proof of the theorem. □

So in general, the output process of an SFSA is not Markov even when its input process is a Markov chain. However, the following theorem shows that if its input process is an i.i.d. process, then under fairly mild conditions, its output process *is* Markov. Its probability transition matrix can be calculated via the probability distribution vector of the input process and the state transition matrices of the SFSA.

Theorem II.7. *If the input process $\boldsymbol{\nu}(k)$ is an i.i.d. process with an $M\times 1$ distribution vector π_{I}, where the η_i-th component $\pi_{\mathrm{I}}(\eta_i) = \Pr\{\boldsymbol{\nu}(k) = \eta_i\}$ for $i = 1, 2, \ldots, M$, which is independent of the initial state of the automaton, $\boldsymbol{z}(0)$, then the output process $\boldsymbol{\theta}(k)$ of the SFSA is an N-state Markov chain with a probability transition matrix*

$$\Pi_{\mathrm{O}} = \left[\Pi^{\eta_1} \quad \Pi^{\eta_2} \quad \ldots \quad \Pi^{\eta_M}\right] \cdot (\pi_{\mathrm{I}} \otimes I_N)\,. \tag{10}$$

Proof. For any $k \in \mathbb{Z}^+$, consider an arbitrary event of the form

$$\mathscr{G}_k := \{z(k), z(k-1), \ldots, z(0)\}\,.$$

Similar to the proof for Theorem II.6, for $k \geq 1$, it follows that

$$\begin{aligned}
\Pr\{\mathscr{G}_k \mid \mathscr{G}_{k-1}\} &= \Pr\{z(k) \mid z(k-1)\} \\
&= \sum_{s=1}^{M} \Pr\{\nu(k-1)\} \Pr\left\{z(k) \mid \big(z(k-1), \nu(k-1)\big)\right\} \\
&= \sum_{s=1}^{M} \pi_{\mathrm{I}}(\nu(k-1)) \left[\Pi^{\nu(k-1)}\right]_{z(k-1)z(k)},
\end{aligned}$$

which implies that the state process $\boldsymbol{z}$ is Markov. From the assumption that the output process is isomorphic to the state process of the SFSA with probability one,

it is immediate that $\boldsymbol{\theta}$ is also Markov with the transition probability

$$[\Pi_{\mathrm{O}}]_{\xi_i\xi_j} := \Pr\{\boldsymbol{\theta}(k+1) = \xi_j \mid \boldsymbol{\theta}(k) = \xi_i\} = \sum_{s=1}^{M} \pi_{\mathrm{I}}(\eta_s)\,[\Pi^{\eta_s}]_{\xi_i\xi_j}.$$

The transition probability matrix of the output process is

$$\Pi_{\mathrm{O}} = \sum_{s=1}^{M} \pi_{\mathrm{I}}(\eta_s)\,\Pi^{\eta_s} = \left[\Pi^{\eta_1} \quad \Pi^{\eta_2} \quad \dots \quad \Pi^{\eta_M}\right] \cdot (\pi_{\mathrm{I}} \otimes I_N),$$

which completes the proof. □

The following corollary shows that if the input process of an SFSA is a constant, then its output process is a Markov chain, which is essentially equivalent to its input–output cross product process. The probability transition matrix can be simply deducted from either (7) or (10).

Corollary II.8. [75] *If the input process $\boldsymbol{\nu}(k) = \eta$ is a constant, then the output process $\boldsymbol{\theta}(k)$ of the SFSA is an N-state Markov chain with a probability transition matrix*

$$\Pi_{\mathrm{O}} = \Pi_{\mathrm{I/O}} = \Pi^{\eta}.$$

The following examples demonstrate some of the utility of these theoretical results.

Example II.1. In this example, the probability transition matrix $\Pi_{\mathrm{I/O}}$ is calculated from Theorem II.6 and compared against simulation. Let $\boldsymbol{\nu}(k) \in \{1, 2\}$ be a two-state Markov chain with $\Pi_{\mathrm{I}} = \left(\begin{smallmatrix} 0.9 & 0.1 \\ 0.7 & 0.3 \end{smallmatrix}\right)$. The state transition matrices Π^1 and Π^2 for the two input symbols are assumed to be

$$\Pi^1 = \begin{bmatrix} 0.8 & 0.1 & 0.1 \\ 0.9 & 0 & 0.1 \\ 0.7 & 0.2 & 0.1 \end{bmatrix} \quad \text{and} \quad \Pi^2 = \begin{bmatrix} 0.9 & 0 & 0.1 \\ 0.7 & 0.1 & 0.2 \\ 0.8 & 0 & 0.2 \end{bmatrix}.$$

Then, according to (7), the probability transition matrix for the input–output cross product process is

$$\Pi_{\mathrm{I/O}} = \begin{bmatrix} 0.72 & 0.09 & 0.09 & 0.08 & 0.01 & 0.01 \\ 0.81 & 0 & 0.09 & 0.09 & 0 & 0.01 \\ 0.63 & 0.18 & 0.09 & 0.07 & 0.02 & 0.01 \\ 0.63 & 0 & 0.07 & 0.27 & 0 & 0.03 \\ 0.49 & 0.07 & 0.14 & 0.21 & 0.03 & 0.06 \\ 0.56 & 0 & 0.14 & 0.24 & 0 & 0.06 \end{bmatrix}.$$

A 50,000-sample simulation using MATLAB shows that

$$\tilde{\Pi}_{\mathrm{I/O}} = \begin{bmatrix} 0.7195 & 0.0921 & 0.0863 & 0.0816 & 0.0110 & 0.0095 \\ 0.8069 & 0 & 0.0836 & 0.1014 & 0 & 0.0081 \\ 0.6241 & 0.1838 & 0.0923 & 0.0712 & 0.0184 & 0.0102 \\ 0.6213 & 0 & 0.0697 & 0.2794 & 0 & 0.0296 \\ 0.5010 & 0.0585 & 0.1190 & 0.2422 & 0.0271 & 0.0522 \\ 0.5203 & 0 & 0.1516 & 0.2578 & 0 & 0.0703 \end{bmatrix}.$$

A simple calculation shows that $\left\| \Pi_{\mathrm{I/O}} - \tilde{\Pi}_{\mathrm{I/O}} \right\|_2 = 2\% \left\| \Pi_{\mathrm{I/O}} \right\|_2$, which is a small error for most applications.

Example II.2. In this example, the probability transition matrix Π_{O} is calculated from Theorem II.7 and compared against simulation. Let $\nu(k) \in \{1, 2, 3\}$ be i.i.d. with a distribution vector $\pi_{\mathrm{I}} = \begin{bmatrix} 0.3 & 0.5 & 0.2 \end{bmatrix}^{\mathrm{T}}$. Assume that Π^1 and Π^2 are as

given in Example II.1. The state transition matrix for the input symbol "3" is

$$\Pi^3 = \begin{bmatrix} 0.2 & 0.7 & 0.1 \\ 0.6 & 0.2 & 0.2 \\ 0.5 & 0.1 & 0.4 \end{bmatrix}.$$

From the theoretical calculation using (10) and a 50,000-sample simulation using MATLAB, it follows, respectively, that

$$\Pi_{\mathrm{O}} = \begin{bmatrix} 0.73 & 0.17 & 0.10 \\ 0.74 & 0.09 & 0.17 \\ 0.71 & 0.08 & 0.21 \end{bmatrix} \quad \text{and} \quad \tilde{\Pi}_{\mathrm{O}} = \begin{bmatrix} 0.7284 & 0.1706 & 0.1010 \\ 0.7336 & 0.0900 & 0.1764 \\ 0.7053 & 0.0768 & 0.2180 \end{bmatrix}.$$

Hence $\left\| \Pi_{\mathrm{O}} - \tilde{\Pi}_{\mathrm{O}} \right\|_2 = 1\% \left\| \Pi_{\mathrm{O}} \right\|_2$. This error is comparable to that in the previous example.

The next subsection shows how to use Theorem II.7 to build an *equivalent* Markov jump-linear system for the stochastic hybrid system shown in Fig. 3. It will be used in the next two chapters to analyze the stability and output performance of a stochastic hybrid system.

II.5.2 Model-Equivalent Markov Jump-Linear System for a Stochastic Hybrid System

Consider the n-dimensional stochastic hybrid system in Fig. 3 with p output signals given by the state space model

$$\boldsymbol{x}(k+1) = A_{\boldsymbol{\theta}(k)}\boldsymbol{x}(k) + G_{\boldsymbol{\theta}(k)}\boldsymbol{w}(k), \quad \boldsymbol{x}(0) = \boldsymbol{x}_0, \ \boldsymbol{\theta}(0) = \boldsymbol{\theta}_0 \tag{11a}$$

$$\boldsymbol{y}(k) = C_{\boldsymbol{\theta}(k)}\boldsymbol{x}(k), \tag{11b}$$

where $\boldsymbol{\theta}(k)$ is a stochastic switching signal produced by the SFSA. Here $\boldsymbol{w}(k)$ is a zero-mean, white noise process with covariance matrix I_m. In general $\boldsymbol{\theta}(k)$ is not necessarily Markov, so letting $\boldsymbol{\rho}(k)$ be the Cartesian product of the input and output processes of the SFSA (see Fig. 15), the n-dimensional Markov jump-linear system

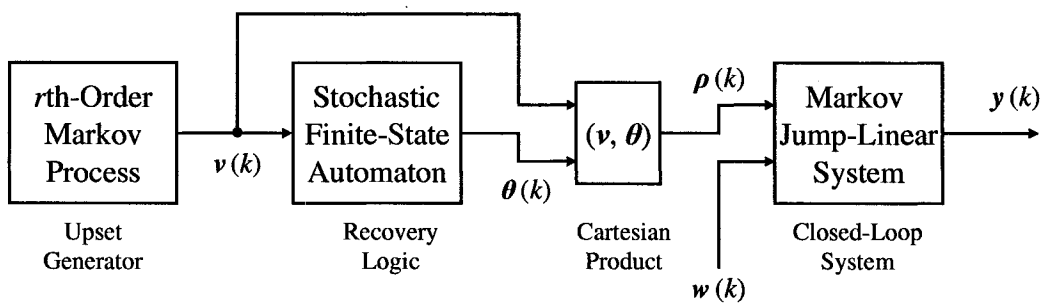

Fig. 15. The equivalent Markov jump-linear model for a stochastic hybrid system driven by an SFSA.

$$\boldsymbol{x}(k+1) = \tilde{A}_{\boldsymbol{\rho}(k)}\boldsymbol{x}(k) + \tilde{G}_{\boldsymbol{\rho}(k)}\boldsymbol{w}(k), \quad \boldsymbol{x}(0) = \boldsymbol{x}_0,\ \boldsymbol{\rho}(0) = \boldsymbol{\rho}_0 \tag{12a}$$

$$\boldsymbol{y}(k) = \tilde{C}_{\boldsymbol{\rho}(k)}\boldsymbol{x}(k), \tag{12b}$$

is *equivalent* to system (11) in the following sense.

Definition II.9 (Model Equivalence). The stochastic hybrid system (11) and the Markov jump-linear system (12) are said to be *model-equivalent* if $\tilde{A}_{\boldsymbol{\rho}(k)} := \tilde{A}_{(\boldsymbol{\nu}(k),\boldsymbol{\theta}(k))} \equiv A_{\boldsymbol{\theta}(k)}$, $\tilde{G}_{\boldsymbol{\rho}(k)} := \tilde{G}_{(\boldsymbol{\nu}(k),\boldsymbol{\theta}(k))} \equiv G_{\boldsymbol{\theta}(k)}$ and $\tilde{C}_{\boldsymbol{\rho}(k)} := \tilde{C}_{(\boldsymbol{\nu}(k),\boldsymbol{\theta}(k))} \equiv C_{\boldsymbol{\theta}(k)}$ for $k \in \mathbb{Z}^+$.

From the definition, the following result is immediate.

Lemma II.10. *When systems* (11) *and* (12) *are model-equivalent, they have the same state process,* $\boldsymbol{x}(k)$*, and the same output process,* $\boldsymbol{y}(k)$*, for* $k \in \mathbb{Z}^+$.

II.6 SUMMARY

In this chapter, the problem of modeling a Boeing 737 in closed-loop with an RCS was addressed in detail. First a conceptual model was introduced. It helped identify the need for certain approximations and motivated a more pragmatic approach. The main mathematical model to be used in subsequent chapters was introduced in three stages. First, system identification techniques were used to obtain the nominal and the recovery dynamics of a Boeing 737 in closed-loop with an RCS. Then an SFSA/FSM was employed to model the rollback recovery of the RCS from a control point of view. Finally, a stochastic hybrid model was used to integrate these submodels. The chapter concluded with the presentation of some properties of the stochastic hybrid model and the notion of a model-equivalent Markov jump-linear model. These results will be used for stability and output performance analyses in the subsequent chapters.

CHAPTER III

STABILITY ANALYSIS OF STOCHASTIC HYBRID SYSTEMS

Stability is a basic requirement of any closed-loop control system. Performance analysis is usually based on the assumption that the system is stable. In this chapter, a variety of stochastic stability definitions are given: mean-square stability (MSS) or second moment stability, exponential second moment stability, stochastic second moment stability and almost sure stability [42]. Under some assumptions, the three second moment stability definitions are equivalent, and they all imply almost sure stability. In this dissertation, only criteria for the MSS of a stochastic hybrid system are presented and applied [20]. As discussed in [80], the advantages of using MSS include:

1. it is easy to test for;
2. it implies stability of the mean dynamics;
3. it yields almost sure asymptotic stability of the zero-input state space trajectories.

This chapter is organized in the following way. Section III.1 defines four notions of stochastic stability. In Section III.2, necessary and sufficient conditions for MSS of a stochastic hybrid system are given in terms of its model-equivalent Markov jump-linear system. The results are then applied to determine the mean-square stability

boundary for a Boeing 737 in closed-loop with an RCS in Section III.3. Finally, a brief summary of the chapter is given in Section III.4.

III.1 DEFINITIONS OF STOCHASTIC STABILITY

As discussed in Section II.5.2, the stochastic hybrid system (11) is model equivalent to the Markov jump-linear system (12) since at each time instant, given identical inputs, both systems possess the same state and output values for all time. Therefore, stability of the stochastic hybrid system (11) can be determined using standard stability results for Markov jump-linear systems. Let $l = (i-1)N + j$ and $\mu_l := (\eta_i, \xi_j)$ for $i = 1, 2, \ldots, M$ and $j = 1, 2, \ldots, N$. The symbol set $\{\mu_l : l = 1, 2, \ldots, MN\}$ labels the elements in the input–output cross product space of the SFSA/FSM, i.e., $\Sigma_{\mathrm{I}} \times \Sigma_{\mathrm{O}}$. The following are standing assumptions:

1. The process $\boldsymbol{\rho}(k)$ is a homogeneous, finite-state Markov chain which takes values from $\{\mu_1, \mu_2, \ldots, \mu_{MN}\}$, where $M, N \in \mathbb{N}$. The probability transition matrix is denoted by $\Pi_{\mathrm{I/O}}$.

2. Both $\boldsymbol{\rho}(0) := \boldsymbol{\rho}_0$ and $\boldsymbol{x}(0) := \boldsymbol{x}_0$ can have any distribution.

The various types of stochastic stability for the Markov jump-linear system (12a) is given next.

Definition III.1. [41, 42] The Markov jump-linear system (12a) with $\boldsymbol{w}(k) \equiv 0$ is said to be:

1. Second moment stable (or mean-square stable), if for any $\boldsymbol{x}_0 \in \mathbb{R}^n$ and any

initial probability distribution $\boldsymbol{\rho}_0$,

$$\lim_{k\to\infty} E\left\{\|\boldsymbol{x}(k)\|^2\right\} = 0.$$

2. Exponentially second moment stable, if for any $\boldsymbol{x}_0 \in \mathbb{R}^n$ and any initial probability distribution $\boldsymbol{\rho}_0$, there exist constants $\alpha, \beta > 0$ independent of $\boldsymbol{x}_0$ and $\boldsymbol{\rho}_0$ such that

$$E\left\{\|\boldsymbol{x}(k)\|\right\}^2 \leq \alpha \|x_0\|^2 \mathrm{e}^{-\beta k}, \forall k \geq 0.$$

3. Stochastically second moment stable, if for any $\boldsymbol{x}_0 \in \mathbb{R}^n$ and any initial probability distribution $\boldsymbol{\rho}_0$,

$$\sum_{k=0}^{\infty} E\left\{\|\boldsymbol{x}(k)\|^2\right\} < +\infty.$$

4. Almost surely stable, if for any $\boldsymbol{x}_0 \in \mathbb{R}^n$ and any initial probability distribution $\boldsymbol{\rho}_0$,

$$\Pr\left\{\lim_{k\to\infty} \|\boldsymbol{x}(k)\| = 0\right\} = 1.$$

The relationship among these types of stochastic stability are given in the following two theorems [41, 49].

Theorem III.2. *For system* (12a) *with* $\boldsymbol{w}(k) \equiv 0$, *mean-square stability, exponentially second-moment stability and stochastically second moment stability are equivalent.*

Theorem III.3. *For system* (12a) *with* $\boldsymbol{w}(k) \equiv 0$, *mean-square stability, exponentially second-moment stability and stochastically second moment stability imply almost sure stability.*

Throughout the remainder of the dissertation only the notion of MSS is employed.

III.2 STABILITY ANALYSIS OF GENERAL MARKOV JUMP-LINEAR SYSTEMS

There are many approaches in the literature for determining the mean-square stability of a Markov jump-linear system. In this section, the spectral radii of two linear operators associated with the system (12) are employed to test for MSS. This technique is ultimately based on Lyapunov's second method. Let $\bar{S} = \left(\bar{S}_{\mu_1}, \bar{S}_{\mu_2}, \ldots, \bar{S}_{\mu_{MN}}\right) \in \mathbb{H}_{MN}^n$ be an MN-tuple with $\bar{S}_{\mu_l} \in \mathbb{M}(\mathbb{R}^n)$ for $l = 1, 2, \ldots, MN$. Define three linear operators in $\mathbb{B}\left(\mathbb{H}_{MN}^n\right)$

$$\mathcal{E}(\cdot) = \left(\mathcal{E}_{\mu_1}(\cdot), \mathcal{E}_{\mu_2}(\cdot), \ldots, \mathcal{E}_{\mu_{MN}}(\cdot)\right)$$

$$\mathcal{L}(\cdot) = \left(\mathcal{L}_{\mu_1}(\cdot), \mathcal{L}_{\mu_2}(\cdot), \ldots, \mathcal{L}_{\mu_{MN}}(\cdot)\right)$$

$$\mathcal{T}(\cdot) = \left(\mathcal{T}_{\mu_1}(\cdot), \mathcal{T}_{\mu_2}(\cdot), \ldots, \mathcal{T}_{\mu_{MN}}(\cdot)\right),$$

such that

$$\mathcal{E}_{\mu_l}\left(\bar{S}\right) = \sum_{q=1}^{MN} \left[\Pi_{\mathrm{I/O}}\right]_{\mu_l \mu_q} \bar{S}_{\mu_q}$$

$$\mathcal{L}_{\mu_l}\left(\bar{S}\right) = A_{\mu_l}^{\mathrm{T}} \mathcal{E}_{\mu_l}(\bar{S}) A_{\mu_l}$$

$$\mathcal{T}_{\mu_l}\left(\bar{S}\right) = \sum_{q=1}^{MN} \left[\Pi_{\mathrm{I/O}}\right]_{\mu_l \mu_q} A_{\mu_l} S_{\mu_l} A_{\mu_l}^{\mathrm{T}}.$$

It is easy to verify that $\mathcal{L}$ is the adjoint of $\mathcal{T}$ and vice versa since $\left\langle \mathcal{L}\left(\bar{S}\right), \bar{V} \right\rangle = \left\langle \bar{V}, \mathcal{T}\left(\bar{S}\right) \right\rangle$ for all $\bar{S}, \bar{V} \in \mathbb{H}_{MN}^n$ [40]. $\mathcal{L}$ is called the observability Gramian operator, and $\mathcal{T}$ is the controllability Gramian operator. It is easily verified that

$$\mathscr{A}_2 := \mathrm{diag}\left(A_{\mu_1}^{\mathrm{T}} \otimes A_{\mu_1}^{\mathrm{T}}, A_{\mu_2}^{\mathrm{T}} \otimes A_{\mu_2}^{\mathrm{T}}, \ldots, A_{\mu_{MN}}^{\mathrm{T}} \otimes A_{\mu_{MN}}^{\mathrm{T}}\right) \left(\Pi_{\mathrm{I/O}} \otimes I_{n^2}\right) \qquad (13)$$

is a matrix representation of $\mathcal{L}$. Similarly, if $\mathscr{A}_1 := \mathscr{A}_2^{\mathrm{T}}$, then $\mathscr{A}_1$ is a matrix representation of the linear operator $\mathcal{T}$. Let $\bar{S} \in \mathbb{H}_{MN}^{n+}$ such that

$$\bar{S}_{\mu_i} = \left[\left[\bar{S}_{\mu_i}\right]_{\cdot 1} \quad \left[\bar{S}_{\mu_i}\right]_{\cdot 2} \quad \cdots \quad \left[\bar{S}_{\mu_i}\right]_{\cdot n} \right],$$

where $\left[\bar{S}_{\mu_i}\right]_{\cdot j} \in \mathbb{R}^n$ for $i = 1, 2, \ldots, MN$ and $j = 1, 2, \ldots, n$. Define two linear column stacking operators $\mathrm{vec} : \mathbb{M}(\mathbb{R}^n) \to \mathbb{R}^{n^2}$ and $\varphi : \mathbb{H}_{MN}^n \to \mathbb{R}^{MNn^2}$ such that

$$\mathrm{vec}\left(\bar{S}_{\mu_i}\right) = \left[\left[\bar{S}_{\mu_i}\right]_{\cdot 1}^{\mathrm{T}} \quad \left[\bar{S}_{\mu_i}\right]_{\cdot 2}^{\mathrm{T}} \quad \cdots \quad \left[\bar{S}_{\mu_i}\right]_{\cdot n}^{\mathrm{T}} \right]^{\mathrm{T}},$$

and

$$\varphi\left(\bar{S}\right) = \left[\mathrm{vec}^{\mathrm{T}}\left(\bar{S}_{\mu_1}\right) \quad \mathrm{vec}^{\mathrm{T}}\left(\bar{S}_{\mu_2}\right) \quad \cdots \quad \mathrm{vec}^{\mathrm{T}}\left(\bar{S}_{\mu_{MN}}\right) \right]^{\mathrm{T}}.$$

It is simple to check that both linear operators are invertible with corresponding inverse operators denoted by vec^{-1} and φ^{-1}, respectively. Fig. 16 illustrates precisely

$$\begin{array}{ccc} \bar{S} & \xrightarrow{\mathcal{T}} & \mathcal{T}\left(\bar{S}\right) \\ {\scriptstyle\varphi^{-1}}\uparrow \downarrow{\scriptstyle\varphi} & & {\scriptstyle\varphi}\downarrow \uparrow{\scriptstyle\varphi^{-1}} \\ \varphi\left(\bar{S}\right) & \xrightarrow{\mathscr{A}_1} & \varphi\left(\mathcal{T}\left(\bar{S}\right)\right) \end{array} \qquad \begin{array}{ccc} S & \xrightarrow{\mathcal{L}} & \mathcal{L}\left(\bar{S}\right) \\ {\scriptstyle\varphi^{-1}}\uparrow \downarrow{\scriptstyle\varphi} & & {\scriptstyle\varphi}\downarrow \uparrow{\scriptstyle\varphi^{-1}} \\ \varphi\left(\bar{S}\right) & \xrightarrow{\mathscr{A}_2} & \varphi\left(\mathcal{L}\left(\bar{S}\right)\right) \end{array}$$

Fig. 16. The relationships between $\mathcal{T}$ and $\mathscr{A}_1$, and $\mathcal{L}$ and $\mathscr{A}_2$.

the relationships between $\mathcal{T}$ and $\mathscr{A}_1$, and $\mathcal{L}$ and $\mathscr{A}_2$. It is well-known that $r_\sigma(\mathcal{L}) = r_\sigma(\mathcal{T})$, since $\mathcal{L}$ and $\mathcal{T}$ are adjoints of each other. (See [66, 81] for additional details.) The following theorem describes a set of mean-square stability criteria for a jump-linear system in terms of these operators.

Theorem III.4. [40] *The following statements are equivalent:*

(*a*) *System* (12a) *with* $\boldsymbol{w}(k) = 0$ *is MSS.*

(*b*) $r_\sigma(\mathscr{A}_2) < 1$.

(*c*) $r_\sigma(\mathcal{L}) < 1$.

(*d*) *(Adjoint Coupled Lyapunov Equations) Given any* $\bar{S} = \left(\bar{S}_1, \bar{S}_2, \ldots, \bar{S}_{MN}\right) > 0$ *in* $\mathbb{H}_{MN}^{n+}$, *there exists* $\bar{P} = \left(\bar{P}_1, \bar{P}_2, \ldots, \bar{P}_{MN}\right) > 0$ *in* $\mathbb{H}_{MN}^{n+}$ *satisfying* $\bar{P} - \mathcal{L}(\bar{P}) = \bar{S}$ *with* $\bar{P} = \sum_{k=0}^{\infty} \mathcal{L}^k\left(\bar{S}\right)$.

(*e*) *For some* $\bar{S} \in \mathbb{H}_{MN}^{n+}, \bar{S} > 0$, *it follows that*

$$\bar{S} - \mathcal{L}\left(\bar{S}\right) > 0.$$

(*f*) *For some* $\beta \geq 1$, *and* $0 < \zeta < 1$, *and for any initial distributions of* $\boldsymbol{x}_0$ *and* $\boldsymbol{\rho}_0$,

$$E\left\{\|\boldsymbol{x}(k)\|^2\right\} \leq \beta\zeta^k \|x_0\|_2^2, \quad k \in \mathbb{Z}^+.$$

(*g*) *For any initial distributions of* $\boldsymbol{x}_0$ *and* $\boldsymbol{\rho}_0$,

$$\sum_{k=0}^{\infty} E\left\{\|\boldsymbol{x}(k)\|^2\right\} < \infty.$$

Note that if system (12a) is MSS, then for any $\bar{S} \in \mathbb{H}_{MN}^{n+}$, there exists a *unique* $\bar{P} \in \mathbb{H}_{MN}^{n+}$ such that $\bar{P} - \mathcal{T}\left(\bar{P}\right) = \bar{S}$ and $\bar{P} - \mathcal{L}\left(\bar{P}\right) = \bar{S}$. If $\bar{S} \geq \bar{T} \geq 0$ (> 0, respectively) and $\bar{P} - \mathcal{T}\left(\bar{P}\right) = \bar{S}$, $\bar{L} - \mathcal{T}\left(\bar{L}\right) = \bar{T}$ or $\bar{P} - \mathcal{L}\left(\bar{P}\right) = \bar{S}$, $\bar{L} - \mathcal{L}\left(\bar{L}\right) = \bar{T}$ then $\bar{P} \geq \bar{L} \geq 0$ (> 0, respectively). The result above also holds when $\mathcal{L}$ is replaced with $\mathcal{T}$, and $\mathscr{A}_2$ is replaced with $\mathscr{A}_1$. In the following context, $\mathcal{L}$ and $\mathscr{A}_2$ will be used, because in the next chapter the observability Gramian will be used to compute the

output performance of the stochastic hybrid system. In regards to the MSS of the stochastic hybrid system (11), from Lemma II.10, the following result is immediate.

Lemma III.5. *A stochastic hybrid system* (11) *is MSS if and only if its model-equivalent Markov jump-linear system* (12) *is MSS.*

III.3 STABILITY ANALYSIS OF THE STOCHASTIC HYBRID MODEL FOR AN AIRCRAFT SYSTEM WITH AN RCS

Using the techniques described in Section III.2, mean-square stability of the Boeing 737 in closed-loop with an RCS can be tested using the models given in Appendices A.2 and A.3. The results provide boundaries for the upset probability under which the hybrid system is MSS. As discussed in Section II.4, the upset process, $\boldsymbol{\nu}(k)$, is a two-state stochastic process: "0" represents there is no upset detected and "1" denotes an upset is detected. It can be modeled either as a first-order Markov chain or an i.i.d. process. These two cases are discussed below.

III.3.1 When the Upset Process Is Modeled as a First-Order Markov Chain

According to the discussion presented in Section II.2, when the upset process is modeled as a Markov chain, it has approximately the probability transition matrix

$$\Pi_{\mathrm{I}} = \begin{bmatrix} 1 - [\Pi_{\mathrm{I}}]_{01} & [\Pi_{\mathrm{I}}]_{01} \\ 1 & 0 \end{bmatrix}. \tag{14}$$

The parameter $[\Pi_{\mathrm{I}}]_{01}$ is the upset probability, which denotes the probability of detecting an upset condition at the next frame given no upset is detected at the current

frame. The second row in the matrix indicates that it is impossible to detect two consecutive upset signals.

The SFSA/FSM used to model the rollback recovery process of the RCS has seven output symbols, i.e., $\boldsymbol{\theta}(k) \in \{\mathrm{N}, \mathrm{R}_1, \mathrm{R}_2, \ldots, \mathrm{R}_6\}$. According to (7), the input–output cross product process $\boldsymbol{\rho}(k)$ has a transition probability matrix

$$\Pi_{\mathrm{I/O}} = \mathrm{diag}\left(\Pi^0, \Pi^1\right) \cdot \left(\Pi_{\mathrm{I}} \otimes I_7\right).$$

According to (13) and Theorem III.4, mean-square stability of the stochastic hybrid system can be determined from the spectral radius of the following matrix:

$$\tilde{\mathscr{A}}_2 := \mathrm{diag}\left(A_{0,\mathrm{N}}^{\mathrm{T}}, A_{0,\mathrm{R}_1}^{\mathrm{T}}, \ldots, A_{0,\mathrm{R}_6}^{\mathrm{T}}; A_{1,\mathrm{N}}^{\mathrm{T}}, A_{1,\mathrm{R}_1}^{\mathrm{T}}, \ldots, A_{1,\mathrm{R}_6}^{\mathrm{T}}\right) \cdot \left(\Pi_{\mathrm{I/O}} \otimes I_{8^2}\right),$$

where $A_{j,\mathrm{N}} \equiv \tilde{A}_{\mathrm{n}} \otimes \tilde{A}_{\mathrm{n}}$ and $A_{j,\mathrm{R}_i} \equiv \tilde{A}_{\mathrm{r}} \otimes \tilde{A}_{\mathrm{r}}$ for $i = 1, 2, \ldots, 6$ and $j = 0, 1$. Since $\tilde{A}_{\mathrm{n}}$ and $\tilde{A}_{\mathrm{r}}$ are eight-dimensional matrices (see Appendix A.2), $\tilde{\mathscr{A}}_2$ has dimension $2 \times 7 \times 8^2 = 896$. This value is much smaller than the dimension of the conceptual model, which was 14,450 (see Section II.2 for details). Fig. 17 shows $r_\sigma\left(\tilde{\mathscr{A}}_2\right)$ plotted as a function of $[\Pi_{\mathrm{I}}]_{01}$. The SFSA stochastic hybrid model is MSS when $[\Pi_{\mathrm{I}}]_{01} < 0.0016$, which is a slightly higher upset probability boundary than that predicted by the FSM hybrid model, namely, $[\Pi_{\mathrm{I}}]_{01} < 0.0015$.

III.3.2 When the Upset Process Is Modeled as an I.I.D. Process

Under the approximations introduced in Section II.2, when the upset signal is modeled as an i.i.d. process, it has the probability distribution:

$$\pi_{\mathrm{I}} = \begin{bmatrix} \pi_{\mathrm{I}}(0) & \pi_{\mathrm{I}}(1) \end{bmatrix} = \begin{bmatrix} 1 - \pi_{\mathrm{I}}(1) & \pi_{\mathrm{I}}(1) \end{bmatrix}, \tag{15}$$

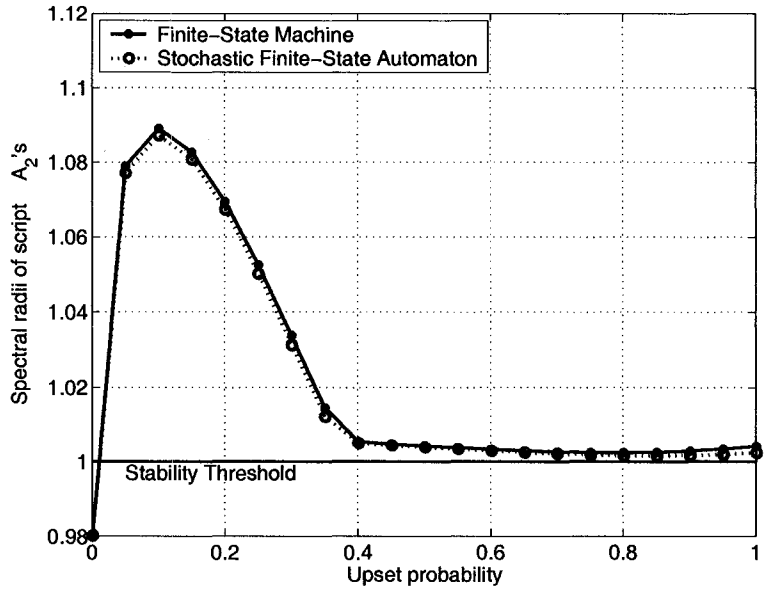

(a) $[\Pi_{\mathrm{I}}]_{01} \in [0, 1]$.

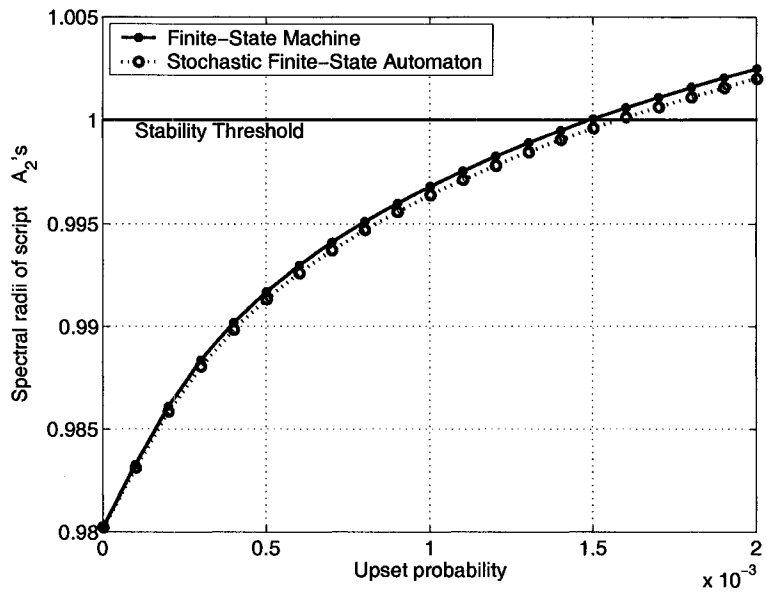

(b) $[\Pi_{\mathrm{I}}]_{01} \in [0, 0.002]$.

Fig. 17. $r_\sigma\left(\tilde{\mathcal{A}}_2\right)$ as a function of upset probability for the SFSA stochastic hybrid model and the FSM hybrid dynamical model.

where the parameter $\pi_{\mathrm{I}}(1)$ is the upset probability. It is equivalent to the probability of detecting an upset signal at each frame. An i.i.d. process can also be considered as a Markov process where each row of the corresponding transition probability matrix is equal to π_{I}. That is,

$$\Pi_{\mathrm{I}} = \begin{bmatrix} \pi_{\mathrm{I}} \\ \pi_{\mathrm{I}} \end{bmatrix} = \begin{bmatrix} 1-\pi_{\mathrm{I}}(1) & \pi_{\mathrm{I}}(1) \\ 1-\pi_{\mathrm{I}}(1) & \pi_{\mathrm{I}}(1) \end{bmatrix}.$$

Then the analysis in Subsection III.3.1 can be applied directly to calculate the upset probability boundaries.

Another analytical technique for the i.i.d. case is to apply the results of Theorem II.7 since the output process $\boldsymbol{\theta}(k)$ is a Markov chain. According to (10), the corresponding probability transition matrix is

$$\Pi_{\mathrm{O}} = \begin{bmatrix} \Pi^0 & \Pi^1 \end{bmatrix} \cdot (\pi_{\mathrm{I}} \otimes I_7).$$

Thus, the mean-square stability of the stochastic hybrid system can be determined from the spectral radius of the following matrix:

$$\breve{\mathscr{A}}_2 := \mathrm{diag}\left(A_{\mathrm{N}}^{\mathrm{T}}, A_{\mathrm{R}_1}^{\mathrm{T}}, \ldots, A_{\mathrm{R}_6}^{\mathrm{T}}\right) \cdot (\Pi_{\mathrm{O}} \otimes I_{8^2}),$$

where $A_{\mathrm{N}} \equiv \tilde{A}_{\mathrm{n}} \otimes \tilde{A}_{\mathrm{n}}$ and $A_{\mathrm{R}_i} \equiv \tilde{A}_{\mathrm{r}} \otimes \tilde{A}_{\mathrm{r}}$ for $i = 1, 2, \ldots, 6$. In this case, the dimension of $\breve{\mathscr{A}}_2$ is 448, which is only half of that for $\tilde{\mathscr{A}}_2$ in the previous subsection. The spectral radius plot of $\breve{\mathscr{A}}_2$ as a function of $\pi_{\mathrm{I}}(1)$ is almost indistinguishable from that shown in Fig. 17. Thus, the *normalized difference* of the spectral radius is used to characterize their difference for a given probability $p_0 \in [0, 1]$. Specifically,

$$\text{normalized difference of } r_\sigma(\mathscr{A}_2) \text{ at } p_0 = \frac{r_\sigma\left(\breve{\mathscr{A}}_2\right)\Big|_{\pi_{\mathrm{I}}(1)=p_0} - r_\sigma\left(\tilde{\mathscr{A}}_2\right)\Big|_{[\Pi_{\mathrm{I}}]_{01}=p_0}}{r_\sigma\left(\tilde{\mathscr{A}}_2\right)\Big|_{[\Pi_{\mathrm{I}}]_{01}=p_0}}.$$

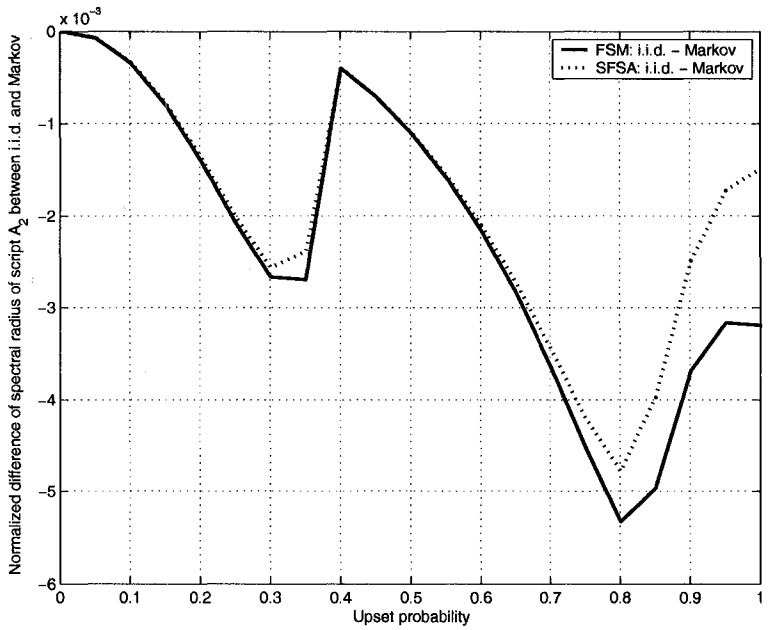

(a) $[\Pi_{\mathrm{I}}]_{01}, \pi_{\mathrm{I}} \in [0, 1]$.

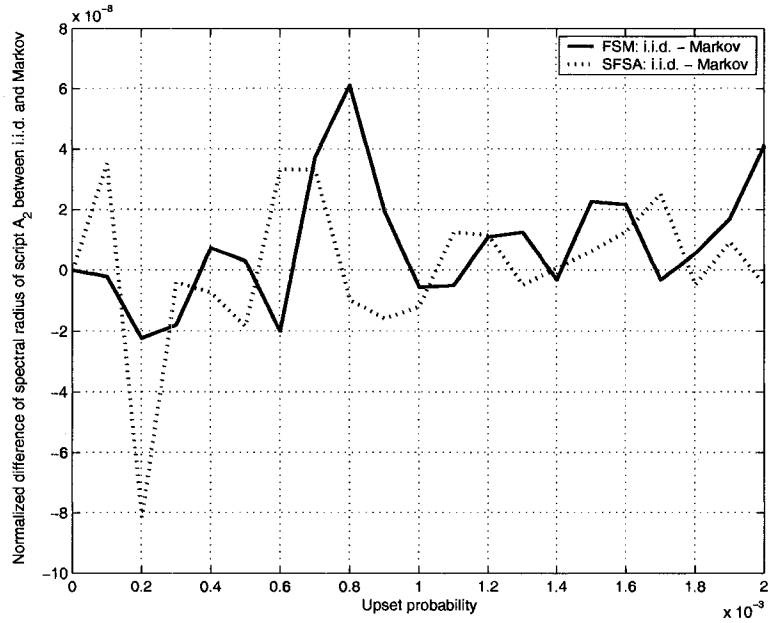

(b) $[\Pi_{\mathrm{I}}]_{01}, \pi_{\mathrm{I}} \in [0, 0.002]$.

Fig. 18. The normalized difference between the spectral radii of the $\breve{\mathscr{A}}_2$ ($r = 0$, namely, i.i.d.) and $\tilde{\mathscr{A}}_2$ ($r = 1$) for typical values of $\pi_{\mathrm{I}}(1)$ and $[\Pi_{\mathrm{I}}]_{01}$.

The normalized difference of $r_\sigma(\mathscr{A}_2)$ is shown in Fig. 18. In general, a lower upset probability leads to a smaller difference. Thus, it is clear, from an MSS point of view, that the i.i.d. and first-order Markov chain are nearly equivalent for modeling the upset process. Either approach works well for the specific application.

III.3.3 Numerical Reliability of the Eigen-Analysis

In Subsections III.3.1 and III.3.2, the spectral radii $r_\sigma\left(\tilde{\mathscr{A}}_2\right)$ and $r_\sigma\left(\check{\mathscr{A}}_2\right)$ were calculated via the MATLAB function `eig`, which uses the `LAPACK` routines [82]. As discussed in [83], for some matrices, eigenvalue computations are sensitive to finite word length effects. For example, small roundoff errors introduced during the computation with floating-point arithmetic can lead to large errors in the eigenvalue estimates. In the following discussion, as a case study, the eigenvalue sensitivities associated with the calculation of $r_\sigma\left(\tilde{\mathscr{A}}_2\right)$ for the SFSA stochastic hybrid model with twenty-one upset probabilities $[\Pi_{\mathrm{I}}]_{01} \in \{0, 0.0001, \ldots, 0.002\}$ (increased by 0.0001) are examined. Let $\tilde{\lambda}_1$ be an estimate of the eigenvalue of $\tilde{\mathscr{A}}_2$ having maximum modulus, namely,

$$\left|\tilde{\lambda}_1\right| = r_\sigma\left(\tilde{\mathscr{A}}_2\right),$$

and $\tilde{v}_1$ be the corresponding eigenvector estimate. If $\tilde{\lambda}_1$ is close to a true eigenvalue of $\tilde{\mathscr{A}}_2$, then the matrix $\tilde{\lambda}_1 I - \tilde{\mathscr{A}}_2$ should be nearly singular. This can be quantified using the *matrix condition number* of $\tilde{\lambda}_1 I - \tilde{\mathscr{A}}_2$, which is defined as

$$\kappa\left(\tilde{\lambda}_1 I - \tilde{\mathscr{A}}_2\right) = \frac{\sigma_{\max}\left(\tilde{\lambda}_1 I - \tilde{\mathscr{A}}_2\right)}{\sigma_{\min}\left(\tilde{\lambda}_1 I - \tilde{\mathscr{A}}_2\right)},$$

where $\sigma_{\max}(\cdot)$ and $\sigma_{\min}(\cdot)$ denote the maximum and the minimum singular values of the matrix, respectively. Using the MATLAB function, `cond`, $\kappa^{-1}\left(\tilde{\lambda}_1 I - \tilde{\mathscr{A}}_2\right)$ was

calculated from $\kappa\left(\tilde{\lambda}_1 I - \tilde{\mathscr{A}}_2\right)$ for the given range of probabilities and found to be of an order between 10^{-19} and 10^{-17} as shown in Fig. 19. For comparison, the result

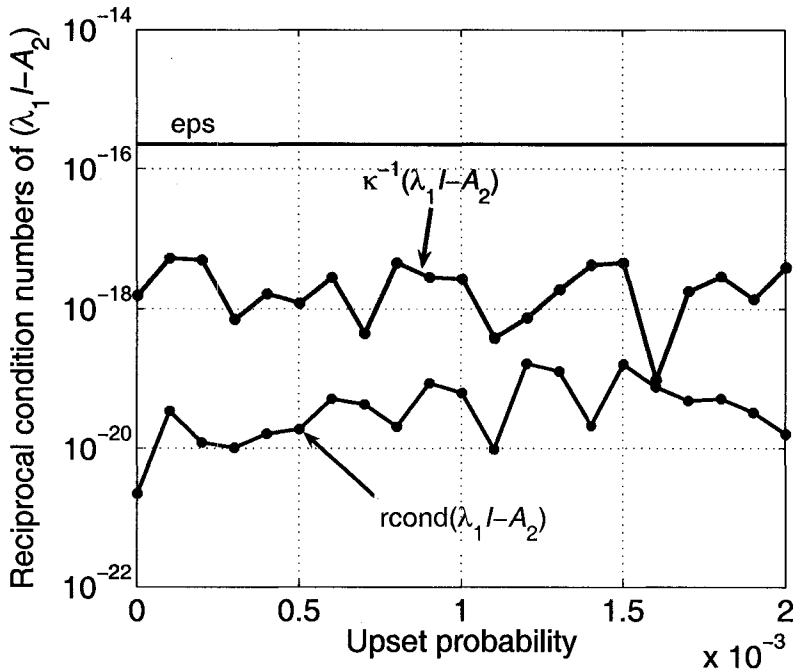

Fig. 19. The reciprocal matrix condition numbers, $\kappa^{-1}\left(\tilde{\lambda}_1 I - \tilde{\mathscr{A}}_2\right)$ and rcond $\left(\tilde{\lambda}_1 I - \tilde{\mathscr{A}}_2\right)$, as a function of the upset probability $[\Pi_{\mathrm{I}}]_{01} \in [0, 0.002]$.

given by the MATLAB function, `rcond`, was also provided, which is more efficient but less reliable than `cond`. The definition of rcond $\left(\tilde{\lambda}_1 I - \tilde{\mathscr{A}}_2\right)$ is given below:

$$\text{rcond}\left(\tilde{\lambda}_1 I - \tilde{\mathscr{A}}_2\right) := \frac{1}{\left\|\tilde{\lambda}_1 I - \tilde{\mathscr{A}}_2\right\|_1 \left\|\left(\tilde{\lambda}_1 I - \tilde{\mathscr{A}}_2\right)^{-1}\right\|_1},$$

where $\|\cdot\|_1$ denotes the 1-norm of a matrix. In each case, the reciprocal condition numbers were smaller than `eps`, namely, 2.2204×10^{-16}, which is the *floating-point relative accuracy* of MATLAB. Thus, for this example, $\tilde{\lambda}_1 I - \tilde{\mathscr{A}}_2$ can be considered to be nearly singular, and $\tilde{\lambda}_1$ is close to a true eigenvalue of $\tilde{\mathscr{A}}_2$ (though not necessarily the one with maximum modulus). Next, if $\left(\tilde{\lambda}_1, \tilde{v}_1\right)$ is a good eigenvalue–eigenvector

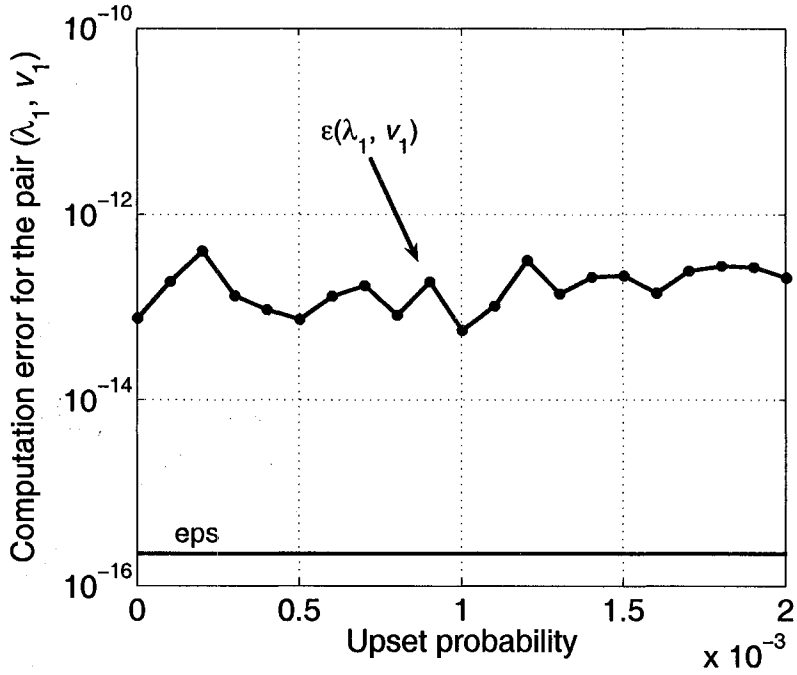

Fig. 20. The computation error for the eigenvalue–eigenvector pair $\left(\tilde{\lambda}_1, \tilde{v}_1\right)$ of $\tilde{\mathscr{A}}_2$ as a function of the upset probability $[\Pi_{\mathrm{I}}]_{01} \in [0, 0.002]$.

estimate of $\tilde{\mathscr{A}}_2$, then the computation error defined as

$$\varepsilon\left(\tilde{\lambda}_1, \tilde{v}_1\right) := \left\|\tilde{\lambda}_1 \tilde{v}_1 - \tilde{\mathscr{A}}_2 \tilde{v}_1\right\|$$

should also be close to zero. As shown in Fig. 20, they were of the order 10^{-13}, which is larger than but still reasonably close to eps. From this analysis, it is concluded that $\left(\tilde{\lambda}_1, \tilde{v}_1\right)$ is a good estimate of an eigenvalue–eigenvector pair of $\tilde{\mathscr{A}}_2$.

For additional eigenvalue sensitivity analysis, the *eigenvalue condition number* was employed. Given a matrix A, the sensitivity for a given eigenvalue, λ, can be evaluated using the eigenvalue condition number,

$$\kappa(\lambda, A) = \frac{\|y\| \, \|x\|}{|y^{\mathrm{T}} x|}, \tag{16}$$

where y^{T} is the left eigenvector of A (i.e., $y^{\mathrm{T}}A = \lambda y^{\mathrm{T}}$), and x is the (right) eigenvector of A (i.e., $Ax = \lambda x$). The eigenvalue condition number provides a worst-case estimate of the computation error one might encounter. It is clear that $\kappa(\lambda, A) \geq 1$, since by the Cauchy-Schwartz inequality $\left|y^{\mathrm{T}}x\right| \leq \|y\| \, \|x\|$. When A is symmetric, it follows that $\left|y^{\mathrm{T}}x\right| = \|y\| \, \|x\|$, since x and y are linearly dependent. Thus, $\kappa(\lambda, A) = 1$, or equivalently, the symmetric eigenvalue problem is *perfectly conditioned.* But in general, the larger the eigenvalue condition number or the smaller its reciprocal is, the more sensitive to roundoff errors the corresponding eigenvalue estimate becomes. The eigenvalue condition numbers can be estimated using the MATLAB function, `condeig`. (Note however that, `condeig` uses `eig` to compute x and y in (16). Therefore, significant inaccuracy in the corresponding eigenvalue condition numbers is possible.) Using `condeig`, the reciprocal eigenvalue condition number, $\kappa^{-1}\left(\tilde{\lambda}_1, \tilde{\mathscr{A}}_2\right)$, was found to have an order between 10^{-12} and 10^{-10} as shown in Fig. 21. It was significantly larger than `eps`, which means that the $\tilde{\lambda}_1$ calculation has the *potential* to be very sensitive to numerical errors. But in general eigenvalue condition numbers only provide upper bounds on numerical errors. That is, they do not say with certainty that at any specific eigenvalue estimate was inaccurately computed. Therefore, this analysis was not conclusive.

A final step in the eigenvalue sensitivity analysis was to use the MATLAB function, `eigs` to compute $r_\sigma\left(\tilde{\mathscr{A}}_2\right)$. This command is usually employed to find the largest eigenvalues/eigenvectors of a sparse matrix. In this case, $\tilde{\mathscr{A}}_2$ is a sparse matrix with no more than 15% of its entries being nonzero. The function `eigs` employs the `ARPACK` library, which is a collection of routines specifically designed to solve

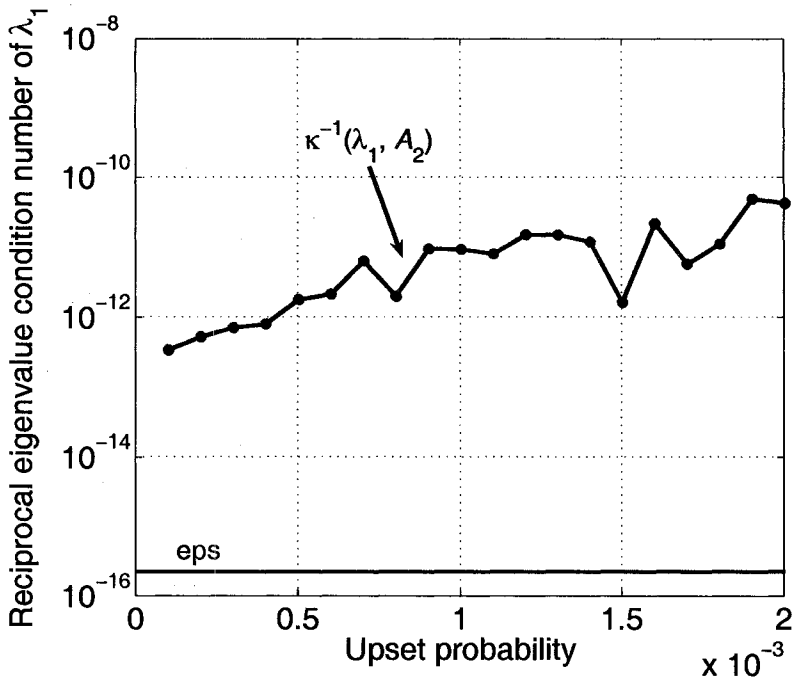

Fig. 21. The reciprocal eigenvalue condition number, $\kappa^{-1}\left(\tilde{\lambda}_1, \tilde{\mathscr{A}}_2\right)$, as a function of the upset probability $[\Pi_{\mathrm{I}}]_{01} \in [0, 0.002]$.

large scale eigenvalue problems [84]. Using `eigs`, nine spectral radii estimates converged. The differences between these two different approaches (`eig` and `eigs`) for those nine spectral radii are shown in Fig. 22 in blue, which were on the order of 10^{-8}. These values are much larger than `eps`. But in this application, the primary interest is in determining how close $r_\sigma\left(\tilde{\mathscr{A}}_2\right)$ is to 1, which means that the two approaches provided nearly indistinguishable spectral radii estimates for the nine upset probabilities. For the other twelve upset probabilities (shown in Fig. 22 as magenta $\times$'s), the `eigs` did not converges properly, and thus there is no basis for comparison.

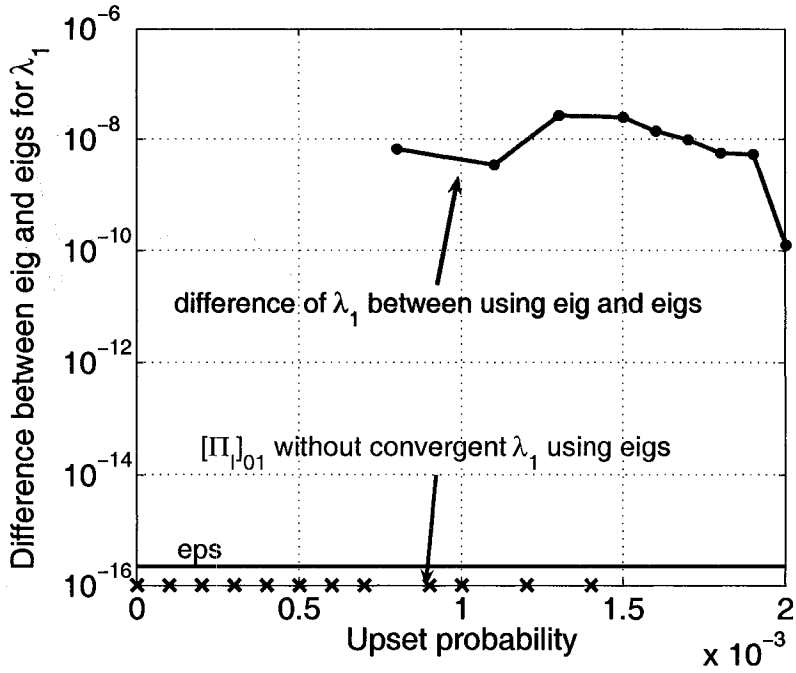

Fig. 22. The difference between `eig` and `eigs` computed $\tilde{\lambda}_1$ as a function of the upset probability $[\Pi_I]_{01} \in [0, 0.002]$.

III.4 SUMMARY

In this chapter, the mean-square stability of a stochastic hybrid system was analyzed via its model-equivalent Markov jump-linear system. First, several analytical techniques for determining the MSS of a Markov jump-linear system were presented. Then, using the models given in Appendices A.2 and A.3, the mean-square stability of the Boeing 737 in closed-loop with an RCS was evaluated for both a Markov chain and an i.i.d. modeled upset process. For this application, it was determined that the aircraft system is MSS when the upset probability is less than 1.5×10^{-3}.

CHAPTER IV

OUTPUT TRACKING PERFORMANCE ANALYSIS OF A RECOVERABLE FLIGHT CONTROL SYSTEM

In this chapter, an output tracking error system is built for studying output performance of a recoverable flight control system. Then performance criteria, including *mean output energy* and *mean output power*, are used to analyze the tracking system mathematically. For a real aircraft system under normal operating conditions, winds and gusts are always present. Therefore, the mean output power is of primary interest for the Boeing 737 in closed-loop with an RCS.

This chapter is organized as follows. In Section IV.1, an output tracking error system is developed to evaluate the performance of a switched system versus a nominal unswitched system. In Section IV.2, the output performance of the stochastic hybrid system (11) is studied by means of its model-equivalent Markov jump-linear model. In Section IV.3, a simple example is given to show how to calculate the output performance analytically. In Section IV.4, the results in Sections IV.2 and IV.3 are applied to predict the output tracking error performance of the Boeing 737 system in closed-loop with an RCS. Section IV.5 briefly summarizes this chapter.

IV.1 THE TRACKING ERROR SYSTEM

As discussed in Chapter I, the closed-loop dynamics of a flight control system with an RCS can be modeled as a jump-linear system with two modes: the nominal

mode and the recovery mode. In general, the system operates in the nominal mode. However, when a neutron encounter produces a detectable SEU in the flight control hardware, the RCS will rollback the state of the controller to its stored value from the previous checkpoint. During this recovery process, the current control output values are frozen until the checkpointed values can be reloaded and made available. During this process, the system is said to be in recovery mode. Therefore, it is important to evaluate the performance difference between the nominal system and the switched system. As shown in Fig. 23, this difference gives rise to an output tracking error

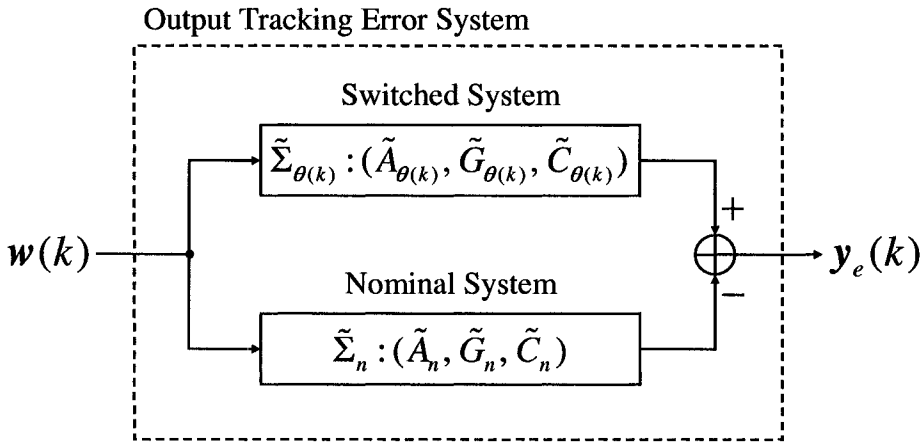

Fig. 23. The output tracking error system.

system described by the state space model

$$\begin{bmatrix} \tilde{\boldsymbol{x}}(k+1) \\ \tilde{\boldsymbol{x}}_{\mathrm{n}}(k+1) \end{bmatrix} = \begin{bmatrix} \tilde{A}_{\boldsymbol{\theta}(k)} & 0 \\ 0 & \tilde{A}_{\mathrm{n}} \end{bmatrix} \begin{bmatrix} \tilde{\boldsymbol{x}}(k) \\ \tilde{\boldsymbol{x}}_{\mathrm{n}}(k) \end{bmatrix} + \begin{bmatrix} \tilde{G}_{\boldsymbol{\theta}(k)} \\ \tilde{G}_{\mathrm{n}} \end{bmatrix} \boldsymbol{w}(k),$$

$$\begin{bmatrix} \tilde{\boldsymbol{x}}(0) \\ \tilde{\boldsymbol{x}}_{\mathrm{n}}(0) \end{bmatrix} = \begin{bmatrix} \tilde{\boldsymbol{x}}_0 \\ \tilde{\boldsymbol{x}}_{\mathrm{n},0} \end{bmatrix}$$

$$\boldsymbol{y}_{\mathrm{e}}(k) = \begin{bmatrix} \tilde{C}_{\boldsymbol{\theta}(k)} & -\tilde{C}_{\mathrm{n}} \end{bmatrix} \begin{bmatrix} \tilde{\boldsymbol{x}}(k) \\ \tilde{\boldsymbol{x}}_{\mathrm{n}}(k) \end{bmatrix}.$$

The random process $\boldsymbol{\theta}(k)$ switches among the symbols $\{\mathrm{n}, \mathrm{r}_1, \mathrm{r}_2, \ldots, \mathrm{r}_6\}$ representing the "nominal" mode and all the "recovery" modes, respectively; $\tilde{\boldsymbol{x}}(k)$ and $\tilde{\boldsymbol{x}}_{\mathrm{n}}(k)$ are the state vectors of the switched and nominal closed-loop systems; $\boldsymbol{w}(k)$ is the white noise process used to generate the wind input; and $\boldsymbol{y}_{\mathrm{e}}(k)$ is the closed-loop output tracking error. Let $\boldsymbol{x}_{\mathrm{e}}(k) = \begin{bmatrix} \tilde{\boldsymbol{x}}^{\mathrm{T}}(k) & \tilde{\boldsymbol{x}}_{\mathrm{n}}^{\mathrm{T}}(k) \end{bmatrix}^{\mathrm{T}}$, $A_{\mathrm{e},\boldsymbol{\theta}(k)} = \mathrm{diag}\left(\tilde{A}_{\boldsymbol{\theta}(k)}, \tilde{A}_{\mathrm{n}}\right)$, $G_{\mathrm{e},\boldsymbol{\theta}(k)} = \begin{bmatrix} \tilde{G}_{\boldsymbol{\theta}(k)}^{\mathrm{T}} & \tilde{G}_{\mathrm{n}}^{\mathrm{T}} \end{bmatrix}^{\mathrm{T}}$ and $C_{\mathrm{e},\boldsymbol{\theta}(k)} = \begin{bmatrix} \tilde{C}_{\boldsymbol{\theta}(k)} & -\tilde{C}_{\mathrm{n}} \end{bmatrix}$. Then the error system can be written concisely as

$$\boldsymbol{x}_{\mathrm{e}}(k+1) = A_{\mathrm{e},\boldsymbol{\theta}(k)}\, \boldsymbol{x}_{\mathrm{e}}(k) + G_{\mathrm{e},\boldsymbol{\theta}(k)} \boldsymbol{w}(k), \quad \boldsymbol{x}_{\mathrm{e}}(0) = \boldsymbol{x}_{\mathrm{e},0}, \quad \boldsymbol{\theta}(0) = \boldsymbol{\theta}_0 \tag{17a}$$

$$\boldsymbol{y}_{\mathrm{e}}(k) = C_{\mathrm{e},\boldsymbol{\theta}(k)} \boldsymbol{x}_{\mathrm{e}}(k), \tag{17b}$$

which is also a jump-linear system with switching signal $\boldsymbol{\theta}(k)$. Therefore, its stability and output performance can be calculated via the same methods applied to systems (11) and (12). The next section develops the theory for the performance analysis of a general Markov jump-linear system.

IV.2 THEORY TO ANALYZE THE OUTPUT PERFORMANCE OF A GENERAL MARKOV JUMP-LINEAR SYSTEM

For an MSS Markov jump-linear system (12), the output performance measure J is defined below:

$$J = \begin{cases} J_0 := E\left\{ \sum_{k=0}^{\infty} \|\boldsymbol{y}(k)\|^2 \right\} & : \quad \boldsymbol{w}(k) \equiv 0 \\ J_w := \lim_{k\to\infty} E\left\{ \|\boldsymbol{y}(k)\|^2 \right\} & : \quad \boldsymbol{w}(k) \not\equiv 0, \end{cases}$$

where J_0 is the *mean output energy*, and J_w is the *mean output power*. The goal of this section is to produce explicit analytical expressions for J via a generalization

of the *observability Gramian* described in [66, 81]. The expression for J_w can be shown to be similar to the output's *power semi-norm* developed in [51] for network controlled systems with data dropouts when both $\tilde{G}$ and $\tilde{C}$ in system (12) are not switched.

Suppose that a Markov chain, $\boldsymbol{\rho}(k)$, has a stationary distribution, and $\boldsymbol{\rho}_{\mathrm{s}}$ is a random variable with this distribution. Then $\pi_{\mathrm{I/O}}(\mu_l) := \Pr\{\boldsymbol{\rho}_{\mathrm{s}} = \mu_l\}$ for $l = 1, 2, \ldots, MN$ is determined by solving the eigen-equation

$$\begin{bmatrix} \pi_{\mathrm{I/O}}(\mu_1) \\ \pi_{\mathrm{I/O}}(\mu_2) \\ \vdots \\ \pi_{\mathrm{I/O}}(\mu_{MN}) \end{bmatrix} = \Pi_{\mathrm{I/O}}^{\mathrm{T}} \begin{bmatrix} \pi_{\mathrm{I/O}}(\mu_1) \\ \pi_{\mathrm{I/O}}(\mu_2) \\ \vdots \\ \pi_{\mathrm{I/O}}(\mu_{MN}) \end{bmatrix}, \tag{18}$$

or, equivalently,

$$\pi_{\mathrm{I/O}}(\mu_j) = \sum_{i=1}^{MN} \left[\Pi_{\mathrm{I/O}}\right]_{\mu_i \mu_j} \pi_{\mathrm{I/O}}(\mu_i) \quad \text{for } j = 1, 2, \ldots, MN. \tag{19}$$

Before addressing the main theory, the following useful identity is presented.

Lemma IV.1. *Given a matrix* $M \in \mathbb{M}\left(\mathbb{R}^{p^2}, \mathbb{R}^{m^2}\right)$ *where* $m, p \in \mathbb{N}$,

$$\mathrm{tr}\left(\mathrm{vec}^{-1}\left(M \,\mathrm{vec}\left(I_p\right)\right)\right) = \mathrm{tr}\left(\mathrm{vec}^{-1}\left(M^{\mathrm{T}} \,\mathrm{vec}\left(I_m\right)\right)\right).$$

Proof. According to the formula (T3.9) in [85],

$$\begin{aligned} \mathrm{tr}\left(\mathrm{vec}^{-1}\left(M \,\mathrm{vec}\left(I_p\right)\right)\right) &= \mathrm{tr}\left(I_m^{\mathrm{T}}\left(\mathrm{vec}^{-1}\left(M \,\mathrm{vec}\left(I_p\right)\right)\right)\right) \\ &= \left(\mathrm{vec}\left(I_m\right)\right)^{\mathrm{T}} \mathrm{vec}\left(\mathrm{vec}^{-1}\left(M \,\mathrm{vec}\left(I_p\right)\right)\right) \\ &= \left(\mathrm{vec}\left(I_m\right)\right)^{\mathrm{T}} M \,\mathrm{vec}\left(I_p\right) \\ &= \left(\mathrm{vec}\left(I_p\right)\right)^{\mathrm{T}} M^{\mathrm{T}} \,\mathrm{vec}\left(I_m\right) \end{aligned}$$

$$= \left(\text{vec}\left(I_p\right)\right)^{\text{T}} \text{vec}\left(\text{vec}^{-1}\left(M^{\text{T}} \text{vec}\left(I_m\right)\right)\right)$$

$$= \text{tr}\left(I_p^{\text{T}}\left(\text{vec}^{-1}\left(M^{\text{T}} \text{vec}\left(I_m\right)\right)\right)\right)$$

$$= \text{tr}\left(\text{vec}^{-1}\left(M^{\text{T}} \text{vec}\left(I_m\right)\right)\right),$$

which proves the lemma. □

The following theorem is a variation of Proposition 8 in [20]. It ultimately provides a mathematical tool to calculate the output performance via the matrix $\mathscr{A}_2$, as presented subsequently in Corollary IV.3.

Theorem IV.2. *For an MSS Markov jump-linear system* (12), *where* $\boldsymbol{\rho}$ *is aperiodic and ergodic, let*

$$\bar{Q}_{\mu_i}(k) := E\left\{\boldsymbol{x}(k)\boldsymbol{x}^{\text{T}}(k)\mathbf{1}_{\{\boldsymbol{\rho}(k)=\mu_i\}}\right\} \text{ for any } k \in \mathbb{Z}^+$$

and

$$\bar{Q}_{\mu_i} := \lim_{k\to\infty} \bar{Q}_{\mu_i}(k).$$

If $\boldsymbol{x}_0$, $\boldsymbol{w}$, *and* $\boldsymbol{\rho}$ *are independent then*

$$\bar{Q}_{\mu_i} = \varphi_{\mu_i}^{-1}\left(\left(I_{MNn^2} - \mathscr{A}_2^{\text{T}}\right)^{-1}\varphi\left(V_{\mu_1}, V_{\mu_2}, \ldots, V_{\mu_{MN}}\right)\right),$$

where $V_{\mu_j} := \sum_{i=1}^{MN}\left[\Pi_{\text{I/O}}\right]_{\mu_i\mu_j} G_{\mu_i} G_{\mu_i}^{\text{T}} \pi_{\text{I/O}}\left(\mu_i\right)$.

Corollary IV.3. *For an MSS Markov jump-linear system* (12), *where* $\boldsymbol{\rho}$ *is aperiodic and ergodic, if* $\boldsymbol{x}_0 = 0$, *and* $\boldsymbol{w}$ *and* $\boldsymbol{\rho}$ *are independent then*

$$J_w = \text{tr}\left(\sum_{j=1}^{MN}\left[\bar{C}_{\mu_j}\bar{Q}_{\mu_j}\right]\right). \tag{20}$$

Proof. For any $k \in \mathbb{Z}^+$,

$$\begin{aligned} J_w &= \lim_{k\to\infty} E\left\{\boldsymbol{y}^{\mathrm{T}}(k)\boldsymbol{y}(k)\right\} \\ &= \lim_{k\to\infty} E\left\{\mathrm{tr}\left(\tilde{C}_{\boldsymbol{\rho}(k)}^{\mathrm{T}}\tilde{C}_{\boldsymbol{\rho}(k)}\boldsymbol{x}(k)\boldsymbol{x}^{\mathrm{T}}(k)\right)\right\} \\ &= \lim_{k\to\infty} \mathrm{tr}\left(\sum_{j=1}^{MN}\left(E\left\{\tilde{C}_{\mu_j}^{\mathrm{T}}\tilde{C}_{\mu_j}\boldsymbol{x}(k)\boldsymbol{x}^{\mathrm{T}}(k)\mathbf{1}_{\{\boldsymbol{\rho}(k)=\mu_j\}}\right\}\right)\right) \\ &= \mathrm{tr}\left(\sum_{j=1}^{MN}\left(\bar{C}_{\mu_j}\cdot\lim_{k\to\infty} E\left\{\boldsymbol{x}(k)\boldsymbol{x}^{\mathrm{T}}(k)\mathbf{1}_{\{\boldsymbol{\rho}(k)=\mu_j\}}\right\}\right)\right) \\ &= \mathrm{tr}\left(\sum_{j=1}^{MN}\left(\bar{C}_{\mu_j}\bar{Q}_{\mu_j}\right)\right), \end{aligned}$$

which completes the proof. □

Shortly, it will be shown in Theorem IV.5 (page 79) that this result concerning J_w can be concisely expressed in terms of a generalized observability Gramian. Before the main output performance results are presented, another useful lemma is given below.

Lemma IV.4. *For an MSS Markov jump-linear system* (12), *given any* $P = (P_1, P_2, \ldots, P_{MN}) \in \mathbb{H}_{MN}^n$:

(a) if $\boldsymbol{w} = 0$, *and* $\boldsymbol{x}_0$ *and* $\boldsymbol{\rho}$ *are independent, then for any* $k \in \mathbb{Z}^+$

$$E\left\{\boldsymbol{x}^{\mathrm{T}}(k+1)P_{\boldsymbol{\rho}(k+1)}\boldsymbol{x}(k+1)\right\} = E\left\{\boldsymbol{x}^{\mathrm{T}}(k)\mathcal{L}_{\boldsymbol{\rho}(k)}(P)\boldsymbol{x}(k)\right\};$$

(b) if $\boldsymbol{x}_0 = 0$, *and* $\boldsymbol{w}$ *and* $\boldsymbol{\rho}$ *are independent, then for any* $k \in \mathbb{Z}^+$

$$\begin{aligned} &E\left\{\boldsymbol{x}^{\mathrm{T}}(k+1)P_{\boldsymbol{\rho}(k+1)}\boldsymbol{x}(k+1)\right\} \\ &\quad = E\left\{\boldsymbol{x}^{\mathrm{T}}(k)\mathcal{L}_{\boldsymbol{\rho}(k)}(P)\boldsymbol{x}(k)\right\} + E\left\{\mathrm{tr}\left(\tilde{G}_{\boldsymbol{\rho}(k)}^{\mathrm{T}}P_{\boldsymbol{\rho}(k+1)}\tilde{G}_{\boldsymbol{\rho}(k)}\right)\right\}. \end{aligned}$$

Proof. (a) For any $k \in \mathbb{Z}^+$, observe

$$
\begin{aligned}
&E\left\{\boldsymbol{x}^{\mathrm{T}}(k+1)P_{\boldsymbol{\rho}(k+1)}\boldsymbol{x}(k+1)\right\} \\
&\quad = E\left\{\boldsymbol{x}^{\mathrm{T}}(k)\tilde{A}^{\mathrm{T}}_{\boldsymbol{\rho}(k)}P_{\boldsymbol{\rho}(k+1)}\tilde{A}_{\boldsymbol{\rho}(k)}\boldsymbol{x}(k)\right\} \\
&\quad = \sum_{i,j=1}^{MN} E\left\{\boldsymbol{x}^{\mathrm{T}}(k)\tilde{A}^{\mathrm{T}}_{\mu_i}P_{\mu_j}\tilde{A}_{\mu_i}\boldsymbol{x}(k)\mathbf{1}_{\{\boldsymbol{\rho}(k)=\mu_i\}}\mathbf{1}_{\{\boldsymbol{\rho}(k+1)=\mu_j\}}\right\} \\
&\quad = \sum_{i,j=1}^{MN} E\left\{E\left\{\boldsymbol{x}^{\mathrm{T}}(k)\tilde{A}^{\mathrm{T}}_{\mu_i}P_{\mu_j}\tilde{A}_{\mu_i}\boldsymbol{x}(k)\mathbf{1}_{\{\boldsymbol{\rho}(k)=\mu_i\}}\mathbf{1}_{\{\boldsymbol{\rho}(k+1)=\mu_j\}} \mid \boldsymbol{x}(k), \boldsymbol{\rho}(k)\right\}\right\} \\
&\quad = \sum_{i,j=1}^{MN} E\left\{\boldsymbol{x}^{\mathrm{T}}(k)\tilde{A}^{\mathrm{T}}_{\mu_i}P_{\mu_j}\tilde{A}_{\mu_i}\boldsymbol{x}(k)\mathbf{1}_{\{\boldsymbol{\rho}(k)=\mu_i\}}E\left\{\mathbf{1}_{\{\boldsymbol{\rho}(k+1)=\mu_j\}} \mid \boldsymbol{x}(k), \boldsymbol{\rho}(k)=\mu_i\right\}\right\} \\
&\quad = \sum_{i,j=1}^{MN} E\left\{\boldsymbol{x}^{\mathrm{T}}(k)\tilde{A}^{\mathrm{T}}_{\mu_i}P_{\mu_j}\tilde{A}_{\mu_i}\boldsymbol{x}(k)\mathbf{1}_{\{\boldsymbol{\rho}(k)=\mu_i\}}E\left\{\mathbf{1}_{\{\boldsymbol{\rho}(k+1)=\mu_j\}} \mid \boldsymbol{\rho}(k)=\mu_i\right\}\right\} \\
&\quad = \sum_{i,j=1}^{MN} E\left\{\boldsymbol{x}^{\mathrm{T}}(k)\tilde{A}^{\mathrm{T}}_{\mu_i}P_{\mu_j}\tilde{A}_{\mu_i}\boldsymbol{x}(k)\mathbf{1}_{\{\boldsymbol{\rho}(k)=\mu_i\}}\left[\Pi_{\mathrm{I/O}}\right]_{\mu_i\mu_j}\right\} \\
&\quad = \sum_{i=1}^{MN} E\left\{\boldsymbol{x}^{\mathrm{T}}(k)\left(\tilde{A}^{\mathrm{T}}_{\mu_i}\sum_{j=1}^{MN}\left[\Pi_{\mathrm{I/O}}\right]_{\mu_i\mu_j}P_{\mu_j}\tilde{A}_{\mu_i}\right)\boldsymbol{x}(k)\mathbf{1}_{\{\boldsymbol{\rho}(k)=\mu_i\}}\right\} \\
&\quad = \sum_{i=1}^{MN} E\left\{\boldsymbol{x}^{\mathrm{T}}(k)\mathcal{L}_{\mu_i}(P)\boldsymbol{x}(k)\mathbf{1}_{\{\boldsymbol{\rho}(k)=\mu_i\}}\right\} \\
&\quad = E\left\{\boldsymbol{x}^{\mathrm{T}}(k)\mathcal{L}_{\boldsymbol{\rho}(k)}(P)\boldsymbol{x}(k)\right\}.
\end{aligned}
$$

(b) For any $k \in \mathbb{Z}^+$, using the independence assumption and the fact that $E\left\{\boldsymbol{w}(k)\boldsymbol{w}^{\mathrm{T}}(l)\right\} = I_m \cdot \mathbf{1}_{\{k=l\}}$ and $E\left\{\boldsymbol{w}(k)\right\} = 0$, it follows that

$$
\begin{aligned}
&E\left\{\boldsymbol{x}^{\mathrm{T}}(k+1)P_{\boldsymbol{\rho}(k+1)}\boldsymbol{x}(k+1)\right\} \\
&\quad = E\Big\{\left[\tilde{A}_{\boldsymbol{\rho}(k)}\boldsymbol{x}(k)+\tilde{G}_{\boldsymbol{\rho}(k)}\boldsymbol{w}(k)\right]^{\mathrm{T}}P_{\boldsymbol{\rho}(k+1)}\left[\tilde{A}_{\boldsymbol{\rho}(k)}\boldsymbol{x}(k)+\tilde{G}_{\boldsymbol{\rho}(k)}\boldsymbol{w}(k)\right]\Big\} \\
&\quad = E\Big\{\boldsymbol{x}^{\mathrm{T}}(k)A^{\mathrm{T}}_{\boldsymbol{\rho}(k)}P_{\boldsymbol{\rho}(k+1)}\tilde{A}_{\boldsymbol{\rho}(k)}\boldsymbol{x}(k)+\boldsymbol{x}^{\mathrm{T}}(k)A^{\mathrm{T}}_{\boldsymbol{\rho}(k)}P_{\boldsymbol{\rho}(k+1)}\tilde{G}_{\boldsymbol{\rho}(k)}\boldsymbol{w}(k)\Big\} \\
&\qquad + \Big\{\boldsymbol{w}^{\mathrm{T}}(k)\tilde{G}^{\mathrm{T}}_{\boldsymbol{\rho}(k)}P_{\boldsymbol{\rho}(k+1)}\tilde{A}_{\boldsymbol{\rho}(k)}\boldsymbol{x}(k)+\boldsymbol{w}^{\mathrm{T}}(k)\tilde{G}^{\mathrm{T}}_{\boldsymbol{\rho}(k)}P_{\boldsymbol{\rho}(k+1)}\tilde{G}_{\boldsymbol{\rho}(k)}\boldsymbol{w}(k)\Big\} \\
&\quad = E\Big\{\boldsymbol{x}^{\mathrm{T}}(k)A^{\mathrm{T}}_{\boldsymbol{\rho}(k)}P_{\boldsymbol{\rho}(k+1)}\tilde{A}_{\boldsymbol{\rho}(k)}\boldsymbol{x}(k)+\boldsymbol{w}^{\mathrm{T}}(k)\tilde{G}^{\mathrm{T}}_{\boldsymbol{\rho}(k)}P_{\boldsymbol{\rho}(k+1)}\tilde{G}_{\boldsymbol{\rho}(k)}\boldsymbol{w}(k)\Big\}
\end{aligned}
$$

$$= E\left\{\boldsymbol{x}^{\mathrm{T}}(k)\mathcal{L}_{\boldsymbol{\rho}(k)}(P)\boldsymbol{x}(k) + \mathrm{tr}\left(\tilde{G}^{\mathrm{T}}_{\boldsymbol{\rho}(k)}P_{\boldsymbol{\rho}(k+1)}\tilde{G}_{\boldsymbol{\rho}(k)}\right)\right\}.$$

The proof of the lemma is complete. □

The main results concerning output performance of the Markov jump-linear system (12) are given next. Specifically, it is shown that the mean output energy, J_0, and the mean output power, J_w, of this system can be concisely written in terms of generalized observability Gramians.

Theorem IV.5. *Consider an MSS stochastic hybrid model with Markov jump-linear system* (12)*, where* $\boldsymbol{\rho}$ *is aperiodic and ergodic.*

(a) If $\boldsymbol{w} = 0$*, and* $\boldsymbol{x}_0$ *and* $\boldsymbol{\rho}$ *are assumed to be independent, then the mean output energy is*

$$J_0 = E\left\{\boldsymbol{x}_0^{\mathrm{T}}\left[\sum_{k=0}^{\infty}\mathcal{L}^k_{\boldsymbol{\rho}_0}(\bar{C})\right]\boldsymbol{x}_0\right\} = \mathrm{tr}(X_0Q_0), \tag{21}$$

where $X_0 := E\left\{\boldsymbol{x}_0\boldsymbol{x}_0^{\mathrm{T}}\right\}$, $Q_0 := E\left\{\sum_{k=0}^{\infty}\mathcal{L}^k_{\boldsymbol{\rho}_0}(\bar{C})\right\}$, *and* $\mathcal{L}^k$ *denotes the composition of* $\mathcal{L}$ k *times* ($\mathcal{L}^0(\bar{C}) := \bar{C}$).

(b) If $\boldsymbol{x}_0 = 0$ *and* $\boldsymbol{w}$ *and* $\boldsymbol{\rho}$ *are assumed to be independent then the mean output power is*

$$J_w = \lim_{k\to\infty} E\left\{\mathrm{tr}\left(\sum_{i=0}^{k-1}\left[\tilde{G}^{\mathrm{T}}_{\boldsymbol{\rho}(k-i-1)}\mathcal{L}^i_{\boldsymbol{\rho}(k-i)}(\bar{C})\tilde{G}_{\boldsymbol{\rho}(k-i-1)}\right]\right)\right\} = \mathrm{tr}\left(E\left\{\bar{G}_{\boldsymbol{\rho}_{\mathrm{s}}}\tilde{Q}_{\boldsymbol{\rho}_{\mathrm{s}}}\right\}\right), \tag{22}$$

where $\bar{G}_{\boldsymbol{\rho}_{\mathrm{s}}} := \tilde{G}_{\boldsymbol{\rho}_{\mathrm{s}}}\tilde{G}^{\mathrm{T}}_{\boldsymbol{\rho}_{\mathrm{s}}}$ *and* $\tilde{Q}_{\boldsymbol{\rho}_{\mathrm{s}}} := \mathcal{E}_{\boldsymbol{\rho}_{\mathrm{s}}}\left(\sum_{k=0}^{\infty}\mathcal{L}^k(\bar{C})\right)$.

Proof. (a) Noting that $\boldsymbol{x}_0$ is independent of $\boldsymbol{\rho}_0$, the result is immediate once it is proven for any $k \in \mathbb{Z}^+$ that

$$E\left\{\|\boldsymbol{y}(k)\|^2\right\} = E\left\{\boldsymbol{x}_0^{\mathrm{T}}\mathcal{L}^k_{\boldsymbol{\rho}_0}(\bar{C})\boldsymbol{x}_0\right\}. \tag{23}$$

When $k = 0$,

$$\begin{aligned} E\left\{\|\boldsymbol{y}(0)\|^2\right\} &= E\left\{\boldsymbol{x}_0^{\mathrm{T}}\tilde{C}_{\boldsymbol{\rho}_0}^{\mathrm{T}}\tilde{C}_{\boldsymbol{\rho}_0}\boldsymbol{x}_0\right\} \\ &= E\left\{\boldsymbol{x}_0^{\mathrm{T}}\bar{C}_{\boldsymbol{\rho}_0}\boldsymbol{x}_0\right\} \\ &= E\left\{\boldsymbol{x}_0^{\mathrm{T}}\mathcal{L}_{\boldsymbol{\rho}_0}^0(\bar{C})\boldsymbol{x}_0\right\}. \end{aligned}$$

For any $k \geq 1$ observe that

$$\begin{aligned} E\left\{\|\boldsymbol{y}(k)\|^2\right\} &= E\left\{\boldsymbol{x}^{\mathrm{T}}(k)\bar{C}_{\boldsymbol{\rho}(k)}\boldsymbol{x}(k)\right\} \\ &= E\left\{\boldsymbol{x}^{\mathrm{T}}(k)\mathcal{L}_{\boldsymbol{\rho}(k)}^0(\bar{C})\boldsymbol{x}(k)\right\}. \end{aligned}$$

Now since $\mathcal{L}^k(\bar{C}) \in \mathbb{H}_{MN}^n$, (23) follows directly by repeatedly applying Lemma IV.4(a) k times.

(b) Since $\boldsymbol{x}_0$, $\boldsymbol{\rho}$ and $\boldsymbol{w}$ are independent, and $E\{\boldsymbol{w}(k)\} = 0$, the natural response of the MSS Markov jump-linear system has zero average power. Hence, there is no loss of generality in assuming that $\boldsymbol{x}_0 = 0$. Trivially then $E\left\{\|\boldsymbol{y}(0)\|^2\right\} = 0$. When $k = 1$,

$$\begin{aligned} E\left\{\|\boldsymbol{y}(1)\|^2\right\} &= E\left\{\boldsymbol{w}^{\mathrm{T}}(0)\tilde{G}_{\boldsymbol{\rho}_0}^{\mathrm{T}}\bar{C}_{\boldsymbol{\rho}(1)}\tilde{G}_{\boldsymbol{\rho}_0}\boldsymbol{w}(0)\right\} \\ &= E\left\{\mathrm{tr}\left(\boldsymbol{w}(0)\boldsymbol{w}^{\mathrm{T}}(0)\cdot\tilde{G}_{\boldsymbol{\rho}_0}^{\mathrm{T}}\bar{C}_{\boldsymbol{\rho}(1)}\tilde{G}_{\boldsymbol{\rho}_0}\right)\right\} \\ &= \mathrm{tr}\left(E\left\{\boldsymbol{w}(0)\boldsymbol{w}^{\mathrm{T}}(0)\right\}\cdot E\left\{\tilde{G}_{\boldsymbol{\rho}_0}^{\mathrm{T}}\bar{C}_{\boldsymbol{\rho}(1)}\tilde{G}_{\boldsymbol{\rho}_0}\right\}\right) \\ &= E\left\{\mathrm{tr}\left(\tilde{G}_{\boldsymbol{\rho}_0}^{\mathrm{T}}\bar{C}_{\boldsymbol{\rho}(1)}\tilde{G}_{\boldsymbol{\rho}_0}\right)\right\} \\ &= E\left\{\mathrm{tr}\left(\tilde{G}_{\boldsymbol{\rho}_0}^{\mathrm{T}}\mathcal{L}_{\boldsymbol{\rho}(1)}^0(\bar{C})\tilde{G}_{\boldsymbol{\rho}_0}\right)\right\}. \end{aligned}$$

For any $k > 1$, simply apply Lemma IV.4(b) $(k-1)$ times, and under the given conditions the first equality of (22) holds. The fact that $\boldsymbol{\rho}(k)$ is aperiodic and

ergodic (i.e., the states of $\boldsymbol{\rho}(k)$ form a single ergodic class) ensures that the limit with respect to k is well defined and independent of $\boldsymbol{\rho}_0$. To validate the second equality of (22), it will be enough to show that (20) and (22) are equivalent. Let

$$Q = (Q_{\mu_1}, Q_{\mu_2}, \ldots, Q_{\mu_{MN}}) := \sum_{k=0}^{\infty} \mathcal{L}^k \left(\bar{C}\right) \tag{24}$$

then

$$\varphi(Q) = \left(I_{MNn^2} - \mathscr{A}_2\right)^{-1} \begin{bmatrix} C_1^{\mathrm{T}} \otimes C_1^{\mathrm{T}} \\ C_2^{\mathrm{T}} \otimes C_2^{\mathrm{T}} \\ \vdots \\ C_{MN}^{\mathrm{T}} \otimes C_{MN}^{\mathrm{T}} \end{bmatrix} \mathrm{vec}\left(I_p\right),$$

and

$$\begin{aligned} \tilde{Q}_{\mu_i} &= \mathcal{E}_{\mu_i}(Q) \\ &= \sum_{j=1}^{MN} \left[\Pi_{\mathrm{I/O}}\right]_{\mu_i\mu_j} Q_{\mu_j} \\ &= \begin{bmatrix} Q_{\mu_1} & Q_{\mu_2} & \cdots & Q_{\mu_{MN}} \end{bmatrix} \left(\begin{bmatrix} \left[\Pi_{\mathrm{I/O}}\right]_{\mu_i\mu_1} \\ \left[\Pi_{\mathrm{I/O}}\right]_{\mu_i\mu_2} \\ \vdots \\ \left[\Pi_{\mathrm{I/O}}\right]_{\mu_i\mu_{MN}} \end{bmatrix} \otimes I_n \right). \end{aligned}$$

In addition,

$$\begin{aligned} &\mathrm{tr}\left(G_{\boldsymbol{\rho}_{\mathrm{s}}}^{\mathrm{T}} \mathcal{E}_{\boldsymbol{\rho}_{\mathrm{s}}}(Q) G_{\boldsymbol{\rho}_{\mathrm{s}}}\right) \\ &= \mathrm{tr}\left(\sum_{i=1}^{MN} \left[G_{\mu_i}^{\mathrm{T}} \mathcal{E}_{\mu_i}(Q) G_{\mu_i} \pi_{\mathrm{I/O}}\left(\mu_i\right)\right]\right) \end{aligned} \tag{25}$$

$$= \mathrm{tr}\left(\sum_{i=1}^{MN}\left[G_{\mu_i}^{\mathrm{T}}\left(\begin{bmatrix}Q_1 & Q_2 & \cdots & Q_{MN}\end{bmatrix}\left(\begin{bmatrix}\left[\Pi_{\mathrm{I/O}}\right]_{\mu_i\mu_1}\\ \left[\Pi_{\mathrm{I/O}}\right]_{\mu_i\mu_2}\\ \vdots \\ \left[\Pi_{\mathrm{I/O}}\right]_{\mu_i\mu_N}\end{bmatrix}\otimes I_n\right)\right)\right.\right.$$

$$\left.\left.\cdot G_{\mu_i}\pi_{\mathrm{I/O}}\left(\mu_i\right)\right]\right)$$

$$= \mathrm{tr}\left(\mathrm{vec}^{-1}\left(\left[\sum_{i=1}^{MN}\left(\left[\pi_{\mathrm{I/O}}\left(\mu_i\right)G_{\mu_i}^{\mathrm{T}}\left(\left[\begin{matrix}\left[\Pi_{\mathrm{I/O}}\right]_{\mu_i\mu_1} & \left[\Pi_{\mathrm{I/O}}\right]_{\mu_i\mu_2}\\ \cdots & \left[\Pi_{\mathrm{I/O}}\right]_{\mu_i\mu_{MN}}\end{matrix}\right]\otimes I_n\right)\right]\otimes G_{\mu_i}^{\mathrm{T}}\right)\right]\left(I_{MNn^2}-\mathscr{A}_2\right)^{-1}\right.\right.$$

$$\left.\left.\cdot\begin{bmatrix}C_{\mu_1}^{\mathrm{T}}\otimes C_{\mu_1}^{\mathrm{T}}\\ C_{\mu_2}^{\mathrm{T}}\otimes C_{\mu_2}^{\mathrm{T}}\\ \vdots \\ C_{\mu_{MN}}^{\mathrm{T}}\otimes C_{\mu_{MN}}^{\mathrm{T}}\end{bmatrix}\mathrm{vec}\left(I_p\right)\right)\right)$$

$$= \mathrm{tr}\left(\mathrm{vec}^{-1}\left(\left[\sum_{i=1}^{MN}\left(\left[\begin{matrix}\left[\Pi_{\mathrm{I/O}}\right]_{\mu_i\mu_1}\pi_{\mathrm{I/O}}\left(\mu_i\right)G_{\mu_i}^{\mathrm{T}} & \left[\Pi_{\mathrm{I/O}}\right]_{\mu_i\mu_2}\pi_{\mathrm{I/O}}\left(\mu_i\right)G_{\mu_i}^{\mathrm{T}}\\ \cdots & \left[\Pi_{\mathrm{I/O}}\right]_{\mu_i\mu_{MN}}\pi_{\mathrm{I/O}}\left(\mu_i\right)G_{\mu_i}^{\mathrm{T}}\end{matrix}\right]\otimes G_{\mu_i}^{\mathrm{T}}\right)\right]\left(I_{MNn^2}-\mathscr{A}_2\right)^{-1}\right.\right.$$

$$\cdot \left[\begin{array}{c} C_{\mu_1}^{\mathrm{T}} \otimes C_{\mu_1}^{\mathrm{T}} \\ C_{\mu_2}^{\mathrm{T}} \otimes C_{\mu_2}^{\mathrm{T}} \\ \vdots \\ C_{\mu_{MN}}^{\mathrm{T}} \otimes C_{\mu_{MN}}^{\mathrm{T}} \end{array} \right] \operatorname{vec}(I_p) \Bigg) \Bigg)$$

$$= \operatorname{tr} \left(\operatorname{vec}^{-1} \left(\left[\sum_{i=1}^{MN} \left(\left[\left[\Pi_{\mathrm{I/O}} \right]_{\mu_i \mu_1} \pi_{\mathrm{I/O}}(\mu_i) G_{\mu_i}^{\mathrm{T}} \otimes G_{\mu_i}^{\mathrm{T}} \right. \right. \right. \right.$$

$$\left. \left. \left. \left. \cdots \quad \left[\Pi_{\mathrm{I/O}} \right]_{\mu_i \mu_{MN}} \pi_{\mathrm{I/O}}(\mu_i) G_{\mu_i}^{\mathrm{T}} \otimes G_{\mu_i}^{\mathrm{T}} \right] \right) \right] \right.$$

$$\left. \cdot \left(I_{MNn^2} - \mathscr{A}_2 \right)^{-1} \left[\begin{array}{c} C_{\mu_1}^{\mathrm{T}} \otimes C_{\mu_1}^{\mathrm{T}} \\ C_{\mu_2}^{\mathrm{T}} \otimes C_{\mu_2}^{\mathrm{T}} \\ \vdots \\ C_{\mu_{MN}}^{\mathrm{T}} \otimes C_{\mu_{MN}}^{\mathrm{T}} \end{array} \right] \operatorname{vec}(I_p) \right) \Bigg) \Bigg)$$

$$= \operatorname{tr} \left(\operatorname{vec}^{-1} \left(M \operatorname{vec}(I_p) \right) \right), \tag{26}$$

where

$$M := \left[\sum_{i=1}^{MN} \left[\Pi_{\mathrm{I/O}} \right]_{\mu_i \mu_1} \pi_{\mathrm{I/O}}(\mu_i) G_{\mu_i}^{\mathrm{T}} \otimes G_{\mu_i}^{\mathrm{T}} \right.$$

$$\left. \cdots \quad \sum_{i=1}^{MN} \left[\Pi_{\mathrm{I/O}} \right]_{\mu_i \mu_{MN}} \pi_{\mathrm{I/O}}(\mu_i) G_{\mu_i}^{\mathrm{T}} \otimes G_{\mu_i}^{\mathrm{T}} \right]$$

$$\cdot \left(I_{MNn^2} - \mathscr{A}_2 \right)^{-1} \left[\begin{array}{c} C_{\mu_1}^{\mathrm{T}} \otimes C_{\mu_1}^{\mathrm{T}} \\ C_{\mu_2}^{\mathrm{T}} \otimes C_{\mu_2}^{\mathrm{T}} \\ \vdots \\ C_{\mu_{MN}}^{\mathrm{T}} \otimes C_{\mu_{MN}}^{\mathrm{T}} \end{array} \right].$$

Next observe that according to Theorem IV.2, if for $j \in \{1, 2, \ldots, MN\}$,

$$V_{\mu_j} := \sum_{i=1}^{MN} \left[\Pi_{\mathrm{I/O}}\right]_{\mu_i \mu_j} G_{\mu_i} G_{\mu_i}^{\mathrm{T}} \pi_{\mathrm{I/O}}\left(\mu_i\right),$$

then for $V = (V_{\mu_1}, V_{\mu_2}, \ldots, V_{\mu_{MN}})$,

$$\begin{aligned}
\varphi(V) &= \begin{bmatrix} \operatorname{vec}\left(V_{\mu_1}\right) \\ \operatorname{vec}\left(V_{\mu_2}\right) \\ \vdots \\ \operatorname{vec}\left(V_{\mu_{MN}}\right) \end{bmatrix} \\
&= \begin{bmatrix} \sum_{i=1}^{MN} \left[\Pi_{\mathrm{I/O}}\right]_{\mu_i \mu_1} \pi_{\mathrm{I/O}}\left(\mu_i\right) G_{\mu_i} \otimes G_{\mu_i} \\ \sum_{i=1}^{MN} \left[\Pi_{\mathrm{I/O}}\right]_{\mu_i \mu_2} \pi_{\mathrm{I/O}}\left(\mu_i\right) G_{\mu_i} \otimes G_{\mu_i} \\ \vdots \\ \sum_{i=1}^{MN} \left[\Pi_{\mathrm{I/O}}\right]_{\mu_i \mu_{MN}} \pi_{\mathrm{I/O}}\left(\mu_i\right) G_{\mu_i} \otimes G_{\mu_i} \end{bmatrix} \operatorname{vec}\left(I_m\right).
\end{aligned}$$

Therefore,

$$\begin{aligned}
\varphi\left(\bar{Q}\right) &= \left(I_{MNn^2} - \mathscr{A}_2^{\mathrm{T}}\right)^{-1} \varphi(V) \\
&= \left(I_{MNn^2} - \mathscr{A}_2^{\mathrm{T}}\right)^{-1} \begin{bmatrix} \sum_{i=1}^{MN} \left[\Pi_{\mathrm{I/O}}\right]_{\mu_i \mu_1} \pi_{\mathrm{I/O}}\left(\mu_i\right) G_{\mu_i} \otimes G_{\mu_i} \\ \sum_{i=1}^{MN} \left[\Pi_{\mathrm{I/O}}\right]_{\mu_i \mu_2} \pi_{\mathrm{I/O}}\left(\mu_i\right) G_{\mu_i} \otimes G_{\mu_i} \\ \vdots \\ \sum_{i=1}^{MN} \left[\Pi_{\mathrm{I/O}}\right]_{\mu_i \mu_{MN}} \pi_{\mathrm{I/O}}\left(\mu_i\right) G_{\mu_i} \otimes G_{\mu_i} \end{bmatrix} \operatorname{vec}\left(I_m\right).
\end{aligned}$$

But according to Corollary IV.3,

$$J_w = \operatorname{tr}\left(\sum_{i=1}^{MN} \left[C_{\mu_j} \bar{Q}_{\mu_j} C_{\mu_j}^{\mathrm{T}}\right]\right)$$

$$= \mathrm{tr}\left(\mathrm{vec}^{-1}\left(\left[C_{\mu_1}\otimes C_{\mu_1} \quad C_{\mu_2}\otimes C_{\mu_2} \quad \cdots \quad C_{\mu_{MN}}\otimes C_{\mu_{MN}}\right]\varphi\left(\bar{Q}\right)\right)\right)$$

$$= \mathrm{tr}\left(\mathrm{vec}^{-1}\left(\left[C_{\mu_1}\otimes C_{\mu_1} \quad C_{\mu_2}\otimes C_{\mu_2} \quad \cdots \quad C_{\mu_{MN}}\otimes C_{\mu_{MN}}\right]\right.\right.$$

$$\left.\left.\cdot\left(I_{MNn^2}-\mathscr{A}_2^{\mathrm{T}}\right)^{-1}\begin{bmatrix}\sum_{i=1}^{MN}\left[\Pi_{\mathrm{I/O}}\right]_{\mu_i\mu_1}\pi_{\mathrm{I/O}}\left(\mu_i\right)G_{\mu_i}\otimes G_{\mu_i}\\ \sum_{i=1}^{MN}\left[\Pi_{\mathrm{I/O}}\right]_{\mu_i\mu_2}\pi_{\mathrm{I/O}}\left(\mu_i\right)G_{\mu_i}\otimes G_{\mu_i}\\ \vdots\\ \sum_{i=1}^{MN}\left[\Pi_{\mathrm{I/O}}\right]_{\mu_i\mu_{MN}}\pi_{\mathrm{I/O}}\left(\mu_i\right)G_{\mu_i}\otimes G_{\mu_i}\end{bmatrix}\mathrm{vec}\left(I_m\right)\right)\right)$$

$$= \mathrm{tr}\left(\mathrm{vec}^{-1}\left(M^{\mathrm{T}}\,\mathrm{vec}\left(I_m\right)\right)\right). \tag{27}$$

According to Lemma IV.1, the right-hand sides of (26) and (27) are equivalent. Thus, the proof is complete. □

The following corollary shows that Theorem 2(b) in [86] is a special case of Theorem IV.5(b).

Corollary IV.6. *In the context of Theorem* IV.5(b), *if* $\tilde{G}_{\mu_i}\equiv\tilde{G}$ *for* $i=1,2,\ldots,MN$ *then*

$$J_w = \mathrm{tr}\left(\tilde{G}_w E\left\{\tilde{Q}_{\boldsymbol{\rho}_{\mathrm{s}}}\right\}\right)\equiv\mathrm{tr}\left(\tilde{G}_w Q_w\right), \tag{28}$$

where $\tilde{G}_w := \tilde{G}\tilde{G}^{\mathrm{T}}$ *and* $Q_w := E\left\{Q_{\boldsymbol{\rho}_{\mathrm{s}}}\right\}$.

Proof. Observe, using (18) and (24), that

$$\begin{aligned}
E\left\{\tilde{Q}_{\rho_s}\right\} &= E\left\{\mathcal{E}_{\rho_s}(Q)\right\} \\
&= E\left\{\sum_{j=1}^{MN}\left[\left[\Pi_{\mathrm{I/O}}\right]_{\rho_s\mu_j} Q_{\mu_j}\right]\right\} \\
&= \sum_{i=1}^{MN}\left[\left(\sum_{j=1}^{MN}\left[\Pi_{\mathrm{I/O}}\right]_{\mu_i\mu_j} Q_{\mu_j}\right)\pi_{\mathrm{I/O}}(\mu_i)\right] \\
&= \sum_{j=1}^{MN}\left[\left(\sum_{i=1}^{MN}\left[\Pi_{\mathrm{I/O}}\right]_{\mu_i\mu_j} \pi_{\mathrm{I/O}}(\mu_i)\right) Q_{\mu_j}\right] \\
&= \sum_{j=1}^{MN}\left[\pi_{\mathrm{I/O}}(\mu_j) Q_{\mu_j}\right] \\
&= E\left\{Q_{\rho_s}\right\} \\
&= Q_w.
\end{aligned}$$

This completes the proof. □

Corollary IV.7. *If $M = N = 1$, then system (12) is a non-switching system with $[\Pi]_{\mathrm{I/O}} = 1$. Let $\tilde{A}_1 = \hat{A}$ with $r_\sigma\left(\hat{A}\right) < 1$, $\tilde{G}_1 = G$ and $\tilde{C}_1 = C$. Then*

$$J_w = \mathrm{tr}\left(G_w \hat{Q}_w\right), \tag{29}$$

where $G_w := GG^{\mathrm{T}}$ and $\hat{Q}_w := \sum_{k=0}^{\infty}\left[\left(\hat{A}^{\mathrm{T}}\right)^k C^{\mathrm{T}} C \hat{A}^k\right]$, which is exactly the observability Gramian matrix.

IV.3 SIMPLE EXAMPLES

When system (12) is MSS, the result in Theorem III.4(d) can be used to calculate J_0 and J_w analytically. From the MSS property, it is clear that Q as defined in (24) is the unique solution to $Q - \mathcal{L}(Q) = \bar{C}$. This adjoint coupled Lyapunov equation can be solved using $\mathscr{A}_2$, which is a matrix representation of $\mathcal{L}$. By means of the

linear column stacking operator φ and its inverse operator φ^{-1}, the adjoint coupled Lyapunov equation can be written as the matrix equation

$$\varphi(Q) - \mathscr{A}_2 \cdot \varphi(Q) = \varphi\left(\bar{C}\right),$$

and hence

$$Q = \varphi^{-1}\left(\left(I_{MNn^2} - \mathscr{A}_2\right)^{-1} \cdot \varphi(\bar{C})\right).$$

Therefore, the tracking error measures can be written in terms of

$$Q_0 = E\left\{\sum_{k=0}^{\infty} \mathcal{L}_{\boldsymbol{\rho}_0}^k(\bar{C})\right\} = \sum_{i=1}^{MN} Q_{\mu_i} \Pr\{\boldsymbol{\rho}_0 = \mu_i\}$$
$$\tilde{Q}_{\boldsymbol{\rho}_s} = \mathcal{E}_{\boldsymbol{\rho}_s}\left(\sum_{k=0}^{\infty} \mathcal{L}^k(\bar{C})\right) = \sum_{j=1}^{MN}\left(\left[\Pi_{\mathrm{I/O}}\right]_{\boldsymbol{\rho}_s \mu_j} Q_{\mu_j}\right)$$

and

$$Q_w = E\left\{\sum_{k=0}^{\infty} \mathcal{L}_{\boldsymbol{\rho}_s}^k(\bar{C})\right\} = \sum_{j=1}^{MN} Q_{\mu_j} \Pr\{\boldsymbol{\rho}_s = \mu_j\}.$$

Specifically, the mean output energy, J_0, and the mean output power, J_w, can be expressed as

$$J_0 = \mathrm{tr}\left(X_0 \sum_{i=1}^{MN} Q_{\mu_i} \Pr\{\boldsymbol{\rho}_0 = \mu_i\}\right)$$
$$J_w = \mathrm{tr}\left(\sum_{i=1}^{MN}\sum_{j=1}^{MN} \left[\Pi_{\mathrm{I/O}}\right]_{\mu_i \mu_j} \bar{G}_{\mu_i} Q_{\mu_j} \Pr\{\boldsymbol{\rho}_s = \mu_i\}\right),$$

and when $\tilde{G}_{\mu_i} \equiv \tilde{G}$ for $i = 1, 2, \ldots, MN$, then

$$J_w = \mathrm{tr}\left(\tilde{G}_w \sum_{j=1}^{MN} Q_{\mu_j} \Pr\{\boldsymbol{\rho}_s = \mu_j\}\right).$$

The following example is used to demonstrate the theoretical results given in Theorem IV.5 and Corollary IV.6 using a simulation.

Example IV.1. Consider a pair of one-dimensional (scalar) systems (A_i, G, C_i), $i = 1, 2$ driven by a Markovian jump-linear system $\boldsymbol{\rho}(k)$ with the parameters given in Table III. Here the transition probability $[\Pi]_{12}$ is varied between $[0, 0.90]$ (which

TABLE III
Parameters for the Simulation Example IV.1

Parameters	Values
A_1	0.99
A_2	1.01
C_1	1.50
C_2	1.50
G	2.00
$\Pr\{\boldsymbol{\rho}_0 = 1\}$	0.50
$\Pr\{\boldsymbol{\rho}_0 = 2\}$	0.50
$\boldsymbol{x}_0$	0 or uniform on $[0, 1]$
$\Pi = \begin{bmatrix} 1 - [\Pi]_{12} & [\Pi]_{12} \\ 0.90 & 0.10 \end{bmatrix}$	$[\Pi]_{12} \in [0,\ 0.9]$

ensures the system is MSS). According to Theorem IV.5 and Corollary IV.6, the plots of J_0 and J_w with respect to $[\Pi]_{12}$ are shown in Fig. 24. It is clear that J_0 and J_w increase as the transition probability $[\Pi]_{12}$ increases. Roughly speaking, the increasing $[\Pi]_{12}$ causes the unstable A_2 to appear more frequently, so that the Markov jump-linear system approaches instability. On the other hand, when $[\Pi]_{12} = 0.05$,

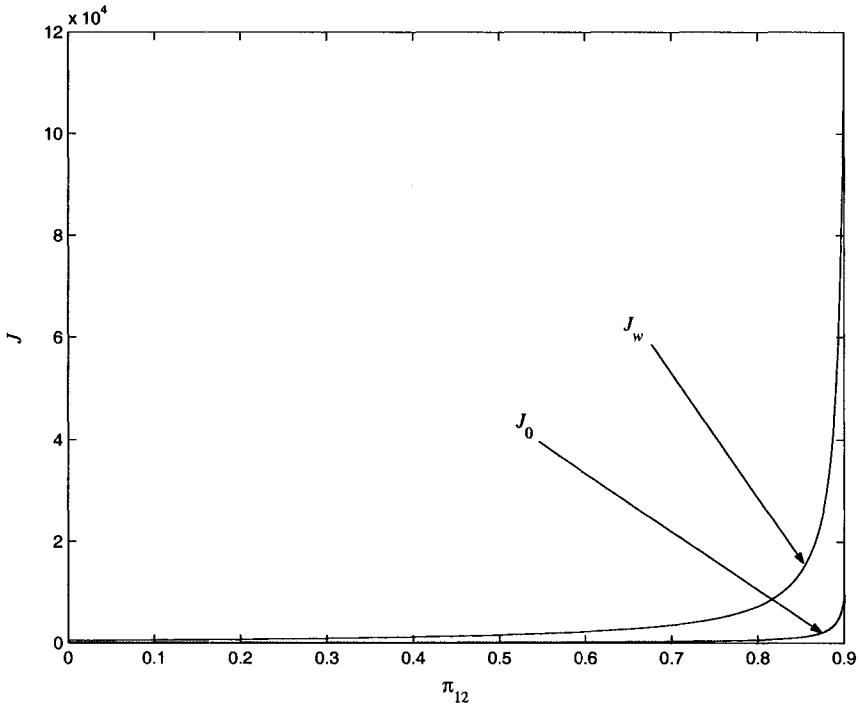

Fig. 24. Plots of J_0 and J_w with respect to the transition probability $[\Pi]_{12}$.

for example, then

$$Q = \begin{bmatrix} Q_1 & Q_2 \end{bmatrix} = \begin{bmatrix} 126.1912 & 131.5214 \end{bmatrix},$$

and thus,

$$Q_0 = Q_1 \cdot \Pr\{\boldsymbol{\rho}_0 = 1\} + Q_2 \cdot \Pr\{\boldsymbol{\rho}_0 = 2\} = 128.8563.$$

Moreover, $X_0 = E\left\{\boldsymbol{x}_0 \boldsymbol{x}_0^{\mathrm{T}}\right\} = \frac{1}{3}$, so by (21) $J_0 = 42.9521$. By comparison, the Monte-Carlo simulation estimate calculated from (12) via $\boldsymbol{y}(k)$ is $J_0 = 42.6461$. In addition, when $\boldsymbol{x}_0 = 0$, it follows that $\Pr\{\boldsymbol{\rho}_{\mathrm{s}} = 1\} = 0.9474$ and $\Pr\{\boldsymbol{\rho}_{\mathrm{s}} = 2\} = 0.0526$. Therefore,

$$Q_w = Q_1 \cdot \Pr\{\boldsymbol{\rho}_{\mathrm{s}} = 1\} + Q_2 \cdot \Pr\{\boldsymbol{\rho}_{\mathrm{s}} = 2\} = 126.4718.$$

Since $G_w = 4$, it follows from (22) that $J_w = 505.8870$. In this case, the Monte-Carlo simulation estimate of $E\left\{\|\boldsymbol{y}(k)\|^2\right\}$ calculated from (12) is shown in Fig. 25. It is in

good agreement with this prediction.

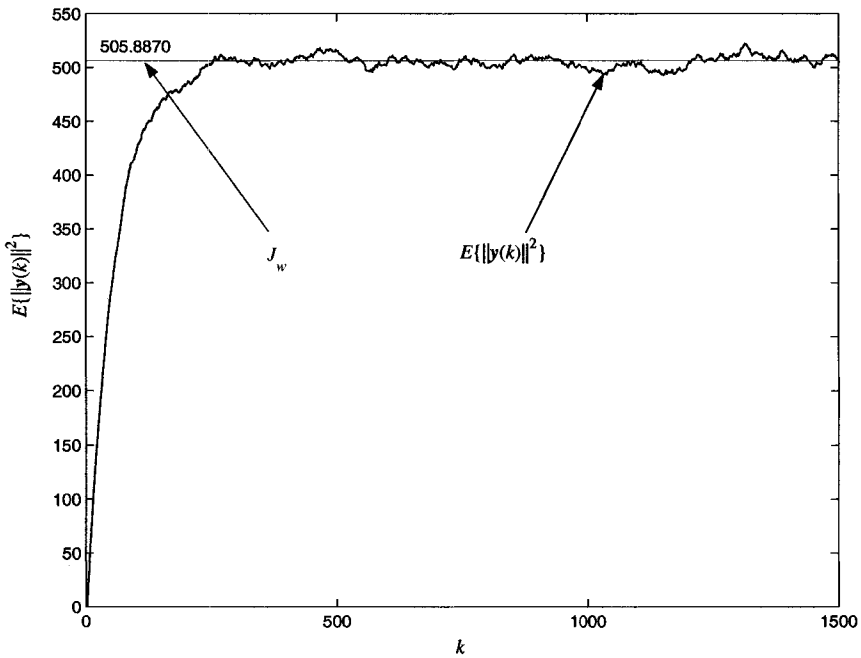

Fig. 25. A plot of $E\{\|\boldsymbol{y}(k)\|^2\}$ from Monte-Carlo simulation and J_w from theoretical calculation when $\boldsymbol{x}_0 = 0$ and $[\Pi]_{12} = 0.05$.

The simple example above demonstrates that the simulation results match well with the theory presented in the preceding section. In the next section, the theory is used to compute the output tracking error of the Boeing 737 system in closed-loop with an RCS subject to SEU's. This provides our central theoretical performance estimate which is compared against the experimental data.

IV.4 OUTPUT TRACKING PERFORMANCE OF THE BOEING 737 IN CLOSED-LOOP WITH AN RCS SUBJECT TO SEU'S

From Section IV.1, it is clear that the output tracking error system is also a stochastic hybrid system, whose structure is similar to system (11). Therefore, all the model-equivalent techniques for the MSS and the output performance of system (11)

can be applied here. For this application, calculations using MATLAB show that the MSS characteristics of the error system are indistinguishable to those described for the closed-loop system (11) given in Section III.3 (see Figs. 17 and 18). Since an aircraft flying at cruising altitude is always disturbed by winds and gusts, the output tracking energy is never finite. Therefore, in this section, only the output tracking power is meaningful for an MSS error system. As discussed in Section III.3, the tracking performance will be analyzed assuming the upset process is modeled as either a Markov chain or an i.i.d. process.

IV.4.1 Tracking Performance When the Upset Process Is Modeled as a First-Order Markov Chain

When the upset process is modeled as a Markov chain with the transition probability matrix, Π_{I}, given in (14), then for the output tracking system,

$$\hat{\mathscr{A}}_2 := \operatorname{diag}\left(\tilde{A}_{0,\mathrm{N}}^{\mathrm{T}}, \tilde{A}_{0,\mathrm{R}_1}^{\mathrm{T}}, \ldots, \tilde{A}_{0,\mathrm{R}_6}^{\mathrm{T}}; \tilde{A}_{1,\mathrm{N}}^{\mathrm{T}}, \tilde{A}_{1,\mathrm{R}_1}^{\mathrm{T}}, \ldots, \tilde{A}_{1,\mathrm{R}_6}^{\mathrm{T}}\right) \cdot \left(\Pi_{\mathrm{I/O}} \otimes I_{16^2}\right),$$

where $\tilde{A}_{j,\mathrm{N}} \equiv \operatorname{diag}\left(\tilde{A}_{\mathrm{n}}, \tilde{A}_{\mathrm{n}}\right) \otimes \operatorname{diag}\left(\tilde{A}_{\mathrm{n}}, \tilde{A}_{\mathrm{n}}\right)$ and $\tilde{A}_{j,\mathrm{R}_i} \equiv \operatorname{diag}\left(\tilde{A}_{\mathrm{n}}, \tilde{A}_{\mathrm{r}}\right) \otimes \operatorname{diag}\left(\tilde{A}_{\mathrm{n}}, \tilde{A}_{\mathrm{r}}\right)$ for $i = 1, 2, \ldots, 6$ and $j = 0, 1$, which are sixteen-dimensional matrices. Thus, the dimension of $\hat{\mathscr{A}}_2$ is 3,584 (i.e., $2 \times 7 \times 16^2$). Let

$$\hat{Q} = \varphi^{-1}\left(\left(I_{2\times 7\times 16^2} - \hat{\mathscr{A}}_2\right)^{-1} \cdot \varphi\left(\hat{C}\right)\right),$$

where

$$\hat{C} = \left(\tilde{C}_{0,\mathrm{N}}, \tilde{C}_{0,\mathrm{R}_1}, \ldots, \tilde{C}_{0,\mathrm{R}_6}; \tilde{C}_{1,\mathrm{N}}, \tilde{C}_{1,\mathrm{R}_1}, \ldots, \tilde{C}_{1,\mathrm{R}_6}\right)$$

with $\tilde{C}_{j,\mathrm{N}} \equiv \operatorname{diag}\left(\tilde{C}_{\mathrm{n}}^{\mathrm{T}}\tilde{C}_{\mathrm{n}}, \tilde{C}_{\mathrm{n}}^{\mathrm{T}}\tilde{C}_{\mathrm{n}}\right)$ and $\tilde{C}_{j,\mathrm{R}_i} \equiv \operatorname{diag}\left(\tilde{C}_{\mathrm{n}}^{\mathrm{T}}\tilde{C}_{\mathrm{n}}, \tilde{C}_{\mathrm{r}}^{\mathrm{T}}\tilde{C}_{\mathrm{r}}\right)$. Similarly, define

$$\hat{G} = \left(\tilde{G}_{0,\mathrm{N}}, \tilde{G}_{0,\mathrm{R}_1}, \ldots, \tilde{G}_{0,\mathrm{R}_6}; \tilde{G}_{1,\mathrm{N}}, \tilde{G}_{1,\mathrm{R}_1}, \ldots, \tilde{G}_{1,\mathrm{R}_6}\right)$$

with $\tilde{G}_{j,\mathrm{N}} \equiv \mathrm{diag}\left(\tilde{G}_{\mathrm{n}}\tilde{G}_{\mathrm{n}}^{\mathrm{T}}, \tilde{G}_{\mathrm{n}}\tilde{G}_{\mathrm{n}}^{\mathrm{T}}\right)$ and $\tilde{G}_{j,\mathrm{R}_i} \equiv \mathrm{diag}\left(\tilde{G}_{\mathrm{n}}\tilde{G}_{\mathrm{n}}^{\mathrm{T}}, \tilde{G}_{\mathrm{r}}\tilde{G}_{\mathrm{r}}^{\mathrm{T}}\right)$. Then the output tracking power of the system, $\hat{J}_w$, can be calculated using (22). Among the three output signals, altitude, calibrated airspeed, and tracking angle, only the altitude is significant numerically. Therefore, $\hat{J}_w$ embodies primarily the altitude variations. The predicted mean output tracking error power, $\hat{J}_w$, is shown in Fig. 26 for the

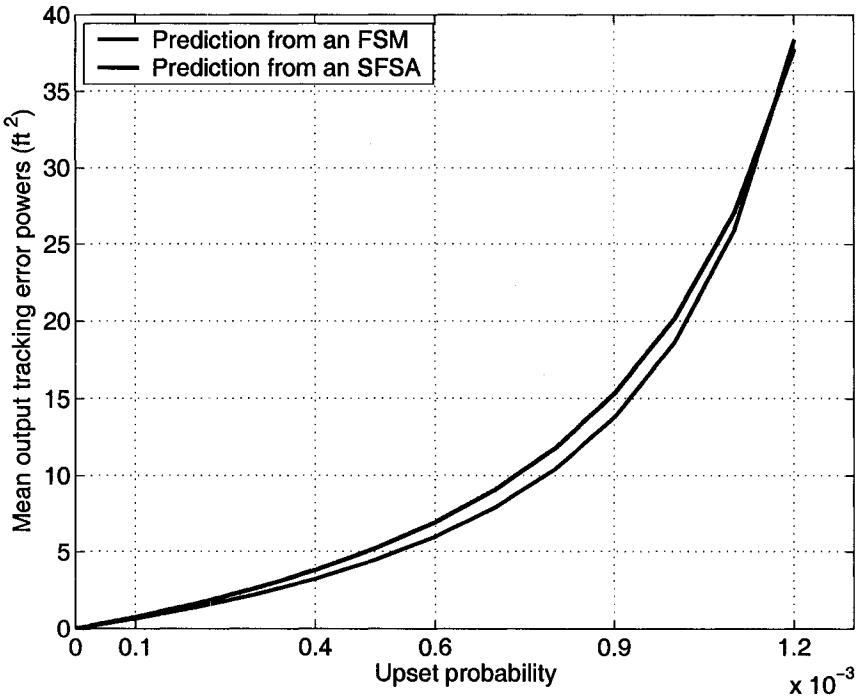

Fig. 26. The SFSA/FSM-predicted mean output tracking error powers as a function of upset probability $[\Pi_{\mathrm{I}}]_{01}$.

SFSA/FSM modeled recovery processes. As might be expected, the higher the upset probability, the larger the output tracking error power. It is unbounded at the stability boundary. The mean tracking error power is less than 40 ft^2 when the upset probability, $[\Pi_{\mathrm{I}}]_{01}$, is less than 1.2×10^{-3}. In this case, the corresponding altitude variation is less ± 6.4 ft at cruising altitude. Therefore, it is predicted that the RCS controlled Boeing 737 system will function well for any upset probability less than 1.2×10^{-3}.

IV.4.2 Tracking Performance When the Upset Process Is Modeled as an I.I.D. Process

When the upset process is i.i.d. with the probability distribution, π_I, given in (15), then one approach to calculating its output tracking power is via Theorem IV.5(b) with

$$\Pi_{\mathrm{I}} = \begin{bmatrix} 1-\pi_{\mathrm{I}}(1) & \pi_{\mathrm{I}}(1) \\ 1-\pi_{\mathrm{I}}(1) & \pi_{\mathrm{I}}(1) \end{bmatrix}.$$

An alternative approach is to use Π_{O}, given in Subsection III.3.2, and

$$\check{\mathscr{A}}_2 := \mathrm{diag}\left(\tilde{A}_{\mathrm{N}}^{\mathrm{T}}, \tilde{A}_{\mathrm{R}_1}^{\mathrm{T}}, \ldots, \tilde{A}_{\mathrm{R}_6}^{\mathrm{T}}\right) \cdot (\Pi_{\mathrm{O}} \otimes I_{16^2})$$

with $\tilde{A}_{\mathrm{N}} \equiv \mathrm{diag}\left(\tilde{A}_{\mathrm{n}}, \tilde{A}_{\mathrm{n}}\right) \otimes \mathrm{diag}\left(\tilde{A}_{\mathrm{n}}, \tilde{A}_{\mathrm{n}}\right)$ and $\tilde{A}_{\mathrm{R}_i} \equiv \mathrm{diag}\left(\tilde{A}_{\mathrm{n}}, \tilde{A}_{\mathrm{r}}\right) \otimes \mathrm{diag}\left(\tilde{A}_{\mathrm{n}}, \tilde{A}_{\mathrm{r}}\right)$ for $i = 1, 2, \ldots, 6$, which are sixteen-dimensional matrices. (Here the dimension of $\check{\mathscr{A}}_2$ is 1,792 (i.e., 7×16^2).) Let

$$\check{Q} = \varphi^{-1}\left(\left(I_{7\times 16^2} - \check{\mathscr{A}}_2\right)^{-1} \cdot \varphi\left(\check{C}\right)\right),$$

where

$$\check{C} = \left(\tilde{C}_{\mathrm{N}}, \tilde{C}_{\mathrm{R}_1}, \ldots, \tilde{C}_{\mathrm{R}_6}\right)$$

with $\tilde{C}_{\mathrm{N}} \equiv \mathrm{diag}\left(\tilde{C}_{\mathrm{n}}^{\mathrm{T}}\tilde{C}_{\mathrm{n}}, \tilde{C}_{\mathrm{n}}^{\mathrm{T}}\tilde{C}_{\mathrm{n}}\right)$ and $\tilde{C}_{\mathrm{R}_i} \equiv \mathrm{diag}\left(\tilde{C}_{\mathrm{n}}^{\mathrm{T}}\tilde{C}_{\mathrm{n}}, \tilde{C}_{\mathrm{r}}^{\mathrm{T}}\tilde{C}_{\mathrm{r}}\right)$. Similarly, define

$$\check{G} = \left(\tilde{G}_{\mathrm{N}}, \tilde{G}_{\mathrm{R}_1}, \ldots, \tilde{G}_{\mathrm{R}_6}\right)$$

with $\tilde{G}_{\mathrm{N}} \equiv \mathrm{diag}\left(\tilde{G}_{\mathrm{n}}\tilde{G}_{\mathrm{n}}^{\mathrm{T}}, \tilde{G}_{\mathrm{n}}\tilde{G}_{\mathrm{n}}^{\mathrm{T}}\right)$ and $\tilde{G}_{\mathrm{R}_i} \equiv \mathrm{diag}\left(\tilde{G}_{\mathrm{n}}\tilde{G}_{\mathrm{n}}^{\mathrm{T}}, \tilde{G}_{\mathrm{r}}\tilde{G}_{\mathrm{r}}^{\mathrm{T}}\right)$. Then the output tracking power of the system, $\check{J}_w$, can be calculated using (22). The plot of $\check{J}_w$ as a function of $\pi_{\mathrm{I}}(1)$ is almost indistinguishable to Fig. 26. Thus, for a given probability p_0 and under the condition that the system is MSS, the *normalized difference* of the

mean output power,

$$\text{normalized difference of } J_w \text{ at } p_0 = \frac{\check{J}_w\big|_{\pi_{\mathrm{I}}(1)=p_0} - \hat{J}_w\big|_{[\Pi_{\mathrm{I}}]_{01}=p_0}}{\hat{J}_w\big|_{[\Pi_{\mathrm{I}}]_{01}=p_0}},$$

is shown in Fig. 27 corresponding to $r = 0$ and $r = 1$. When $p_0 \in [0, 1.4 \times 10^{-3}]$, the

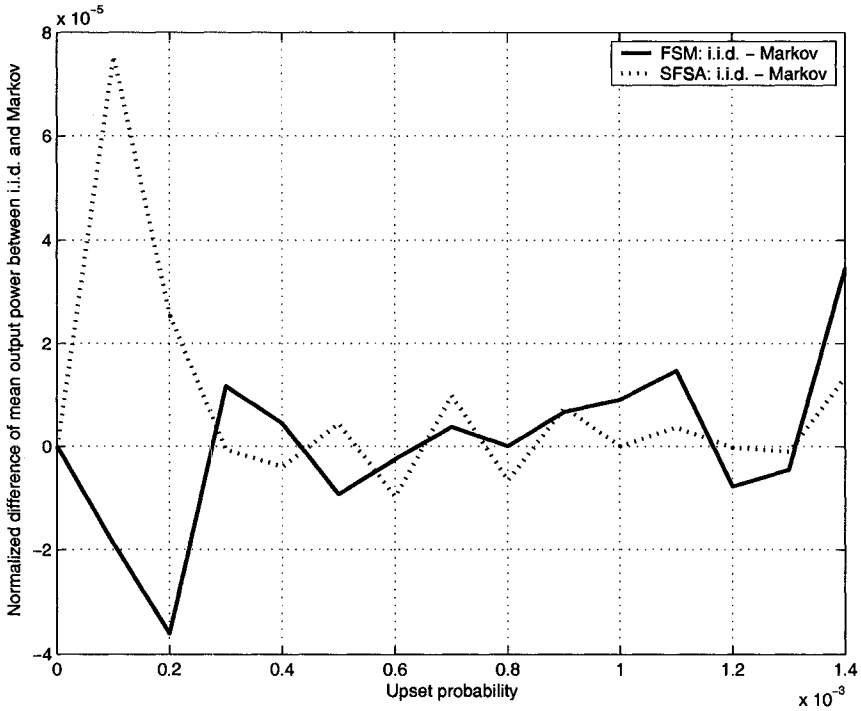

Fig. 27. The normalized difference between the output performances when $r = 0$ (i.i.d.) and $r = 1$ for typical values of $\pi_{\mathrm{I}}(1)$ and $[\Pi_{\mathrm{I}}]_{01}$.

normalized difference is less than 10^{-4}. Thus, it is clear, from a mean output power point of view that modeling the upset process as an i.i.d. process or a first-order Markov chain produces approximately the same theoretical performance prediction.

IV.5 SUMMARY

In this chapter, theory to compute the output performance of a stochastic hybrid system was presented via its model-equivalent Markov jump-linear system. It was shown that both mean output energy and mean output power could be expressed

in terms of a generalized output observability Gramian. The analytical expressions were derived under the condition that the system is MSS, which guaranteed their finiteness. Then the theory was applied to calculate the mean output power of the Boeing 737 in closed-loop with an RCS subject to either a Markov or an i.i.d. upset process. For this specific application, the mean tracking error power was less than 40 ft^2 when the upset probability was less than 1.2×10^{-3}. Thus, the corresponding altitude variation was around ± 6.4 ft at cruising altitude, an acceptable performance level given the circumstances.

CHAPTER V

EXPERIMENTS FOR EVALUATING THE TRACKING ERROR PERFORMANCE OF A RECOVERABLE FLIGHT CONTROL SYSTEM

In this chapter, two RCS experiments are described. One experiment was conducted in a *high intensity* neutron environment at the Los Alamos National Laboratory (see [87] for additional details). The primary goal here was to gather real neutron performance data in order to assess any potential safety hazards due to SEU's for RCS controlled aircraft flying under *normal* atmospheric conditions. The other experiment was conducted in a *simulated* neutron environment at the NASA Langley Research Center. The main purpose of this experiment was to validate the hybrid model for the recoverable flight control system developed in Chapter II by evaluating the accuracy of the theoretical prediction of the system's mean output tracking performance presented in Chapter III.

This chapter is organized in the following way. First, descriptions of the RCS experiments conducted at LANSCE and NASA Langley are given in Section V.1. Then in Section V.2, the experimental data obtained from NASA Langley will be analyzed and the results will be compared against the theoretical performance predictions obtained in Chapter IV. In Section V.3, the experimental data obtained from the LANSCE will be analyzed in a similar fashion. Finally, a summary of the main experimental conclusions is given in Section V.4.

V.1 DESCRIPTION OF THE RCS EXPERIMENTS

Two experiments were designed and conducted to evaluate the output tracking performance of an RCS controlled flight system: one was performed at LANSCE in Los Alamos, New Mexico and the other conducted at the NASA Langley SAFETI Laboratory in Hampton, Virginia. At LANSCE, RCS performance was measured under a *high intensity* neutron environment. As will be discussed shortly, this data can be used to assess the performance of an RCS controlled flight system under normal atmospheric conditions. At NASA Langley, the tests were conducted in a *simulated* neutron environment, which was used to validate the mean output tracking power prediction model. Aside from the difference in the environments, both experiments were conducted in as similar conditions as possible: same hardware, same software, identical flight configurations, etc.

V.1.1 Description of the High Intensity Neutron Experiment at LANSCE

The experimental configuration at LANSCE was described in Chapter I. The layout of the experimental environment is shown again in Fig. 28. A concrete wall separates the laboratory into two sections. The section below the concrete wall depicts the control room containing the host computers, one for the flight simulation of the Boeing 737 system and one for data acquisition. It is also a safe environment for the personnel operating and controlling the experiment. The actual control room at LANSCE is shown in Fig. 29. The section above the concrete wall depicts the radiation chamber, where the free neutron beam source was directed at the RCS

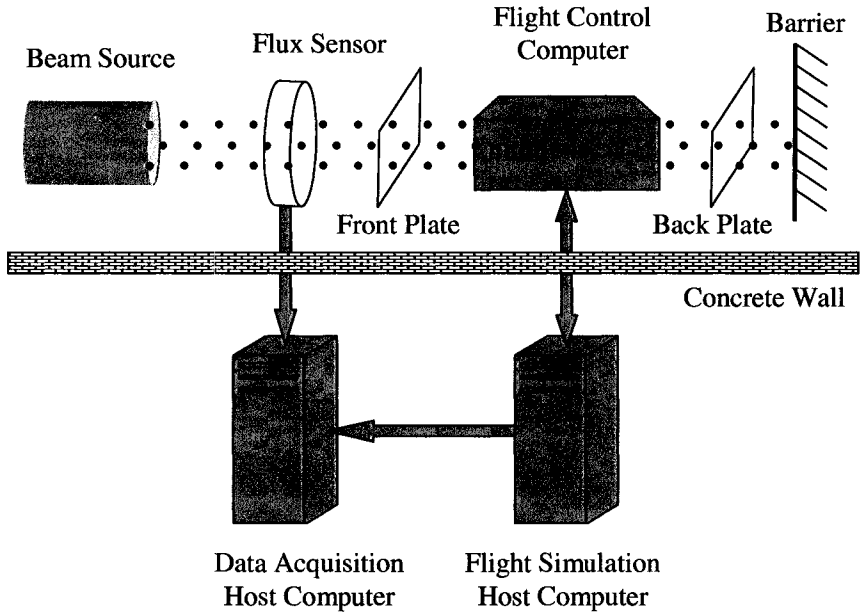

Fig. 28. The layout of the experimental environment at LANSCE.

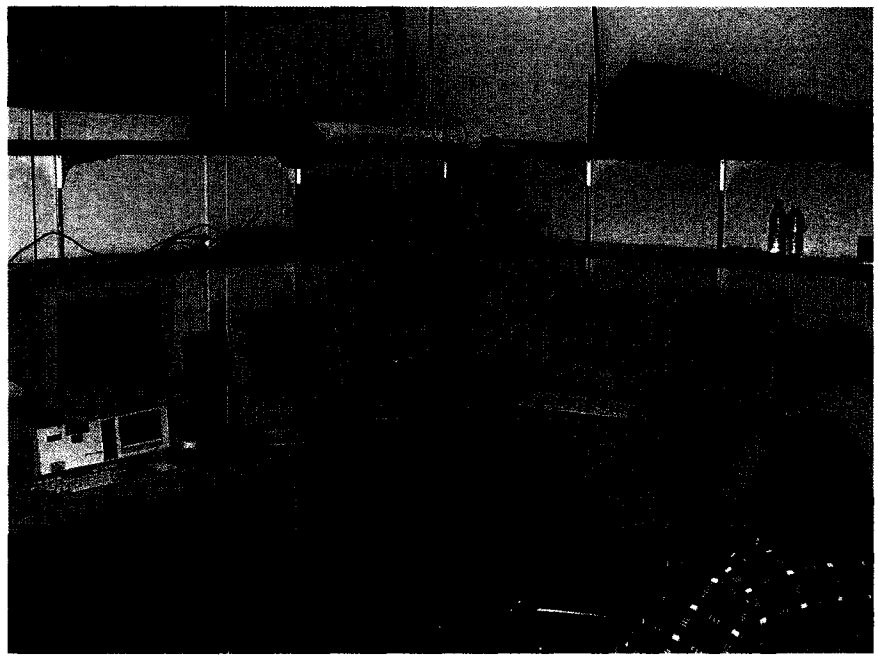

Fig. 29. The control room at LANSCE.

through a flux sensor. The flux sensor was used to measure the neutron intensity. It sent a signal to the data acquisition computer, which could be converted into a time-varying flux measurements. In addition, an image plate (*front plate*) was placed between the flux sensor and the RCS in order to measure the position and diameter of the beam before striking the RCS. Another image plate (*back plate*) was placed between the RCS and the barrier which created an image of the chip set within the RCS exposed to neutrons. The real radiation chamber with the RCS in the beam path is shown in Fig. 30. (The back plate is not visible here.) Since the diameter

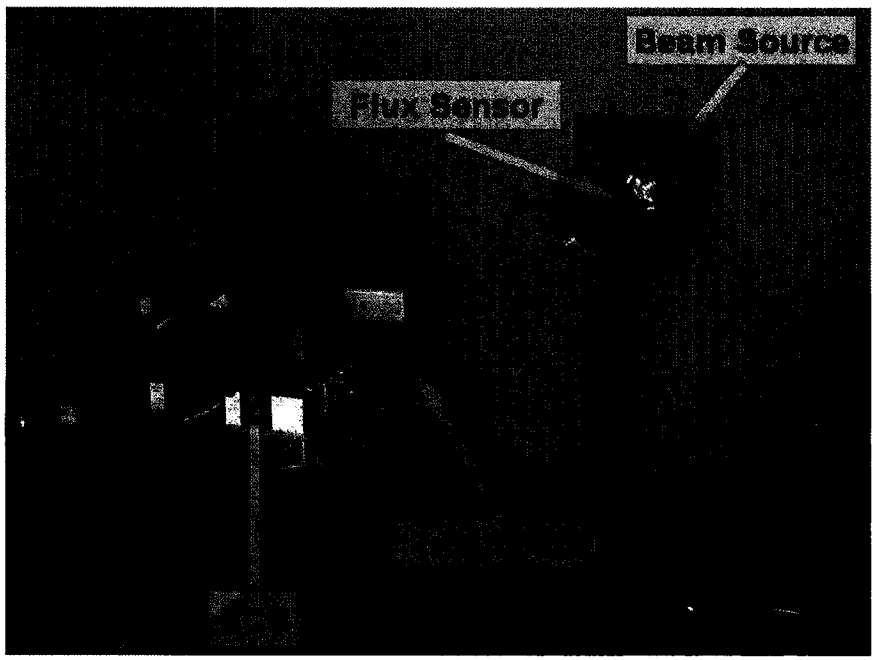

Fig. 30. The LANSCE neutron radiation chamber.

of the neutron beam (adjustable between 1–3 in) is smaller than the dimensions of the RCS (20.5 in $\times$ 7.25 in $\times$ 6 in), only a portion of the RCS can be targeted at any one time. Fig. 31 shows a *virtual* RCS used to select neutron targets. The beam path (denoted in pink) is just below the dual CPU's (shown in red). A wide variety of target positions were investigated (see [87] for an overview), but in general

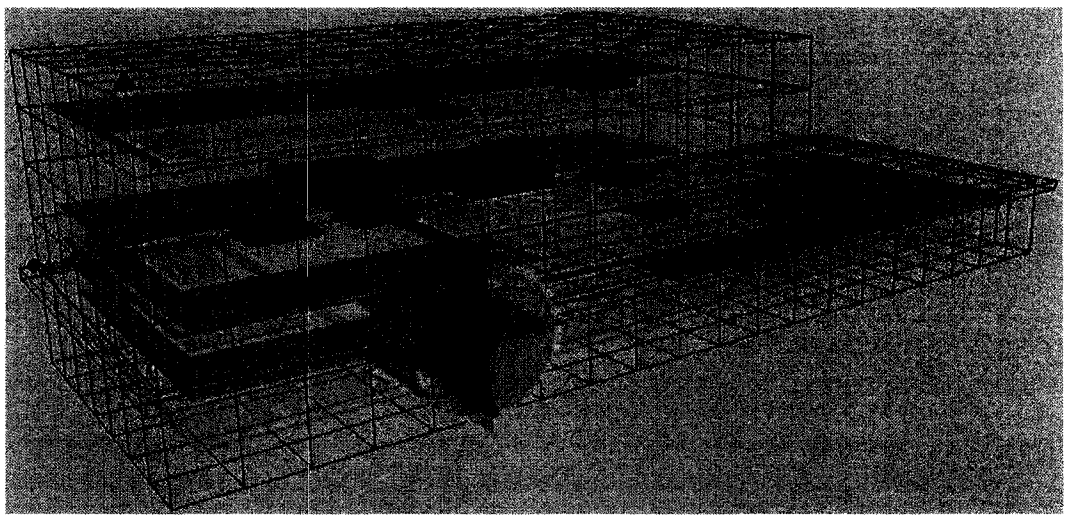

Fig. 31. A beam path (shown in pink) just below the dual CPU's (depicted in red).

those located in the vicinity of the CPU's were the most sensitive. With the beam path selected, Fig. 32 shows how the front and back image plates record which chip sets received neutrons. After a neutron beam passed through the front plate for several hours, a circular white region was recorded as shown in Fig. 32(a). As the neutron beam passed through the RCS, it was partially absorbed by the electronics, which then produced a back plate image as shown in Fig. 32(b). A typical target was exposed to the beam between three to ten hours depending on the number of recoveries observed. A total of 87 experimental runs were produced in three days. As this was the very first test of its kind, target selection was often done on an ad hoc basis. In addition, the LANSCE facility is reserved by users 365 days a year. This means that only a limited number of good data sets can be collected and used for our analysis. In this case, no more than 15% of the 87 runs contained significant statistical information. Of those, only six were used for Markovianess analysis of the upset signals (see Subsection V.3.1) and eleven were used for the output tracking

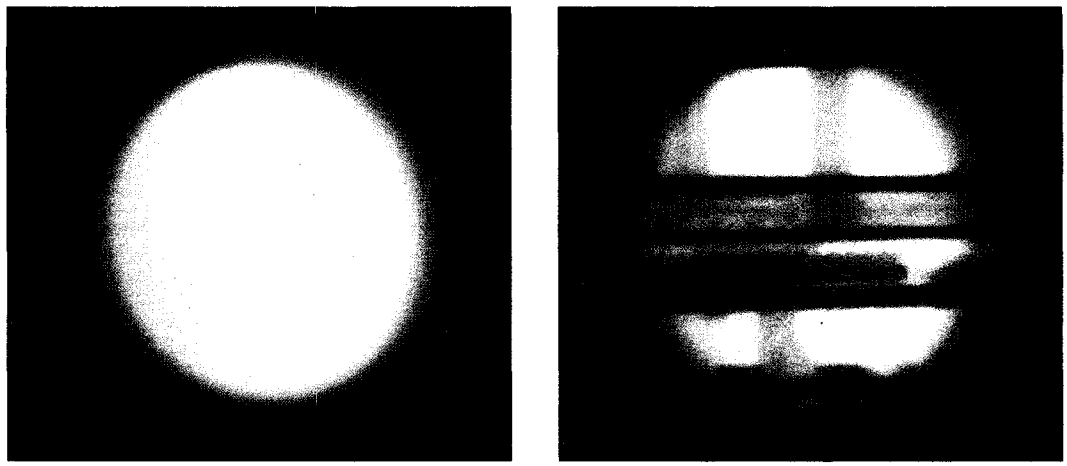

(a) Front plate. (b) Back plate.

Fig. 32. The front and back image plates used to record which chip sets received neutrons. (The horizontal lines are printed circuit boards.)

performance analysis (see Subsection V.3.2). Nevertheless, the experiment provided a usable set of data describing how neutron-induced SEU's can interfere with digital closed-loop systems.

V.1.2 Description of the Simulated Neutron Experiment at NASA Langley

The experiment at NASA Langley had a similar configuration as the one at LANSCE (see Fig. 33), except that there was no real neutron source. Instead, the neutron interactions were simulated by triggering rollback recoveries according to pre-determined Markov or i.i.d. upset processes, which were characterized by sets of *upset trigger* sequences. The main advantage to testing the RCS in this manner is that the upset signals could be simulated using software triggers having a precisely known and controllable probability distribution, unlike what was possible at LANSCE. As discussed in Chapter II, the upset signals were assumed to be either a first-order

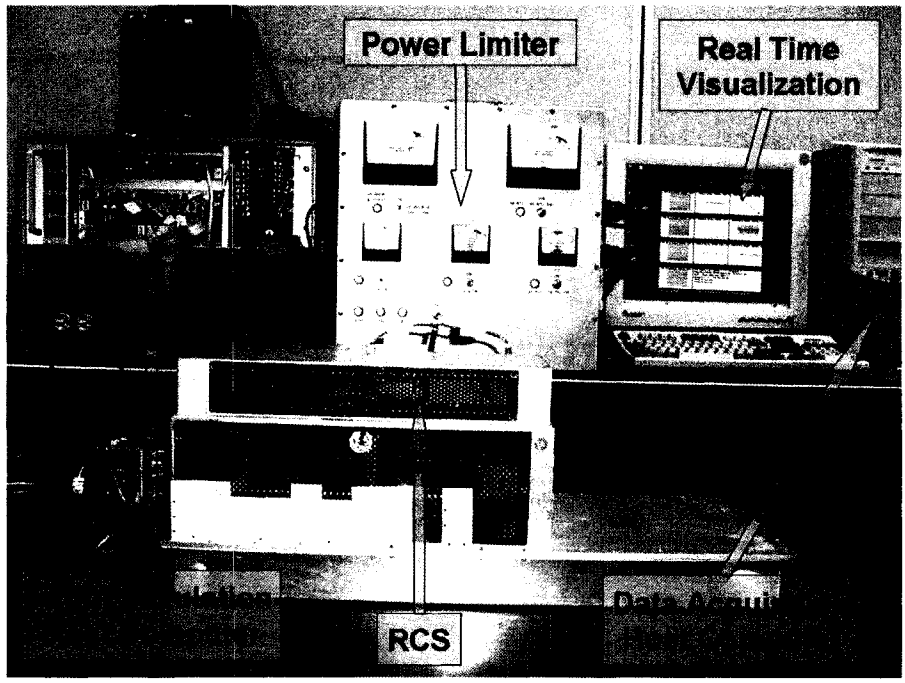

Fig. 33. The RCS experimental environment in the SAFETI Laboratory at NASA Langley.

Markov chain or an i.i.d. process. Thus, two corresponding groups of RCS tests were conducted to simulate the neutron environment. For each group, ten sets of experimental data were collected for each of the following six upset probabilities, $[\Pi_{\mathrm{I}}]_{01}$, in the Markov test or, $\pi_{\mathrm{I}}(1)$, in the i.i.d. test: 0, 0.0001, 0.0004, 0.0006, 0.0009, and 0.0012. That is, in total there were 60 one hour runs for each group. These probabilities were selected such that the closed-loop system was MSS, and thus, the output tracking power was finite. In each case, different sample functions from the corresponding Markov or i.i.d. process, $\boldsymbol{\nu}(k)$, were used to supply the RCS with a series of recovery requests for the closed-loop system. A summary of the experimental parameters is listed in Table IV (see also Tables XII and XIII in Appendix B.2 for the MATLAB data files).

TABLE IV
The Parameters of Markov and I.I.D. Tests for the RCS

	Markov tests	I.I.D. tests
Probability transition or probability distribution	$\Pi_{\mathrm{I}} = \begin{bmatrix} 1-[\Pi_{\mathrm{I}}]_{01} & [\Pi_{\mathrm{I}}]_{01} \\ 1 & 0 \end{bmatrix}$	$\pi_{\mathrm{I}} = \begin{bmatrix} 1-\pi_{\mathrm{I}}(1) & \pi_{\mathrm{I}}(1) \end{bmatrix}$
Upset probability	$[\Pi_{\mathrm{I}}]_{01}$	$\pi_{\mathrm{I}}(1)$
Values of upset probability	0, 0.0001, 0.0004, 0.0006, 0.0009, and 0.0012	
Sample period for each run	0.05 sec/sample (or sec/frame)	
Duration of each run	60 mins	
Number of samples for each run	72,000 samples (or frames)	
Total number of runs	60 for each group	
Magnitude of the winds	1 ft/sec	

Since the RCS is a prototype device, it was also necessary to perform a variety of pretests to guarantee the device and the experimental configuration worked as expected. Those pretests are described below.

1. Repeatability test:

   To establish a baseline, it was first important to test the *repeatability* of the software, the hardware and the communication units in the following sense: if given the same upset trigger sequence and the same sample function from the wind process, the system should to some degree produce the same recovery process and same output signal. Six test runs were conducted under these conditions. An example of the result is given in Fig. 34. In Fig. 34(a), the altitude (`ALT`) deviations (i.e., the deviations from the 34,000 ft cruising altitude) of two runs[1] are shown. The difference between these runs is shown in Fig. 34(b). The primary reason that the difference signal is not zero is that the connection between the RCS and the flight simulation is asynchronous. Thus, the communication between the units during the course of an hour is slightly different for each experimental trial. On average, the difference between runs was around 8% of the deviations from cruising altitude.

2. Upset trigger type test:

   There are several types of trigger signals that the RCS might employ: edge triggers, state triggers and time triggers. For example, the trigger signal[2] shown in Fig. 35(a), from Frame 1,049 to Frame 1,050, forms a rising (positive) edge

[1]Experiment data for run 1 is `RCS5_29.mat` and for run 2 is `RCS_Pre2_09.mat` (See Table XI in Appendix B.2).

[2]Experiment data set is `upsets_test_0629.mat` (see Table XIV in Appendix B.2).

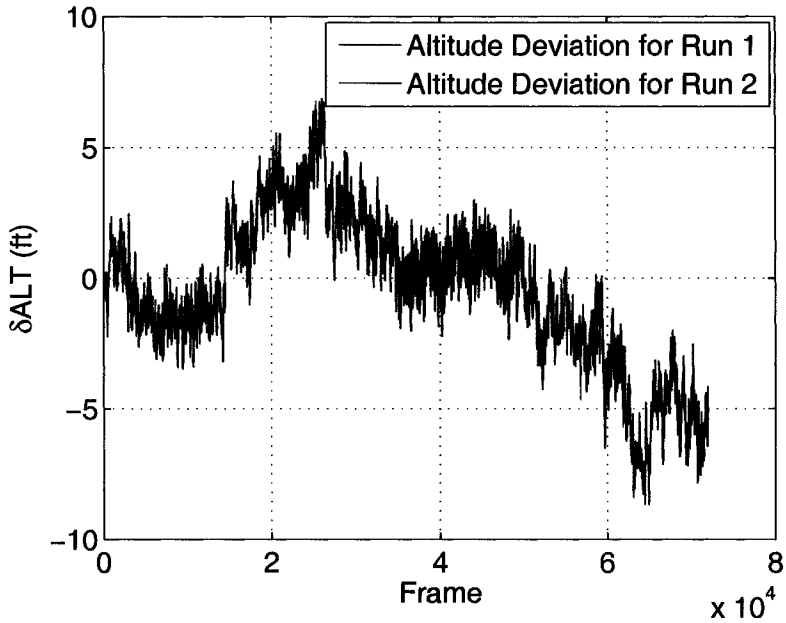

(a) Altitude deviations from 34,000 ft of two experimental runs.

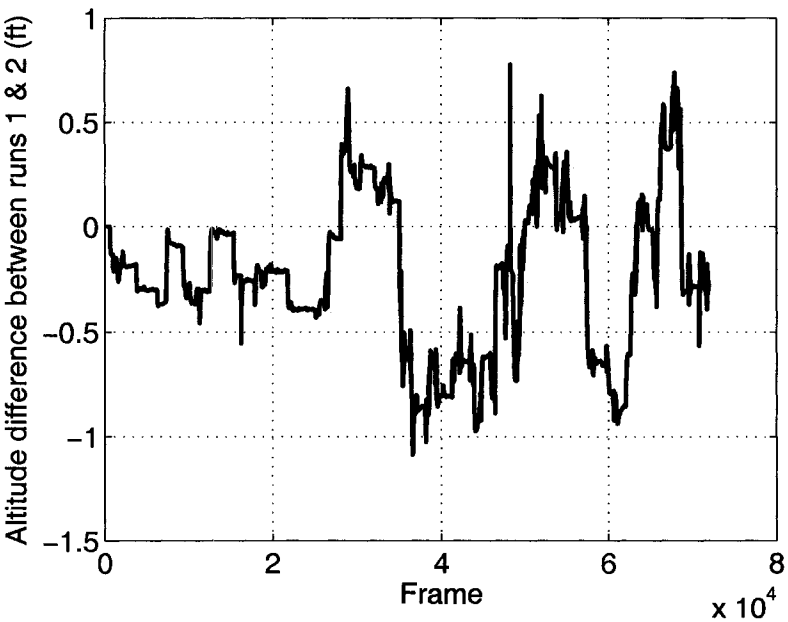

(b) Altitude difference between two experimental runs.

Fig. 34. Comparing the altitudes of the aircraft for two experimental runs with the exact same configuration.

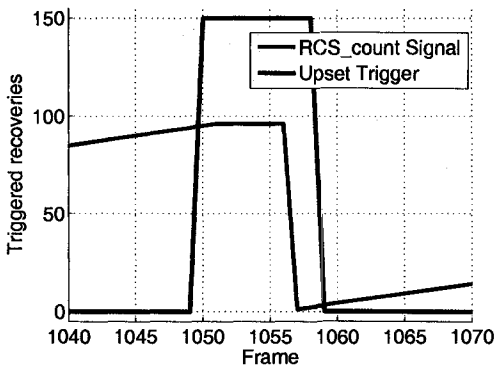

(a) No response to state triggering.

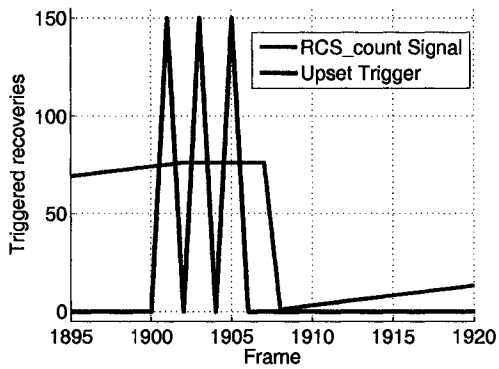

(b) No response to triggering during an active recovery.

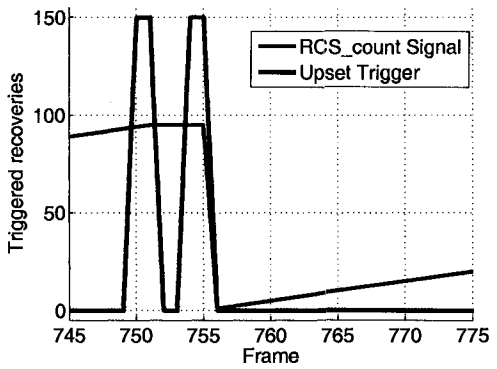

(c) No response to falling edge triggering.

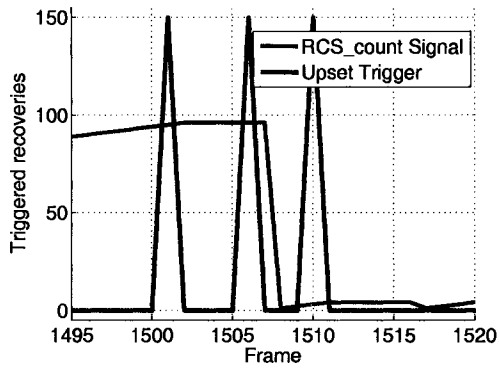

(d) Response to triggering after a full recovery.

Fig. 35. Response of the RCS to various trigger signals.

trigger, then from Frame 1,050 to Frame 1,058, forms a set of state triggers, and from Frame 1,058 to Frame 1,059, it forms a falling (negative) trigger. During this test it was discovered that the rollback recovery mechanism of the RCS would only react to a rising edge upset trigger. Furthermore, it would only respond to the *first* upset trigger if a sequence of consecutive upset triggers was injected. Critical in this analysis is the internal variable `RCS_count` of the RCS experiment[3] (see Fig. 35). The main characteristics of `RCS_count` are: if there is no upset trigger, its value increases from 0 to 255, one increment per frame, and then the process is restarted. If an upset trigger is detected, the current value of `RCS_count` is held till the rollback process finishes, and then its value is reset to 0. For example, Fig. 35(a) shows that the RCS does not respond to the state triggers during Frames 1,050–1,058. Fig. 35(b) indicates that the RCS ignores any new upset triggers which occur during a recovery period. Specifically, the upset triggers at Frames 1,903 and 1,905 are ignored. Fig. 35(c) shows that the RCS does not respond to a falling edge trigger at Frame 755. Fig. 35(d) shows that it will respond to another rising edge upset trigger at Frame 1,510 immediately after finishing the current recovery.

3. Recovery recognition test:

   This test was important in order to obtain statistical information concerning the recovery lengths. It was done primarily by monitoring the internal variable `RCS_count`. Take Fig. 36 as an example: Fig. 36(a)[4] shows that two recoveries are detected. A closer view of the first recovery event is given in Fig. 36(b). Here

[3]Experiment data set is `RCS5_1.mat` (see Table XIV in Appendix B.2).
[4]Experiment data is `RCS_Pre2_09.mat` (see Table XI in Appendix B.2).

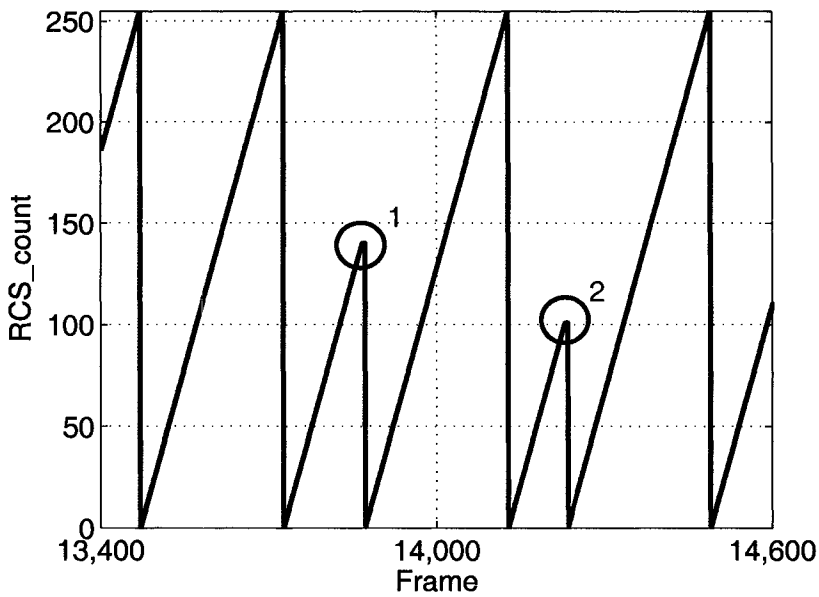

(a) Recovery processes detected from RCS_count.

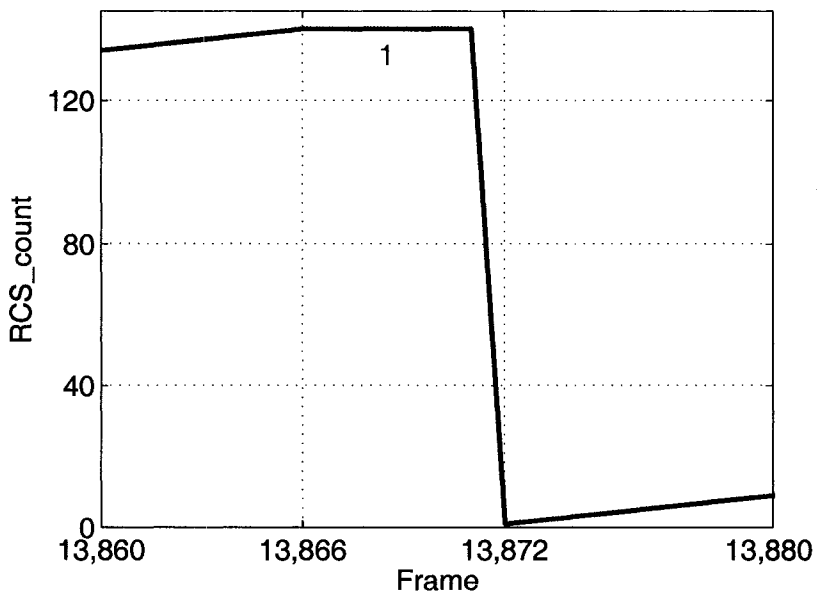

(b) Closer view of the first recovery event.

Fig. 36. Recognition of recovery processes using the internal variable RCS_count.

it can be seen that recovery period is six frames in length (from Frame 13,866 to Frame 13,872). A series of such tests revealed that approximately 20% of the recovery periods were five frames in length and 80% were six frames in length.

4. MSS tests:

MSS could not tested directly in the experimental environment since the hardware employs nonlinear protective devices such as limiters to prevent the system variables from becoming unbounded. In other words, the linear model was obtained for one trim condition of the flight system. However, some obviously unstable phenomena could still be observed for high upset probabilities. For example, Fig. 37 shows that when the upset probability is $[\Pi_{\mathrm{I}}]_{01} = 0.26$, the al-

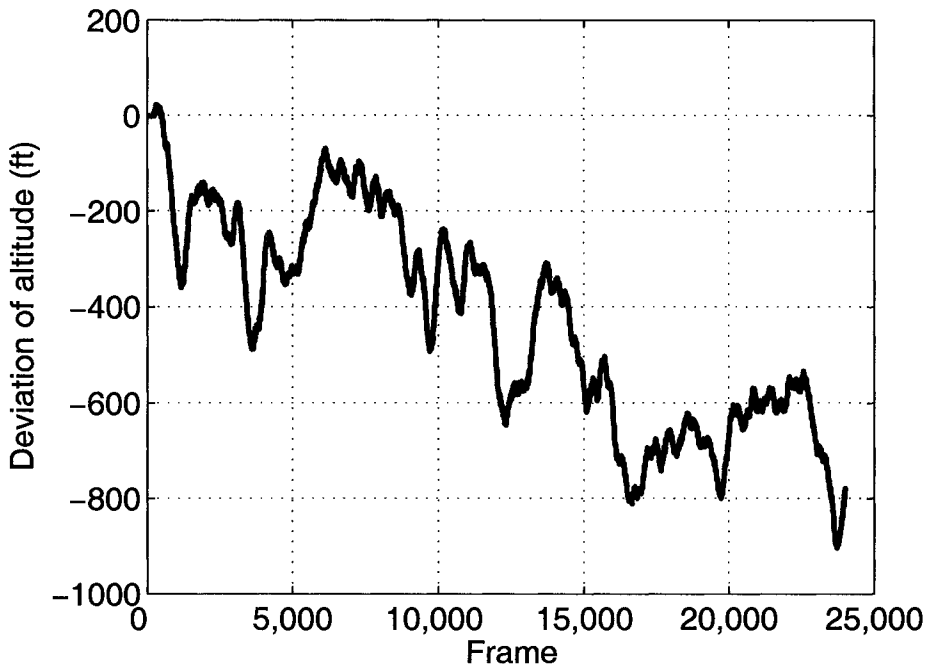

Fig. 37. A stability test of the recoverable flight system when $[\Pi_{\mathrm{I}}]_{01} = 0.26$.

titude deviation increases dramatically.[5] MSS results presented in Section III.2

[5]Experiment data is `RCS5_11.mat` (see Table XIV in Appendix B.2).

predicted that the system would not be MSS for this upset probability.

V.2 ANALYZING THE EXPERIMENTAL DATA FROM NASA LANGLEY

In this section, the experimental data obtained from the NASA Langley test-bed are analyzed to produce an *experimental* mean output tracking power. In the analysis, the aircraft's output variables are compared against nominal flights, i.e., ones with no rollback recoveries (when $[\Pi_{\mathrm{I}}]_{01} = 0$ for the first-order Markov chain or $\pi_{\mathrm{I}}(1) = 0$ for the i.i.d. process) but identical wind conditions. The tracking error statistics are then computed using the output errors. The results are finally compared against the theoretical predictions developed in Chapter IV to validate the hybrid model presented in Chapter II. In particular, Subsection V.2.1 presents the results obtained using Markov upset processes, while Subsection V.2.2 presents the results obtained using i.i.d. upset processes.

V.2.1 Performance Analysis for the Markov Tests

For the Markov upset signals, the ten experimental output tracking error powers for each value of $[\Pi_{\mathrm{I}}]_{01} \in \mathbb{U} := \{0, 0.0001, 0.0004, 0.0006, 0.0009, 0.0012\}$ are shown in Fig. 38. In the calculation, only the altitude output signal (in units of feet) was considered because it is more significant in magnitude than the calibrated airspeed and the tracking angle. Cluster analysis, a tool for analyzing under sampled data sets, was used to exclude the outliers for each probability [88,89]. Specifically, as shown in Fig. 39, *hierarchical clustering* diagrams were used based on the Euclidean distances between the measured output powers. The red-dotted lines denote experimental data

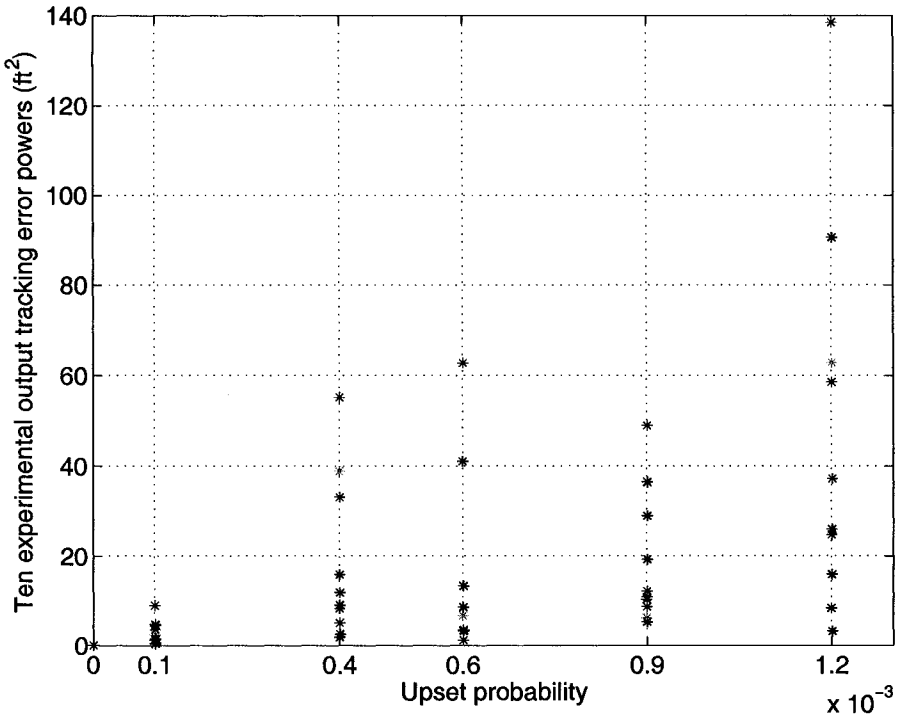

Fig. 38. The distribution of ten output tracking error powers for six specific upset probabilities for Markov upset signals.

which was discarded because it was far away from the main clusters (indicated in solid lines). Here the one or two highest links were removed if they were approximately four times higher than the other links. After using the cluster analysis, effects from outliers were obviously reduced. Fig. 40 compares the averages and standard deviations of the experimental mean output tracking powers at each upset probability $[\Pi_{\mathrm{I}}]_{01}$ before and after employing the cluster analysis technique. The black-dotted line denotes the average power before the cluster analysis. The magenta-solid line denotes the average power after the cluster analysis, which is smoother. The blue dot-dash and the green-dashed lines are used to denote their standard deviations, respectively. The standard deviation before the cluster analysis is larger than that after the cluster analysis. More details are given in Table V, where the *deviation reduction ratio* is

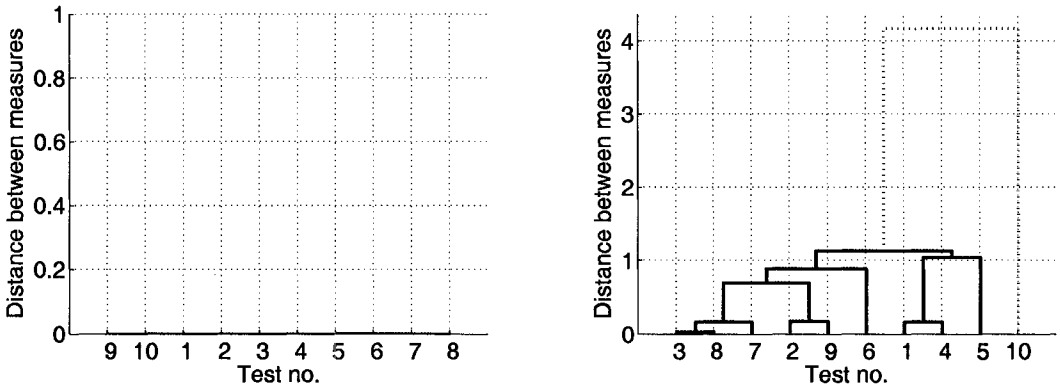

(a) $[\Pi_{\mathrm{I}}]_{01} = 0.$ (b) $[\Pi_{\mathrm{I}}]_{01} = 0.0001.$

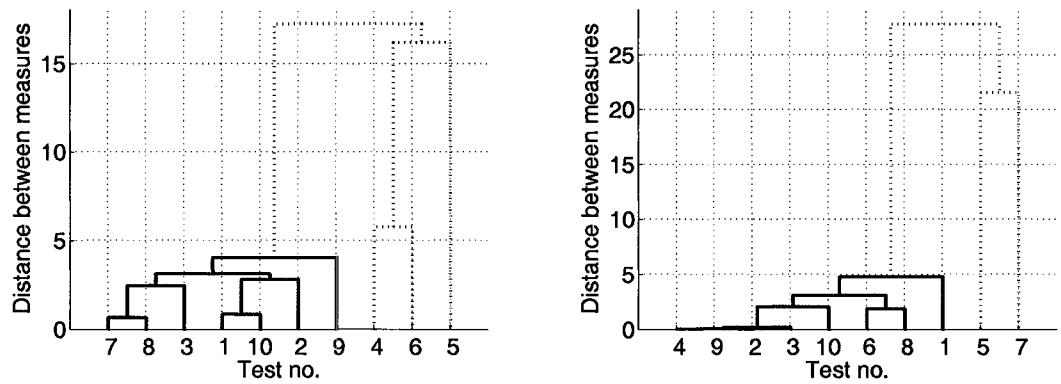

(c) $[\Pi_{\mathrm{I}}]_{01} = 0.0004.$ (d) $[\Pi_{\mathrm{I}}]_{01} = 0.0006.$

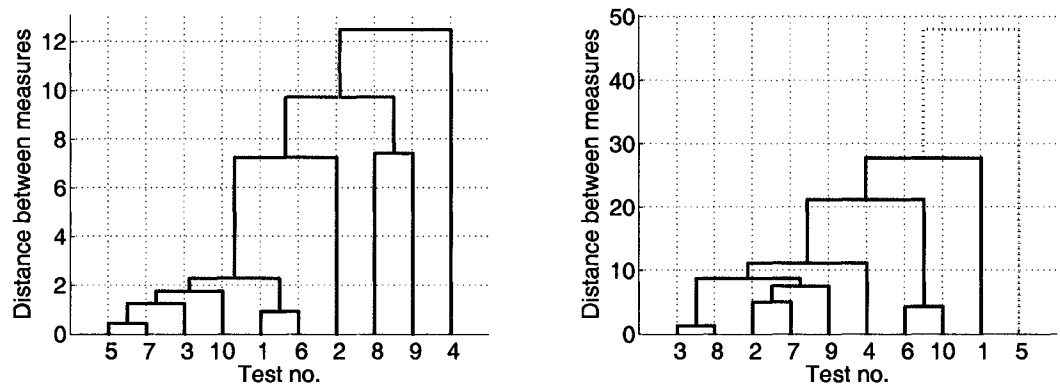

(e) $[\Pi_{\mathrm{I}}]_{01} = 0.0009.$ (f) $[\Pi_{\mathrm{I}}]_{01} = 0.0012.$

Fig. 39. The cluster analysis diagrams for six specific upset probabilities for the Markov upset signals.

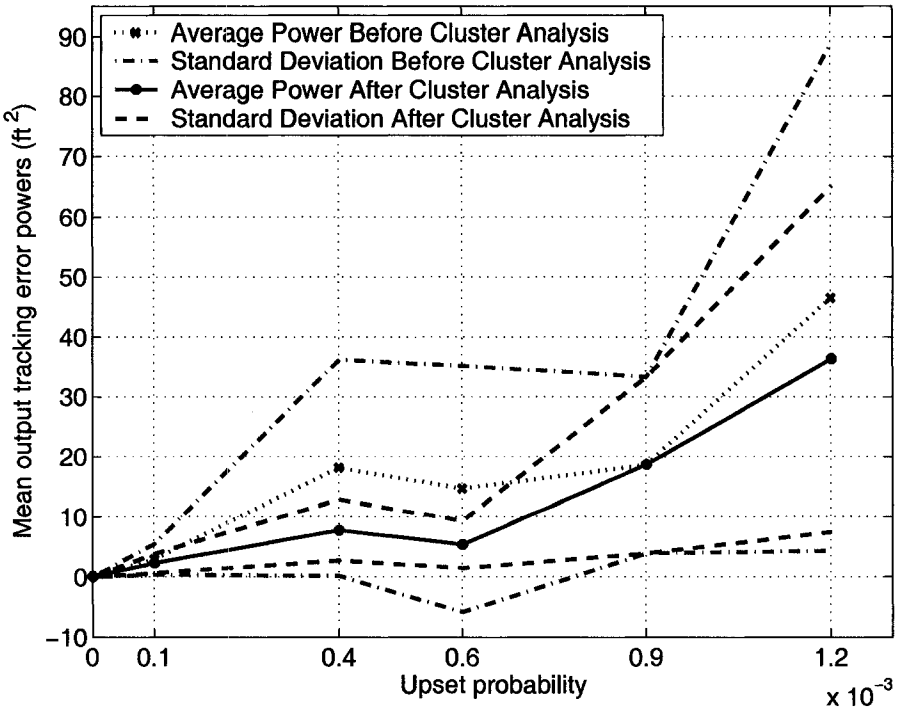

Fig. 40. The averages and standard deviations of the experimental output tracking powers before and after applying cluster analysis for Markov tests.

TABLE V
Comparison Between the Standard Deviation of the Output Tracking Powers Before and After the Cluster Analysis for Markov Upsets

Upset probability	Standard deviation before cluster analysis	Standard deviation after cluster analysis	Deviation reduction ratio	Number of outliers removed after cluster analysis
0	0	0	1	0
0.0001	2.5846	1.6183	0.6261	1
0.0004	18.0319	5.0544	0.2803	3
0.0006	20.5188	3.9220	0.1911	2
0.0009	14.7303	14.7303	1	0
0.0012	42.2334	28.8601	0.6833	1

used to describe the degree to which the cluster analysis eliminates the outliers. It is defined as

$$\text{deviation reduction ratio} = \frac{\text{standard deviation after the cluster analysis}}{\text{standard deviation before the cluster analysis}}.$$

Therefore, the smaller the deviation reduction ratio, the more effect the elimination procedure. If the ratio is less one, then some outliers are said to be *effectively* eliminated. For example, in Table V, the cluster analysis works well at $[\Pi_{\mathrm{I}}]_{01} = 0.0006$ but is not effective at $[\Pi_{\mathrm{I}}]_{01} = 0.0009$.

The average output tracking error powers for the six probabilities were computed empirically from the experimental output data within the main cluster. The results are shown in Fig. 41 and compared against the theoretical predictions using both

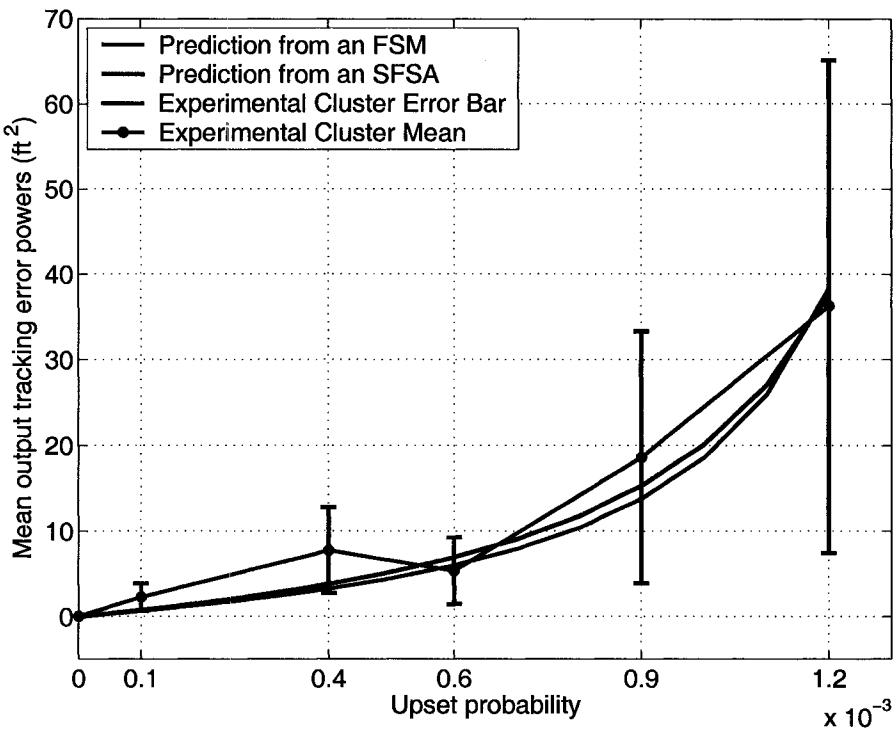

Fig. 41. The average power after cluster analysis and the theoretical predictions from the FSM and the SFSA for Markov upset signals.

the SFSA and the FSM. The SFSA prediction is better, as it is slightly closer to

the experimental curve. In order to accurately characterize the error between the theoretical predictions and the experimental estimates, the *normalized error* and *mean-square normalized error* (MS error) are utilized. These statistics are defined as

$$\text{normalized error at } p_1 = \frac{\text{estimate at } p_1 - \text{prediction at } p_1}{\text{estimate at } p_1}$$

for $p_1 \in \mathbb{U}$, and

$$\text{mean-square normalized error} = \sqrt{\sum_{p_1 \in \mathbb{U}} (\text{normalized error at } p_1)^2},$$

respectively. Negative normalized error means that the prediction is larger than the estimate and vice versa. The smaller the error is, the closer the prediction and estimate are. The error statistics for the Markov upsets are shown in Table VI.

TABLE VI
Normalized Errors Between Experimental Estimates and Theoretical Predictions of the Output Tracking Powers for Markov Upsets

Upset probability	Normalized error before cluster analysis		Normalized error after cluster analysis	
	FSM	SFSA	FSM	SFSA
0	0	0	0	0
0.0001	-3.6184	-2.8412	-2.5691	-1.9685
0.0004	-4.6035	-3.7359	-1.3941	-1.0234
0.0006	-1.4418	-1.0979	0.1081	0.2337
0.0009	-0.3498	-0.2117	-0.3498	0.2117
0.0012	-0.2133	-0.2323	0.0533	0.0384
MS error	6.0441	4.8305	2.9463	2.2413

It can be seen that the normalized errors before the cluster analysis is applied are significant. In addition, the predictions from the SFSA modeled recovery process are slightly better than the predictions from the FSM models. However, the MS normalized errors are small for both cases when compared to the 34,000 ft cruising altitude. Thus, the model works well for this application under the assumption that the upset process is a first-order Markov chain.

V.2.2 Performance Analysis of the I.I.D. Tests

This subsection basically repeats the analysis in Subsection V.2.1 for the tests which used the i.i.d. upset sequences where $\pi_I(1) \in \mathbb{U}$. In this case, the ten experimental output tracking error powers for each value of $\pi_I(1)$ are shown in Fig. 42. The

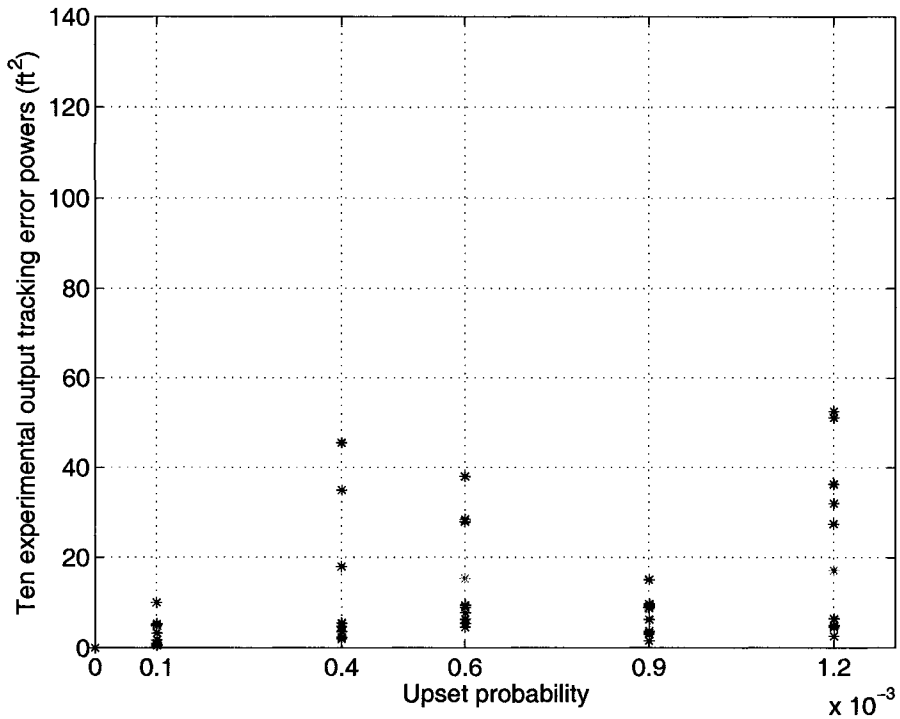

Fig. 42. The distribution of ten output tracking error powers for six specific upset probabilities for i.i.d. upset signals.

corresponding hierarchical clustering diagrams are shown in Fig. 43. The outliers are

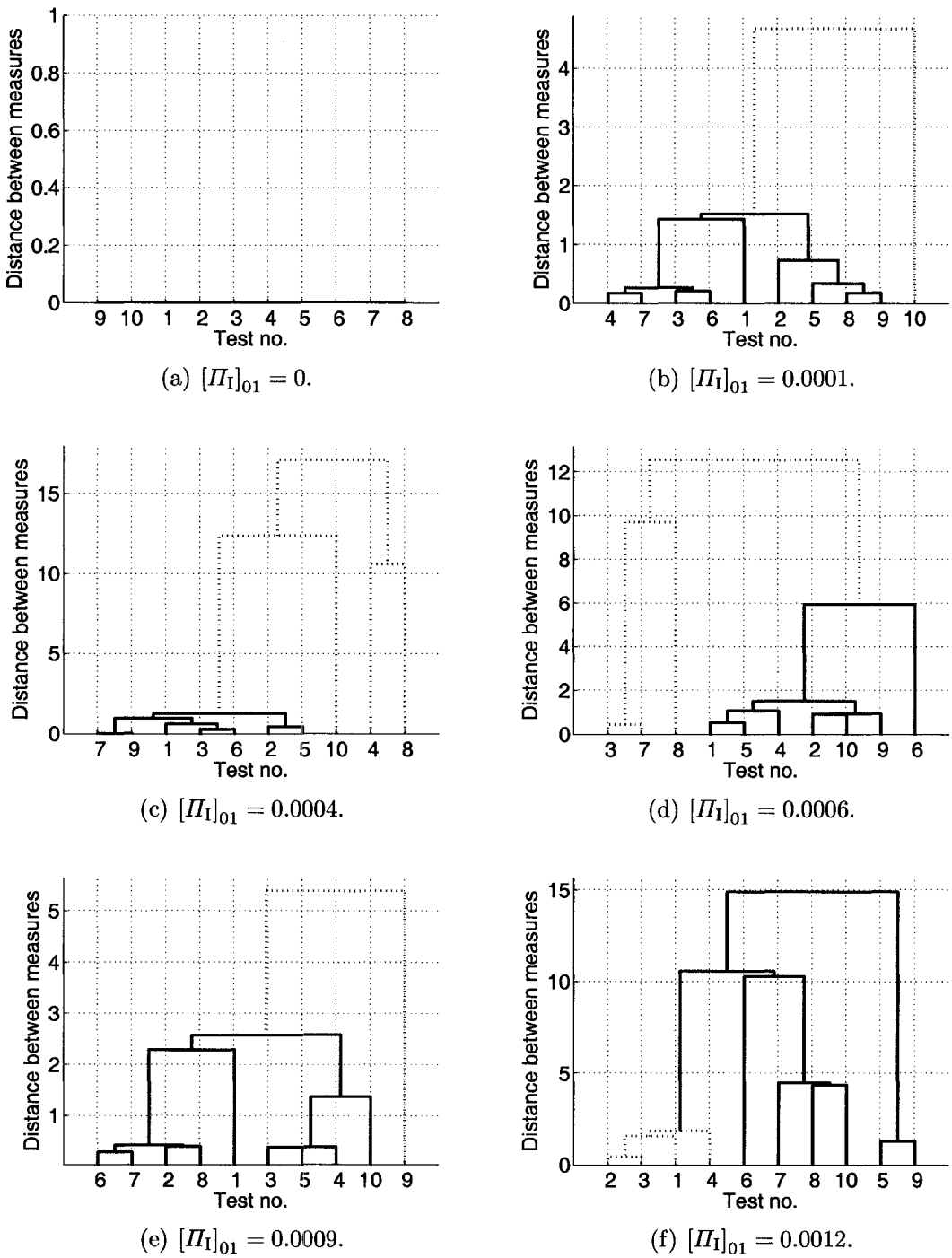

(a) $[\Pi_{\mathrm{I}}]_{01} = 0.$ (b) $[\Pi_{\mathrm{I}}]_{01} = 0.0001.$

(c) $[\Pi_{\mathrm{I}}]_{01} = 0.0004.$ (d) $[\Pi_{\mathrm{I}}]_{01} = 0.0006.$

(e) $[\Pi_{\mathrm{I}}]_{01} = 0.0009.$ (f) $[\Pi_{\mathrm{I}}]_{01} = 0.0012.$

Fig. 43. The cluster analysis diagrams for six specific upset probabilities for the i.i.d. upset signals.

linked in red-dotted line. The averages and standard deviations of the experimental mean output tracking powers at each upset probability, $\pi_I(1)$, before and after employing the cluster analysis technique are compared in Fig. 44. As expected, the

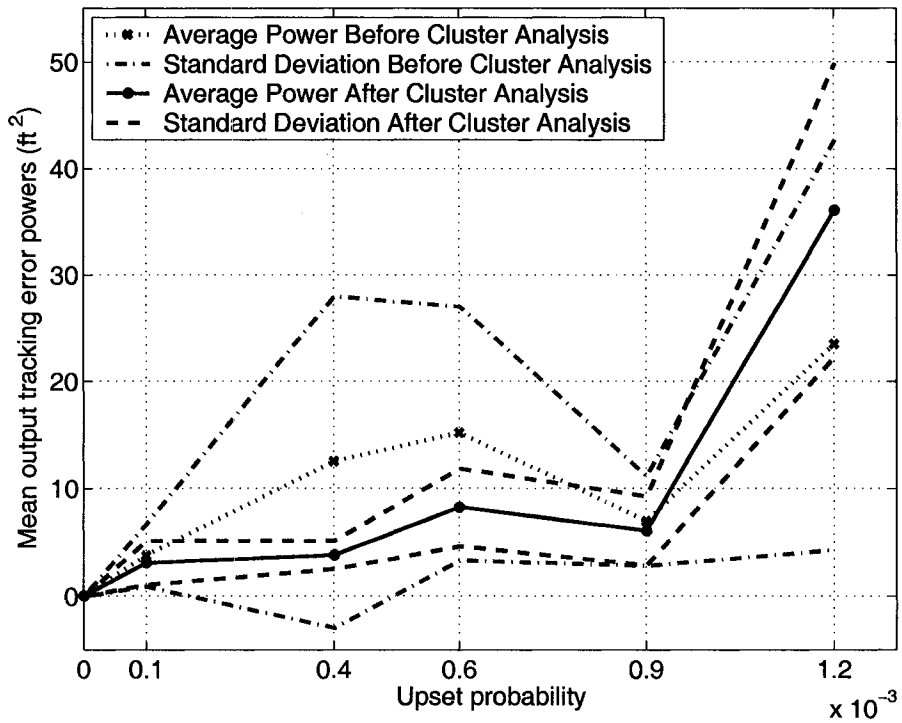

Fig. 44. The averages and standard deviations of the experimental output tracking powers before and after applying cluster analysis for i.i.d. tests.

standard deviations before the cluster analysis is applied are larger than those after the cluster analysis is employed. The details are summarized in Table VII, where it is clear that when $\pi_I(1) = 0.0004$, the cluster analysis is the most effective at excluding the outliers. The average output tracking error powers for the six probabilities were computed empirically from the experimental output data within the main cluster. The results are shown in Fig. 45 and compared against the theoretical predictions using both the SFSA and the FSM. Again, the SFSA prediction is better, as it is slightly closer to the experimental curve. The *normalized errors* and *MS (normalized) errors* for i.i.d. upsets are shown in Table VIII. The normalized errors before

TABLE VII
Comparison Between the Standard Deviation of the Output Tracking Powers Before and After the Cluster Analysis for I.I.D. Upsets

Upset probability	Standard deviation before cluster analysis	Standard deviation after cluster analysis	Deviation reduction ratio	Number of outliers removed after cluster analysis
0	0	0	1	0
0.0001	2.9317	2.0540	0.7006	1
0.0004	15.5031	1.3141	0.0848	3
0.0006	11.8691	3.6152	0.3046	3
0.0009	4.1638	3.1974	0.7679	1
0.0012	19.1979	13.7766	0.7176	4

the cluster analysis are much larger, and the predictions from the SFSA modeled recovery process are slightly better than the predictions from the FSM models. But as in the Markov case, the MS normalized errors are small for both cases. Thus, the hybrid model works well for this application under the assumption that the upset process is an i.i.d. process.

In summary, the hybrid model developed in Chapter II and the output performance produced in Chapter IV faithfully model the output tracking performance of the Boeing 737 system in closed-loop with an RCS subject to either a Markov or an i.i.d. upset process. From Tables VI and VIII, it is obvious that the difference of the tracking performance between Markov and i.i.d. upset processes is small.

TABLE VIII
Normalized Errors Between Experimental Estimate and Theoretical Prediction of the Output Tracking Powers for I.I.D. Upsets

Upset probability	Normalized error before cluster analysis		Normalized error after cluster analysis	
	FSM	SFSA	FSM	SFSA
0	0	0	0	0
0.0001	-5.0250	-4.0112	-3.9179	-3.0904
0.0004	-2.8716	-2.2721	-0.1840	-0.0007
0.0006	-1.5360	-1.1788	-0.3776	-0.1836
0.0009	0.4938	0.5456	0.5597	0.6047
0.0012	0.3869	0.3773	0.0596	0.0448
MS error	6.0207	4.8043	3.9804	3.1547

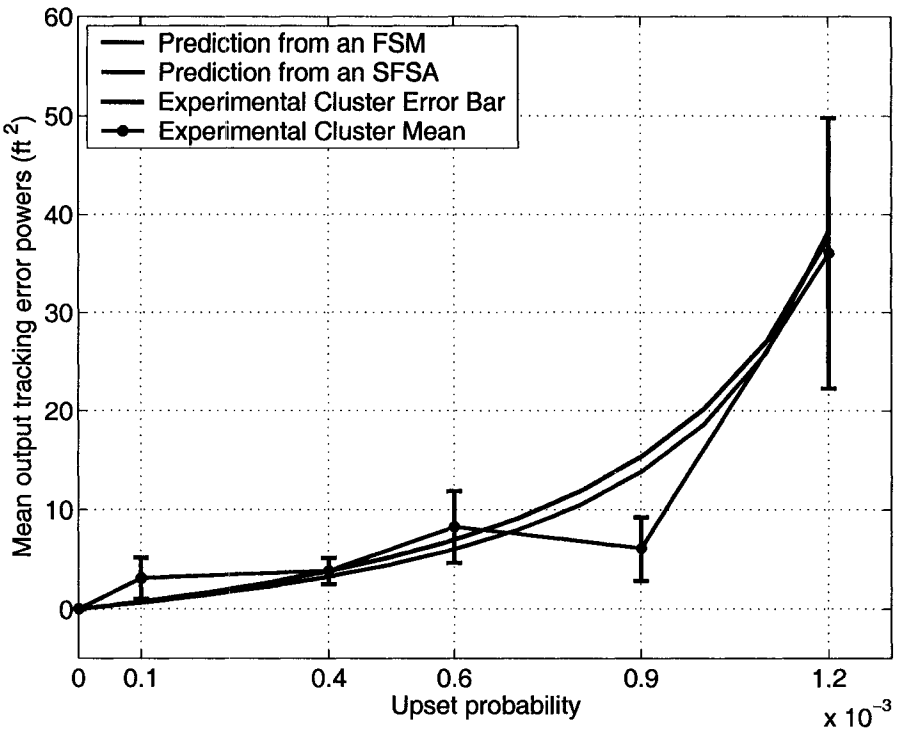

Fig. 45. The average power after cluster analysis and the theoretical predictions from the FSM and the SFSA for i.i.d. upset signals.

V.3 ANALYZING THE EXPERIMENTAL DATA FROM LOS ALAMOS

In this section, the data obtained from the LANSCE testbed is analyzed and compared against the experimental outcomes from NASA Langley and the theoretical predictions. In Subsection V.3.1, the Markovian nature of the SEU's is characterized. In Subsection V.3.2, the output tracking power is computed from the LANSCE data and then used to estimate the performance of the RCS under normal atmospheric conditions using the hybrid model.

V.3.1 Statistical Data Analysis of the Markovianess of SEU's

In Chapter II, when modeling the flight control system in closed-loop with an RCS, the upset process was assumed to be either a first-order Markov chain ($r = 1$) or an i.i.d. process ($r = 0$). In this subsection, this assumption will be investigated using the *high intensity* neutron test data obtained from LANSCE. This section is based on the work presented in [17, 18]. Out of 87 total trials, six experimental runs with 44,850 samples each were chosen because they contained the most recovery activity observed during the experiment. The number of rollbacks, believed to be caused by neutron-induced SEU's, for each of the six experimental runs is shown in Table IX (see Table X in Appendix B.1 for additional information). It should

TABLE IX
Recoveries Caused by Neutron-Induced SEU's in the Experiments Conducted at Los Alamos

Los Alamos test number	Recovery count
RCS_106	14
RCS_107	13
RCS_113	16
RCS_114	10
RCS_136	20
RCS_151	31

be noted from the onset that the Markovianess of the upset signal, $\boldsymbol{\nu}(k)$, cannot be determined *directly* from this data since $\boldsymbol{\nu}(k)$ could not be measured with the instrumentation available. Instead, the switching signal $\boldsymbol{\theta}(k)$, a filtered version of $\boldsymbol{\nu}(k)$

via the recovery logic of the SFSA (see, for example, Figs. 2 and 3), was measured using the internal variable `RCS_count`. The signal $\boldsymbol{\theta}(k)$ takes the value 1 only during the recovery period and is 0 otherwise. For example, in Fig. 36(b) on page 108, from Frame 13,860 to Frame 13,880, $\boldsymbol{\theta}(k) = 1$ for $k = 13866, 13867, \ldots, 13871$ and $\boldsymbol{\theta}(k) = 0$, otherwise. The *claim* is that $\boldsymbol{\nu}(k)$ is i.i.d. because $\boldsymbol{\theta}(k)$ is a first-order Markov chain (see Theorem II.7).

The procedure to determine the Markovianess of $\boldsymbol{\theta}(k)$ was based on χ^2 hypothesis testing. In this application, two types of χ^2 hypothesis tests were employed to analyze the $\boldsymbol{\theta}(k)$ sequences: one for testing the homogeneity and the other for selecting the best order fit of a Markov chain to the data [90]. The two tests are described briefly as follows (see [17, 18] for additional details).

For testing the homogeneity, two hypotheses were considered:

$$H_0 : \text{The } \boldsymbol{\theta}(k) \text{ sequences are homogeneous,}$$

$$H_1 : \text{The } \boldsymbol{\theta}(k) \text{ sequences are non-homogeneous.}$$

Let s be the total number of tests and K the length of the data sequences. (In our context, $s = 6$ and $K = 44,580$.) For $i, j \in \{0, 1\}$ and $k = 1, 2, \ldots, K$, $n_i(k-1)$ is used to denote the total number of instances in the s data sets such that $\boldsymbol{\theta}(k-1) = i$. Let $\hat{p}_{ij}(k)$ denote the non-homogeneous transition probability from $\boldsymbol{\theta}(k-1) = i$ to $\boldsymbol{\theta}(k) = j$ based on the s data sets at time k. $\hat{p}_{ij}$ denotes the homogeneous transition probability from i to j based on the total sK data. A homogeneity test can be conducted using the following test statistic

$$\chi^2_{\text{TS}} = \sum_{k=1}^{K-1} \sum_{i,j \in \{0,1\}} \frac{n_i(k-1)\left[\hat{p}_{ij}(k) - \hat{p}_{ij}\right]^2}{\hat{p}_{ij}},$$

where as $sK \rightarrow \infty$, the test statistic is a χ^2 distribution with $2(K-1)$ degrees of freedom. The critical value, χ^2_{CV}, for the hypothesis test is determined by the degrees of freedom and a specified α-error, which is the conditional probability of choosing H_1 given that the true hypothesis is H_0. Specifically, H_0 cannot be rejected if $\chi^2_{\mathrm{TS}} < \chi^2_{\mathrm{CV}}$, and it is rejected if $\chi^2_{\mathrm{TS}} \geq \chi^2_{\mathrm{CV}}$. Using the experimental data from LANSCE, the χ^2 homogeneity test results are shown in Fig. 46. The test statistic

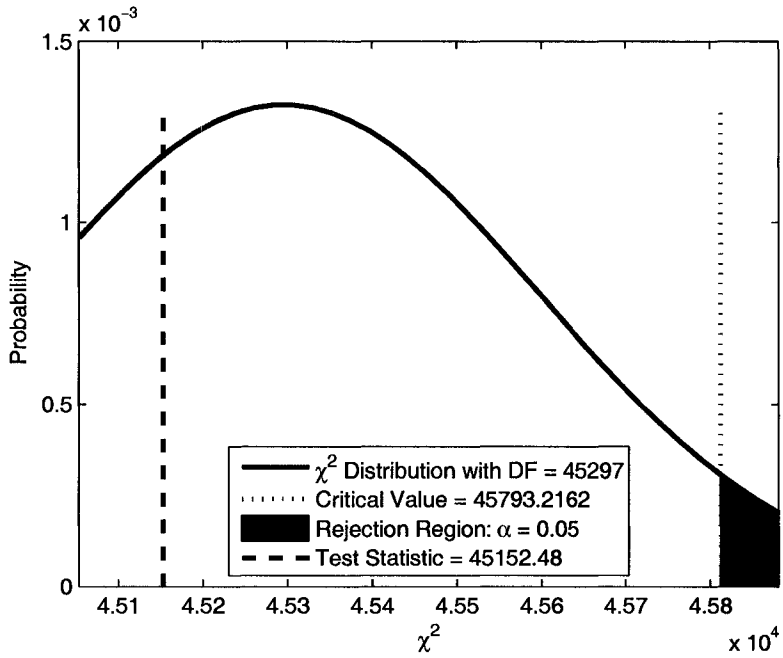

Fig. 46. Homogeneity results from the LANSCE experiments.

was found to be $\chi^2_{\mathrm{TS}} = 45152.48$. The χ^2 critical value for an α-error of 0.05 with 45,297 degrees of freedom is $\chi^2_{\mathrm{CV}} = 45793.22$. Since $\chi^2_{\mathrm{TS}} < \chi^2_{\mathrm{CV}}$, the data was deemed to be homogeneous.

For fitting a Markov chain model to the data, another pair of hypotheses was considered:

$\tilde{H}_0$: The $\boldsymbol{\theta}(k)$ sequences can be fitted to an $(r-1)$th-order Markov Chain,

$\tilde{H}_1$: The $\boldsymbol{\theta}(k)$ sequences can be fitted to an rth-order Markov Chain.

The hypothesis tests are iteratively executed starting with a specified upperbound for r. Let $ij\ldots kl$ be a specific binary word of length $r+1$. $n_{ij\ldots kl}$ is used to denote the number of occurrences of this word in the sK data, and let $n_{ij\ldots k*} = \sum_{l\in\{0,1\}} n_{ij\ldots kl}$. The (homogeneous) transition probabilities for an rth-order Markov chain is denoted by $\hat{p}_{ij\ldots kl}$, and for an $(r-1)$th-order Markov chain it is denoted by $\hat{p}_{j\ldots kl}$, where $j\ldots kl$ is of length r. The test statistic for an rth-order Markov chain is then defined as:

$$\tilde{\chi}^2_{\mathrm{TS}} = \sum_{i,j,\ldots,k,l\in\{0,1\}} \frac{n_{ij\ldots k*}\left[\hat{p}_{ij\ldots kl} - \hat{p}_{j\ldots kl}\right]^2}{\hat{p}_{j\ldots kl}}.$$

As $sK \to \infty$, this test statistic has a χ^2 distribution with 2^{r-1} degrees of freedom. The critical value, $\tilde{\chi}^2_{\mathrm{CV}}$, can also be determined by the degrees of freedom and a specified α-error. $\tilde{H}_0$ cannot be rejected if $\tilde{\chi}^2_{\mathrm{TS}} < \tilde{\chi}^2_{\mathrm{CV}}$, and it is rejected if $\tilde{\chi}^2_{\mathrm{TS}} \geq \tilde{\chi}^2_{\mathrm{CV}}$. The Markovianess analysis of the data from LANSCE is shown in Fig. 47. The graph indicates, for $\alpha = 0.05$, that the test statistic values for each hypothesis test are greater than the corresponding critical values. Thus, all the $\tilde{H}_0$'s are rejected; that is, in this case, the data cannot be fitted with a fourth or lower order Markov process. However, for a significantly smaller α-value, $\alpha = 10^{-10}$, it indicates that $\boldsymbol{\theta}(k)$ can be fitted to a first-order Markov chain. Of particular interest is the fact that the test statistic increased by three orders of magnitude in the $r = 1$ case. This is strong evidence that $\boldsymbol{\theta}(k)$ is a first-order Markov process, which, in turn, suggests that the upset process, $\boldsymbol{\nu}(k)$, can be modeled as an i.i.d. process. Therefore, the experimental output tracking powers should be compared with the corresponding theoretical predictions and simulated-neutron experimental results for the i.i.d. case.

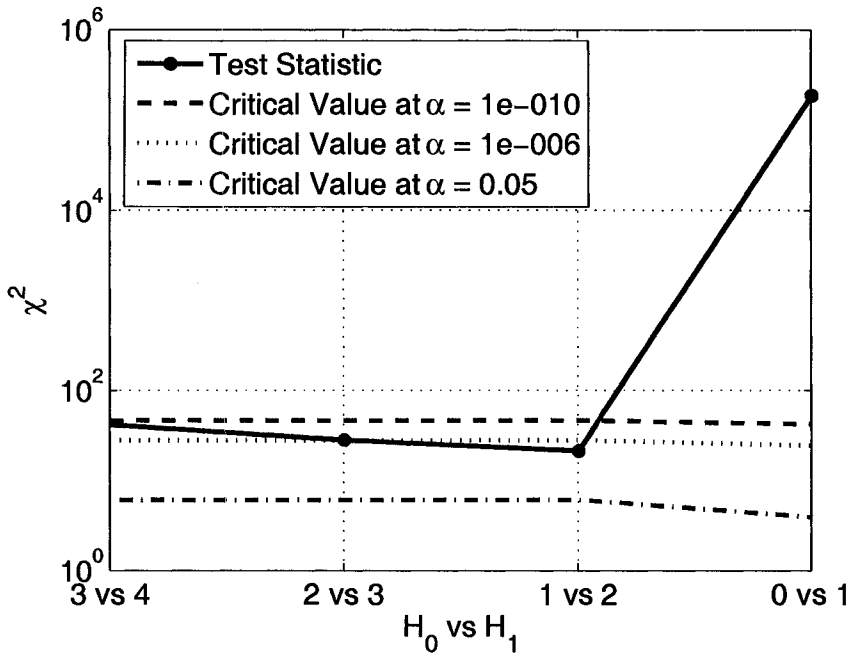

Fig. 47. Fitting a Markov chain to the LANSCE experimental data.

V.3.2 Output Tracking Performance Analysis in the LANSCE Neutron Environment

In this subsection, the output tracking power was computed for eleven trials from the LANSCE neutron experiment. The upset probability was estimated using the ratio of the number of rollback recoveries for each test to the total number of frames in this test, that is,

$$\hat{\pi}_{\mathrm{I}}(1) = \frac{\text{number of rollback recovery processes}}{\text{total number of frames}}.$$

In the analysis, the aircraft's output variables were compared against nominal flights, i.e., ones with no rollback recoveries (in this case, $\pi_{\mathrm{I}}(1) = 0$). The tracking error statistics were then computed using the output errors. The results were finally compared against those from the NASA experiment and the theoretical predictions. In Fig. 48,

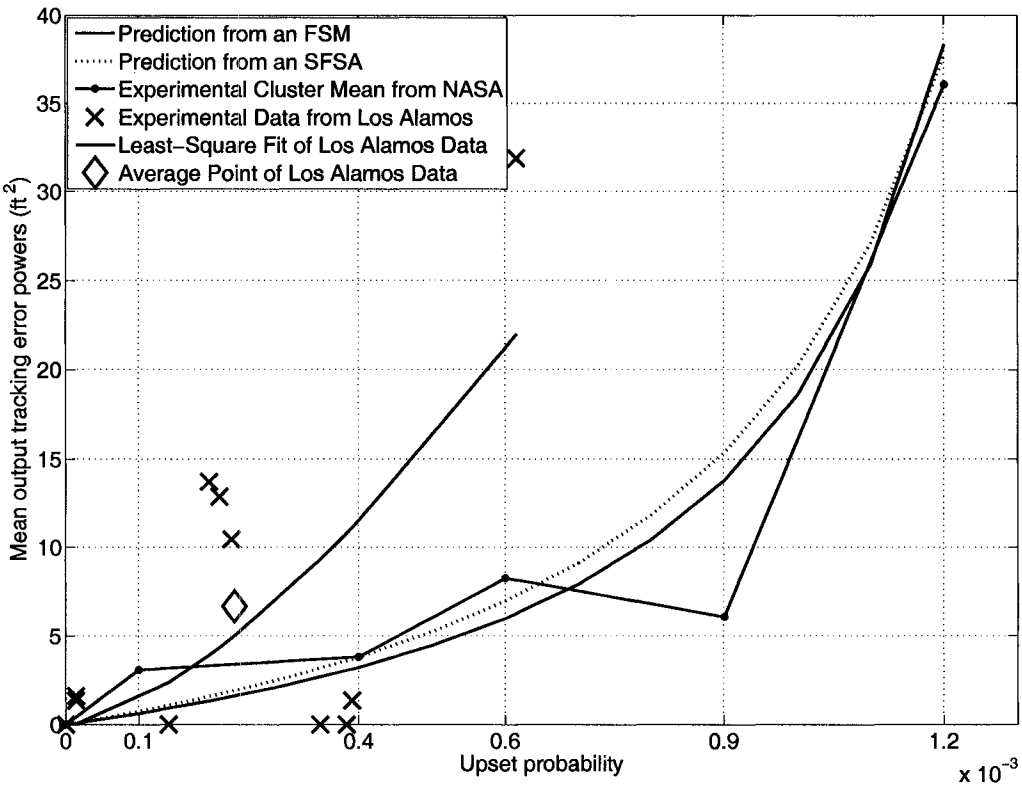

Fig. 48. Comparing the mean output tracking powers obtained from the theoretical predictions, the simulated neutron environment at NASA Langley (after cluster analysis) and the high intensity neutron environment at LANSCE.

predictions from the hybrid models with an FSM and an SFSA recovery logic unit are denoted in blue-dotted and red-solid lines, respectively. The experiment data from NASA Langley with an i.i.d. upset process is denoted with a magenta curve. The experimental data from LANSCE is denoted using single black dots in the figure. The standard deviation of the output tracking power is 9.9917. A least-square fit of the data is given in a green-solid line. The *average point* is denoted as a red diamond point. It represents the average upset probability and the average output tracking power pair $(0.0002, 6.6567)$. If cluster analysis is employed, which will eliminate the outlier $(0.0006, 31.8958)$ (see Fig. 49), the new average point pair is $(0.0002, 4.1328)$,

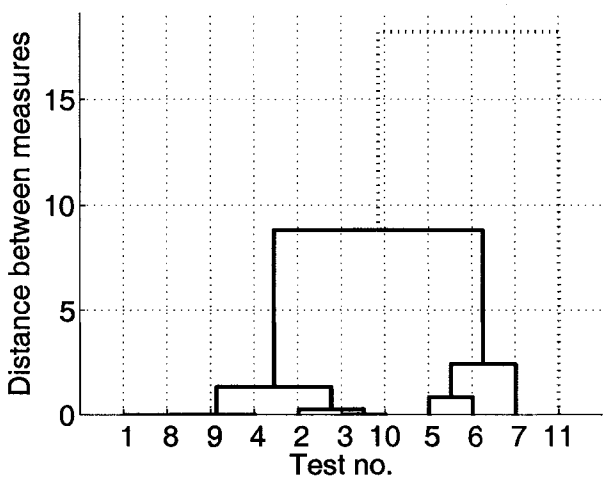

Fig. 49. The cluster analysis diagram for the output tracking power estimates from LANSCE.

and the standard deviation of the output power is 5.7506. The deviation reduction ratio for the output power is $0.5755 < 1$, thus the cluster analysis effectively deletes the outlier. The new least-square fitting curve also significantly improves. Fig. 50 shows the LANSCE experimental estimates after the cluster analysis. Therefore, at the average point, when $\hat{\pi}_I(1) = 0.0002$, under the high intensity neutron environment, the rollback recovery process of the RCS introduces a deviation less than

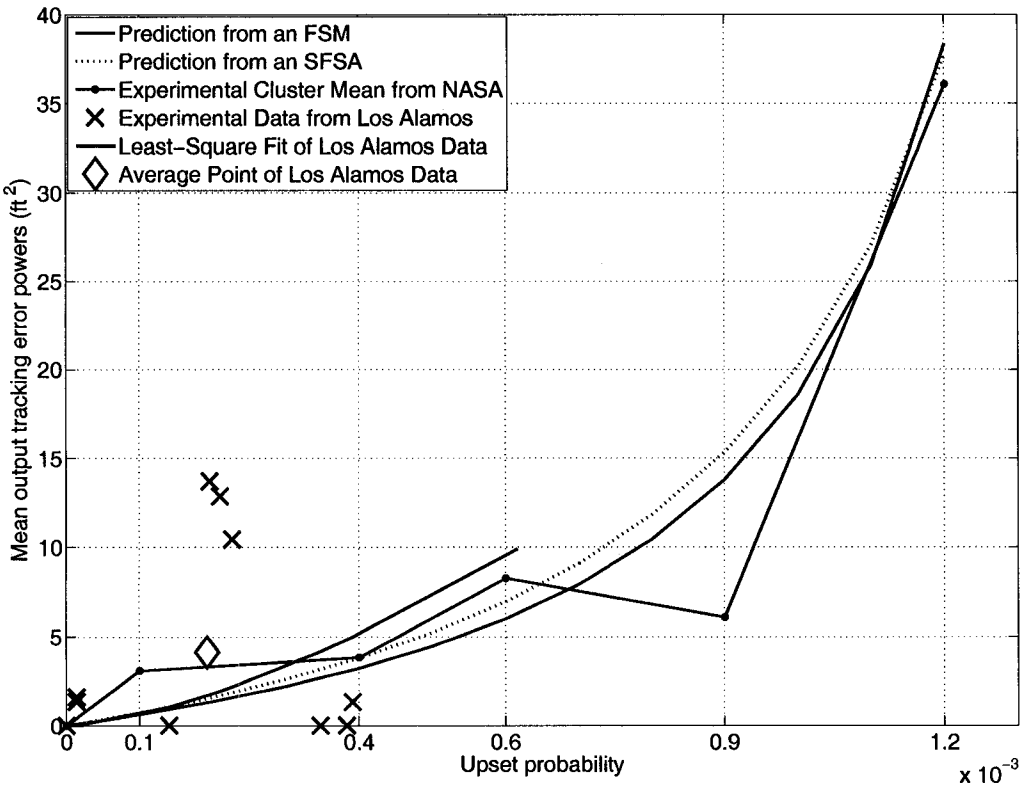

Fig. 50. Comparing the mean output tracking powers obtained from the theoretical predictions, the simulated neutron environment at NASA Langley (after cluster analysis) and the high intensity neutron environment at LANSCE (after cluster analysis).

± 3 ft from the cruising altitude (34,000 ft). Since the upset probability under normal atmospheric conditions is much lower than this, using the performance theory, the output tracking performance will also be much smaller (see Fig. 6). Specifically, the neutron intensity at LANSCE is around 10^5 higher than the normal atmospheric conditions, so the deviation under normal atmospheric conditions is estimated to be smaller than ± 0.01 ft. This means that the recoverable flight control system, when functioning as designed, provides reliable control performance in the presence of the neutron induced single-event upsets at normal atmospheric levels.

V.4 SUMMARY

In this chapter, two RCS experiments were described: one experiment was performed at LANSCE in a real neutron environment; the other was conducted at the NASA Langley in a simulated-neutron environment. Mean output tracking power was calculated using the data obtained from NASA and compared with the theoretical prediction. The results validated that the stochastic hybrid system could be used to predict output tracking performance of the recoverable flight control system. The LANSCE experimental data was used to analyze the Markovianess nature of the SEU's. The mean output tracking power was also computed using this data, which was then rescaled to assess the tracking performance of the RCS controlled aircraft system under normal atmospheric conditions.

CHAPTER VI

CONCLUSIONS AND FUTURE RESEARCH

In this final chapter, the main contributions and conclusions of this dissertation are summarized in Section VI.1, and future research topics are described in Section VI.2.

VI.1 MAIN CONCLUSIONS

The general contributions of this dissertation are, from a theoretical point of view, constructing a stochastic hybrid model class for a recoverable flight control system and developing mathematical tools for stability and output tracking performance analysis. From an application point of view, the contributions are modeling a Boeing 737 in closed-loop with an RCS and analyzing its tracking performance in a real neutron environment in order to determine the efficiency of the fault tolerant architecture.

The specific research conclusions in this dissertation are summarized as follows:

1. A class of stochastic hybrid models was introduced for modeling recoverable closed-loop systems. In this model, the upset processes were modeled as either (first-order) Markovian or i.i.d. processes; the nominal and recovery modes were modeled by linear state space realizations; and the rollback recovery processes of the RCS were approximated using an SFSA (or an FSM).

2. A mean-square stability criterion for the stochastic hybrid system was developed by analyzing its model-equivalent Markov jump-linear system. It was shown that if the hybrid system is MSS, its output performance can be characterized in terms of a new generalized observability Gramian. This model was then applied to the recoverable Boeing 737 control system to generate output tracking performance predictions.

3. A series of tests performed in a simulated neutron environment at NASA Langley, where the upsets were triggered by software-injected signals, validated the theoretical performance predictions.

4. The performance analysis tools were used to *rescale* the performance estimates derived from real (accelerated) neutron tests conducted at LANSCE to atmospheric levels. The main conclusion of the dissertation is that the recoverable flight control system, when functioning as designed, will provide reliable control performance in the presence of neutron-induced single-event upsets under normal atmospheric conditions.

VI.2 FUTURE RESEARCH

Some interesting open problems related to this dissertation are presented in the following subsections.

VI.2.1 Model Reduction Improvements

The model-equivalent Markov jump-linear system used for the recoverable flight control system is an 8-dimensional system with a 14-state input–output cross product

process. The dimension of $\mathscr{A}_2$ is 896 (i.e., $8^2 \times 14$). This size limits the accuracy of the calculations for the stability and the output performance since the spectral radius and the matrix inverse must be computed. For the output tracking error system, which is of dimension 3,584 (i.e., $(2 \times 8)^2 \times 14 = 896 \times 4$), the situation is even worse. Therefore, it will be interesting to consider some type of model reduction. Some ideas in this direction are:

1. To use only the output signals of the SFSA in the analysis. Is it possible to extend the theory presented in this dissertation to a non-stationary Markov/non-Markov jump-linear system? If so, only the output signals of the SFSA need be considered. In this case, the dimension of the hybrid model is exactly half of the Markov jump-linear system.

2. To use the fact that all the six recovery states "$R_1, R_2, \ldots, R_6$" of the SFSA share the same dynamics. These dynamics were replicated six times in the stability and performance calculations. Is it possible to avoid this redundancy? In this case, the dimension will be reduced from 896 to 128 for the hybrid system and from 896×4 to 128×4 for the tracking error system.

3. To employ partial switching. Only two control signals (those for the aileron and the elevator) have the recovery capability. The idea is to partition the controller dynamics, and then employ system identification to the two subsystems individually. A conceptual view of this idea is given in Fig. 51. Assume, for example, that the controller dynamics for the aileron and the elevator are 2-dimensional and the other part is 6-dimensional. Then the dimension of $\mathscr{A}_2$

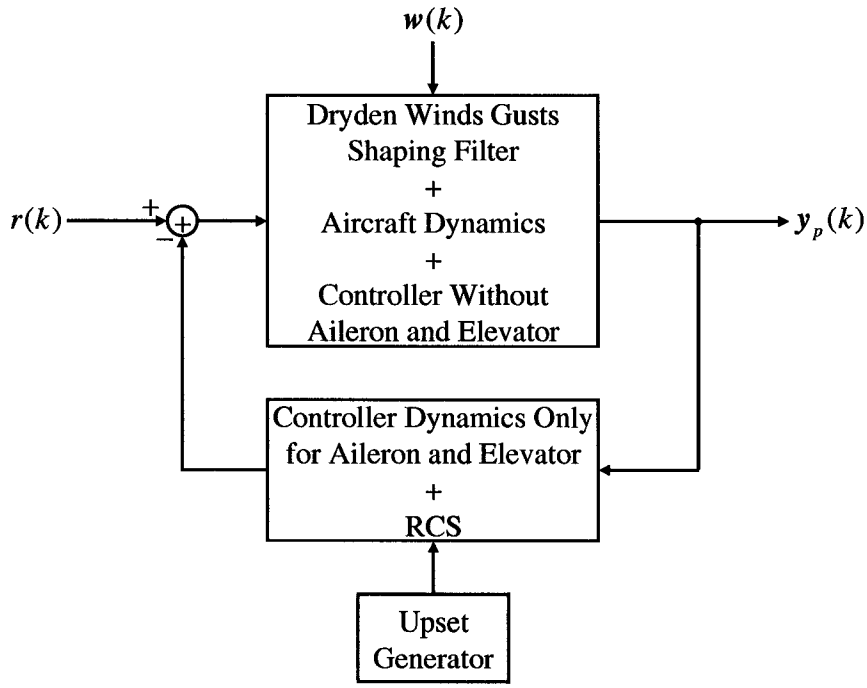

Fig. 51. A conceptual view of a partial switching system.

with the 14-state cross product switching process is $2^2 \times 14 = 56$ and the dimension of the whole system is $56 + 6 = 62$. For the tracking error system, the total dimension is 230 (i.e., $56 \times 4 + 6$).

4. To use a different model class, for example, stochastic nonlinear systems. But in this case, it may be difficult to analytically calculate the output tracking performance.

VI.2.2 RCS Algorithm Improvement

This dissertation did not address the problem of how to apply the results to improving the RCS device. However, the hardware might be improved at least in two ways:

1. To improve the efficiency of rollback recovery algorithm itself. The current

rollback recovery algorithm simply rolls all the states back to previously saved values when it is doing a recovery. Therefore, the recovery periods are five to six frame in length, which in turn reduces the system performance. If only the *critical states* are rolled back, then the algorithm may operate faster. Thus, the performance may also be improved. There should be some system theoretic method to determine what the *critical states* are for a given application.

2. Improve the fault detection and correction algorithm. At present, only detected upset signals are corrected. But how can one know for sure whether some upsets are missed, and thus uncorrected? One idea is to compare the output performance *prediction* with the actual system performance at each checkpoint. If the actual performance is significantly worse than the prediction, it is possible that there were missed detections, and an additional rollback is necessary.

VI.2.3 Other Interesting Topics

It was shown in Section II.3 that the nominal mode has a higher dimensional state space realization than the recovery mode. A state augmentation technique was used to equate the dimensions by adding two auxiliary states to the recovery mode. But another approach is to decouple the states of the nominal mode into two parts: one part with two states which are non-switched and the other part with six states which are switched with the recovery mode. In this case, no state embedding is needed. One could also remove two states from the nominal mode, so that both the nominal and the recovery modes are six-dimensional. But how can this be done systematically? Another technique is to develop a mathematical tool for analyzing a

system switching between dynamics of different dimensions.

The main application for the theory in this dissertation was a Boeing 737 simulation system. It would be interesting to apply the theory to another aircraft system or perhaps a UAV. The methodology can also be extended to other safety critical applications like nuclear power plant control systems.

BIBLIOGRAPHY

[1] R. B. Mendell and S. A. Korff, "Fast-neutron flux in the atmosphere," *J. Geophys. Res.*, vol. 68, no. 19, pp. 5487–5495, 1963.

[2] J. F. Ziegler, "Terrestrial cosmic rays," *IBM J. Res. Develop.*, vol. 40, no. 1, pp. 19–39, 1996.

[3] E. Normand and T. J. Baker, "Altitude and latitude variations in avionics SEU and atmospheric neutron flux," *IEEE Trans. Nucl. Sci.*, vol. 40, no. 6, pp. 1484–1490, 1993.

[4] K. E. Holbert, "Single event effects." [Online]. Available: http://www.eas.asu.edu/~holbert/eee460/see.html

[5] G. C. Messenger and M. S. Ash, *The Effects of Radiation on Electronic Systems*, 2nd ed. New York: Van Nostrand Reinhold, 1992.

[6] T. J. O'Gorman, J. M. Ross, A. H. Taber, J. F. Ziegler, H. P. Muhlfeld, C. J. Montrose, H. W. Curtis, and J. L. Walsh, "Field testing for cosmic ray soft errors in semiconductor memories," *IBM J. Res. Develop.*, vol. 40, no. 1, pp. 41–50, 1996.

[7] J. F. Ziegler, H. P. Muhlfeld, C. J. Montrose, H. W. Curtis, T. J. O'Gorman, and J. M. Ross, "Accelerated testing for cosmic soft-error rate," *IBM J. Res. Develop.*, vol. 40, no. 1, pp. 51–72, 1996.

[8] W. S. Gray, O. R. González, and M. Doğan, "Stability analysis of digital linear flight controllers subject to electromagnetic disturbances," *IEEE Trans. Aerosp. Electron. Syst.*, vol. 36, no. 4, pp. 1204–1218, 2000.

[9] O. R. González, W. S. Gray, and A. Tejada, "Analytical tools for the design and verification of safety critical control systems," *2001 SAE Transact.—J. Aerosp.*, vol. 110, no. 1, pp. 481–490, 2002.

[10] R. Hess, "Computing platform architectures for robust operation in the presence of lightning and other electromagnetic threats," in *16th Digital Avionics Systems Conf. Proceedings*, Irvine, California, 1997, pp. 4.3–9–16.

[11] ——, "Options for aircraft function preservation in the presence of lightning," in *Proc. 1999 International Conf. Lightning Static Electricity*, Toulouse, France, 1999, paper no. 106.

[12] M. Malekpour and W. Torres, "Characterization of a recoverable flight control computer system," in *Proc. 1999 IEEE Int. Conf. Contr. Appl.*, Kohala Coast-Island of Hawaii, Hawaii, 1999, pp. 1519–1524.

[13] ——, "Characterization of a flight control computer with rollback recovery," in *19th Digital Avionics Systems Conf. Proceedings*, Philadelphia, Pennsylvania, 2000, pp. 3.C.4–1–8.

[14] R. Narasimhan, D. J. Rosenkrantz, and S. S. Ravi, "Early comparison and decision strategies for datapaths that recover from transient faults," *IEEE Trans. Circuits Syst.—I: Fundam. Theory Appl.*, vol. 44, no. 5, pp. 435–438, 1997.

[15] A. Ranganathan and S. J. Upadhyaya, "Performance evaluation of rollback-recovery techniques in computer programs," *IEEE Trans. Reliab.*, vol. 42, no. 2, pp. 220–226, 1993.

[16] A. Tejada, "Analysis of error recovery effects on digital flight control systems," Master's thesis, Department of Electrical and Computer Engineering, Old Dominion University, 2002.

[17] A. V. Lakdawala, H. Zhang, O. R. González, and W. S. Gray, "Markovian statistical data analysis of single-event upsets triggered by high intensity neutrons," in *Proc. 38th IEEE Southeastern Symp. System Theory*, Cookeville, Tennessee, 2006, pp. 349–353.

[18] A. V. Lakdawala, "A Markovian statistical analysis of single-event upsets on closed-loop flight control systems," Master's thesis, Department of Electrical and Computer Engineering, Old Dominion University, 2006.

[19] S. Patilkulkarni, "Stability analysis of jump-linear systems driven by finite-state machines with Markovian inputs," Ph.D. dissertation, Department of Electrical and Computer Engineering, Old Dominion University, 2004.

[20] O. L. V. Costa and M. D. Fragoso, "Stability results for discrete-time linear systems with Markovian jumping parameters," *J. Math. Anal. Appl.*, vol. 179, pp. 154–178, 1993.

[21] J. B. R. do Val and E. F. Costa, "Numerical solution for linear-quadratic control problems of Markov jump linear systems and weak detectability concept," *J. Optim. Theory Appl.*, vol. 114, no. 1, pp. 69–96, 2002.

[22] T. Kailath, *Linear Systems*, ser. Prentice-Hall Information and System Sciences Series, T. Kailath, Ed. Englewood Cliffs, New Jersey: Prentice-Hall, Inc., 1980.

[23] G. C. Messenger and M. S. Ash, *Single Event Phenomena.* New York: Chapman & Hall, 1997.

[24] W. Heidergott, "SEU tolerant device, circuit and processor design," in *Proc. 42nd Design Automation Conf.*, Anaheim, California, 2005, pp. 5–10.

[25] E. Normand, "Single event upset at ground level," *IEEE Trans. Nucl. Sci.*, vol. 43, no. 6, pp. 2742–2750, 1996.

[26] M. Ceschia, M. Violante, M. Sonza Reorda, A. Paccagnella, P. Bernardi, M. Rebaudengo, D. Bortolato, M. Bellato, P. Zambolin, and A. Candelori, "Identification and classification of single-event upsets in the configuration memory of SRAM-based FPGAs," *IEEE Trans. Nucl. Sci.*, vol. 50, no. 6, pp. 2088–2094, 2003.

[27] H. T. Nguyen, Y. Yagil, N. Seifert, and M. Reitsma, "Chip-level soft error estimation method," *IEEE Trans. Device Mater. Reliab.*, vol. 5, no. 3, pp. 365–381, 2005.

[28] N. Renaud, "How to cope with SEU/SET at chip level? The example of a microprocessor family," in *Proc. 11th IEEE International On-Line Testing Symp.*, Saint Raphael, French Riviera, France, 2005, pp. 313–314.

[29] A. Tiwari and K. A. Tomko, "Enhanced reliability of finite-state machines in FPGA through efficient fault detection and correction," *IEEE Trans. Reliab.*, vol. 54, no. 3, pp. 459–467, 2005.

[30] D. M. Newberry, "Investigation of single event effects at the system level," in *Proc. 2nd European Conf. Radiation Effects Components Systems*, Saint Malo, France, 1993, pp. 113–120.

[31] Y. Blaquière, G. Gagné, Y. Savaria, and C. Évéquoz, "A new efficient algorithmic-based SEU tolerant system architecture," *IEEE Trans. Nucl. Sci.*, vol. 42, no. 6, pp. 1599–1606, 1995.

[32] L. Schiano, M. Ottavi, and F. Lombardi, "Markov models of fault-tolerant memory systems under SEU," in *Records 2004 IEEE International Workshop Memory Technology Design Testing*, San Jose, California, 2004, pp. 38–43.

[33] M. Pignol, "How to cope with SEU/SET at system level?" in *Proc. 11th IEEE International On-Line Testing Symp.*, Saint Raphael, French Riviera, France, 2005, pp. 315–318.

[34] C.-Y. Liu, "A study of flight-critical computer system recovery from space radiation-induced error," *IEEE Aerosp. Electron. Syst. Mag.*, vol. 17, no. 7, pp. 19–25, 2002.

[35] R. A. DeCarlo, M. S. Branicky, S. Pettersson, and B. Lennartson, "Perspectives and results on the stability and stabilizability of hybrid systems," *Proc. IEEE*, vol. 88, no. 7, pp. 1069–1082, 2000.

[36] A. Gollu and P. O. Varaiya, "Hybrid dynamical systems," in *Proc. 28th IEEE Conf. Decision Control*, Tampa, Florida, 1989, pp. 2708–2712.

[37] R. W. Brockett, "Hybrid models for motion control systems," in *Essays on Control: Perspectives in the Theory and Its Applications*, ser. Progress in Systems and Control Theory, H. L. Trentelman and J. C. Willems, Eds. Boston, Massachusetts: Birkhäuser, 1993, vol. 14, pp. 29–53.

[38] J. Hu, J. Lygeros, and S. Sastry, "Towards a theory of stochastic hybrid systems," in *Hybrid Systems: Computation and Control*, ser. Lecture Notes in Computer Science, N. Lynch and B. Krogh, Eds. Berlin: Springer-Verlag, 2000, vol. 1790, pp. 160–173.

[39] G. Pola, M. Bujorianu, J. Lygeros, and M. D. Di Benedetto, "Stochastic hybrid models: An overview," in *Proc. IFAC Conf. Analysis Design Hybrid Systems*, Saint-Malo, Brittany, France, 2003, pp. 45–50.

[40] O. L. V. Costa, M. D. Fragoso, and R. P. Marques, *Discrete-Time Markov Jump Linear Systems*, ser. Probability and Its Applications, J. Gani, C. C. Heyde, P. Jagers, and T. G. Kurtz, Eds. London: Springer-Verlag, 2005.

[41] Y. Ji, H. J. Chizeck, X. Feng, and K. A. Loparo, "Stability and control of discrete-time jump linear systems," *Control—Theory Adv. Technol.*, vol. 7, no. 2, pp. 247–270, 1991.

[42] Y. Fang and K. A. Loparo, "Stochastic stability of jump linear systems," *IEEE Trans. Automat. Contr.*, vol. 47, no. 7, pp. 1204–1208, 2002.

[43] O. L. V. Costa and M. D. Fragoso, "Comments on 'Stochastic stability of jump linear systems'," *IEEE Trans. Automat. Contr.*, vol. 49, no. 8, pp. 1414–1416, 2004.

[44] V. Dragan and T. Morozan, "Stability and robust stabilization to linear stochastic systems described by differential equations with Markovian jumping and multiplicative white noise," *Stoch. Analy. Appl.*, vol. 20, no. 1, pp. 33–92, 2002.

[45] P. Bolzern, P. Colaneri, and G. De Nicolao, "On almost sure stability of discrete-time Markov jump linear systems," in *Proc. 43rd IEEE Conf. Decision Control*, Atlantis, Paradise Island, Bahamas, 2004, pp. 3204–3208.

[46] H. J. Chizeck and Y. Ji, "Optimal quadratic control of jump linear systems with Gaussian noise in discrete time," in *Proc. 27th IEEE Conf. Decision Control*, Austin, Texas, 1988, pp. 1989–1993.

[47] V. Dragan, T. Morozan, and A. Stoica, "H^2 optimal control for linear stochastic systems," *Automatica*, vol. 40, pp. 1103–1113, 2004.

[48] H. J. Chizeck, A. S. Willsky, and D. Castanon, "Discrete-time Markovian-jump quadratic optimal control," *Int. J. Control*, vol. 43, no. 1, pp. 213–231, 1986.

[49] T. Morozan, "Optimal stationary control for dynamic systems with Markov perturbations," *Stoch. Analy. Appl.*, vol. 3, no. 1, pp. 299–325, 1983.

[50] Q. Ling and M. D. Lemmon, "Robust performance of soft real-time networked control systems with data dropouts," in *Proc. 41st IEEE Conf. Decision Control*, Las Vegas, Nevada, 2002, pp. 1225–1230.

[51] ——, "Soft real-time scheduling of networked control systems with dropouts governed by a Markov chain," in *Proc. 2003 Amer. Control Conf.*, Denver, Colorado, 2003, pp. 4845–4850.

[52] ——, "Optimal dropout compensation in networked control systems," in *Proc. 42nd IEEE Conf. Decision Control*, Maui, Hawaii, 2003, pp. 670–675.

[53] A. Stoica and I. Yaesh, "Jump Markovian-based control of wing deployment for an uncrewed air vehicle," *J. Guid. Control Dyn.*, vol. 25, no. 2, pp. 407–411, 2002.

[54] O. L. V. Costa and E. F. Tuesta, "H_2-control and the separation principle for discrete-time Markovian jump linear systems," *Math. Control Signals Syst.*, vol. 16, no. 4, pp. 320–350, 2004.

[55] J. B. R. do Val and T. Başar, "Receding horizon control of jump linear systems and a macroeconomic policy problem," *J. Econ. Dynam. Contr.*, vol. 23, no. 8, pp. 1099–1131, 1999.

[56] P. Seiler and R. Sengupta, "Analysis of communication losses in vehicle control problems," in *Proc. 2001 Amer. Control Conf.*, Arlington, Virginia, 2001, pp. 1491–1496.

[57] S. Roy and A. Saberi, "Static decentralized control of a single-integrator network with Markovian sensing topology," *Automatica*, vol. 41, no. 11, pp. 1867–1877, 2005.

[58] E. Vidal, F. Thollard, C. de la Higuera, F. Casacuberta, and R. C. Carrasco, "Probabilistic finite-state machines—Parts I & II," *IEEE Trans. Pattern Anal. Mach. Intell.*, vol. 27, no. 7, pp. 1013–1039, 2005.

[59] J. Lunze and B. Nixdorf, "Representation of hybrid systems by means of stochastic automata," *Math. Comput. Modelling Dyn. Syst.*, vol. 7, no. 4, pp. 383–422, 2001.

[60] A. Megretski, "Robustness of finite state automata," in *Multidisciplinary Research in Control—The Mohammed Dahleh Symp. 2002*, ser. Lecture Notes in Control and Information Sciences, L. Giarré and B. Bamieh, Eds. New York: Springer, 2003, vol. 289, pp. 147–160.

[61] G. Riccardi, R. Pieraccini, and E. Bocchieri, "Stochastic automata for language modeling," *Computer Speech and Language*, vol. 10, pp. 265–293, 1996.

[62] S. Bangalore and G. Riccardi, "Stochastic finite-state models for spoken language machine translation," *Machine Translation*, vol. 17, pp. 165–184, 2002.

[63] J. Bryans, H. Bowman, and J. Derrick, "Model checking stochastic automata," *ACM Trans. Comput. Logic*, vol. 4, no. 4, pp. 452–492, 2003.

[64] S. Patilkulkarni, H. Herencia-Zapana, W. S. Gray, and O. R. González, "On the stability of jump-linear systems driven by finite-state machines with Markovian inputs," in *Proc. 2004 Amer. Control Conf.*, Boston, Massachusetts, 2004, pp. 2534–2539.

[65] D. Marculescu and R. Marculescu, "Information-theoretic bounds for switching activity analysis in finite-state machines under temporally correlated inputs," in *Proc. IEEE Asilomar Conf. Signals Systems Computers*, Pacific Grove, California, 1999, pp. 369–373.

[66] O. L. V. Costa and R. P. Marques, "Mixed H_2/H_∞-control of discrete-time Markovian jump linear systems," *IEEE Trans. Automat. Contr.*, vol. 43, no. 1, pp. 95–100, 1998.

[67] H. Zhang, W. S. Gray, and O. R. González, "Performance analysis of digital flight control systems with rollback error recovery subject to simulated neutron-induced upsets," *IEEE Trans. Control Syst. Technol.*, 2005, under review.

[68] H. Zhang, W. S. Gray, and O. R. González, "Markov jump-linear performance models for recoverable flight control computers," in *Proc. 36th IEEE Southeastern Symp. System Theory*, Atlanta, Georgia, 2004, pp. 408–412.

[69] ——, "Performance analysis and validation of a recoverable flight control system in a simulated neutron environment," in *Proc. 2005 AIAA Guidance, Navigation, and Control Conf. and Exhibit*, San Francisco, California, 2005, paper no. 6430.

[70] E. F. Hogge, "B-737 linear autoland Simulink model," NASA, Langley Research Center, Hampton, Virginia, Tech. Rep. CR-2004-213021, 2004.

[71] E.-E. Doberkat, *Stochastic Automata: Stability, Nondeterminism, and Prediction*, ser. Lecture Notes in Computer Science, G. Goos and J. Hartmanis, Eds. Berlin: Springer-Verlag, 1981, vol. 113.

[72] P. R. D'Argenio, J.-P. Katoen, and E. Brinksma, "An algebraic approach to the specification of stochastic systems (extended abstract)," in *Programming Concepts and Methods*, D. Gries and W.-P. de Roever, Eds. London, UK: Chapman & Hall, 1998, pp. 126–147.

[73] P. R. D'Argenio, "A compositional translation of stochastic automata into timed automata," Department of Computer Science, University of Twente, Enschede, The Netherlands, Tech. Rep. CTIT00-08, 2000.

[74] C. Ünsal, "Intelligent navigation of autonomous vehicles in an automated highway system: Learning methods and interacting vehicles approach," Ph.D. dissertation, The Bradley Department of Electrical and Computer Engineering, Virginia Polytechnic Institute and State University, 1997.

[75] J. T. Tou, "Stochastic automata and discrete systems theory," in *Applied Automata Theory*, ser. Electrical Science Series, J. T. Tou, Ed. New York: Academic Press, 1968, pp. 55–80.

[76] A. A. Lorenz, *Stochastic Automata: Constructive Theory.* New York: John Wiley & Sons, 1974, translated from Russian by D. Louvish.

[77] K. Horbacz, "Random dynamical systems with jumps," *J. Appl. Prob.*, vol. 41, no. 3, pp. 890–910, 2004.

[78] A. Tejada, O. R. González, and W. S. Gray, "On the Markov property for nonlinear discrete-time systems with Markovian inputs," in *Proc. 2006 Amer. Control Conf.*, Minneapolis, Minnesota, 2006, pp. 899–904.

[79] L. Arnold and W. Kliemann, "Qualitative theory of stochastic systems," in *Probability Analysis and Related Topics*, A. T. Bharucha-Reid, Ed. New York: Academic Press, Inc., 1983, vol. 3, pp. 1–79.

[80] W. S. Gray and O. González, "Modeling electromagnetic disturbances in closed-loop computer controlled flight systems," in *Proc. 1998 Amer. Control Conf.*, Philadelphia, Pennsylvania, 1998, pp. 359–364.

[81] O. L. V. Costa and R. P. Marques, "Robust H_2-control for discrete-time Markovian jump linear systems," *Int. J. Control*, vol. 73, no. 1, pp. 11–21, 2000.

[82] E. Anderson, Z. Bai, C. Bischof, S. Blackford, J. Demmel, J. Dongarra, J. Du Croz, A. Greenbaum, S. Hammarling, A. McKenney, and D. Sorensen, *LAPACK Users' Guide*, 3rd ed. Philadelphia, Pennsylvania: SIAM, 1999.

[83] C. B. Moler, *Numerical Computing with MATLAB.* Philadelphia, Pennsylvania: SIAM, 2004.

[84] R. B. Lehoucq, D. C. Sorensen, and C. Yang, *ARPACK Users' Guide: Solution of Large-Scale Eigenvalue Problems with Implicitly Restarted Arnoldi Methods.* Philadelphia, Pennsylvania: SIAM, 1998.

[85] J. W. Brewer, "Kronecker products and matrix calculus in system theory," *IEEE Trans. Circuits Syst.*, vol. 25, no. 9, pp. 772–781, 1978.

[86] W. S. Gray, H. Zhang, and O. R. González, "Closed-loop performance measures for flight controllers subject to neutron-induced upsets," in *Proc. 42nd IEEE Conf. Decision Control*, Maui, Hawaii, 2003, pp. 2465–2470.

[87] K. Eure, C. M. Belcastro, D. Koppen, R. Hess, K. Stange, L. Vahala, and M. Ferguson, "Closed-loop neutron particle effects testing on a recoverable flight control computer," in *23rd Digital Avionics Systems Conf. Proceedings*, Salt Lake City, Utah, 2004, pp. 6.C.3–1–12.

[88] D. M. Hawkins, *Identification of Outliers*, ser. Monographs on Applied Probability and Statistics, D. R. Cox, Ed. London: Chapman & Hall, 1980, vol. 13.

[89] C. Hennig, "Clusters, outliers, and regression: Fixed point clusters," *J. Multivar. Anal.*, vol. 86, no. 1, pp. 183–212, 2003.

[90] T. W. Anderson and L. A. Goodman, "Statistical inference about Markov chains," *Ann. Math. Statist.*, vol. 28, no. 1, pp. 89–110, 1957.

APPENDIX A

LINEAR MODELS FOR THE BOEING 737 AIRCRAFT SYSTEM IN CLOSED-LOOP WITH AN RCS

A.1 THE IDENTIFIED LINEAR MODELS FOR THE BOEING 737 AIRCRAFT SYSTEM IN CLOSED-LOOP WITH AN RCS

The state space representations of the identified models for the RCS controlled Boeing 737 closed-loop system are given in this section. The inputs of the system were: forward, side and down components of the wind signal, and the outputs were: altitude, calibrated airspeed, and track angle. $\Sigma_{\rm n} : (A_{\rm n}, G_{\rm n}, C_{\rm n})$ is an eight-dimensional system for the nominal mode, and $\Sigma_{\rm r} : (A_{\rm r}, G_{\rm r}, C_{\rm r})$ is a six-dimensional system for the recovery mode.

$$A_{\rm n} = \begin{bmatrix} -0.1526 & -0.0210 & 0.1555 & -0.1927 & 0.1286 & 0.3234 & 0.5743 & 0.0103 \\ -0.5528 & 0.8558 & 0.0794 & -0.0914 & 0.0847 & 0.1713 & -0.0400 & 0.0156 \\ 0.8182 & 0.4362 & 0.6091 & -0.1658 & -0.1018 & -0.1013 & 0.4448 & 0.0811 \\ -0.1970 & 0.0157 & 0.2102 & 1.0813 & 0.0295 & -0.0324 & -0.3494 & -0.0306 \\ -0.1518 & -0.0151 & 0.1142 & 0.0343 & 0.9900 & 0.0909 & -0.4197 & -0.0556 \\ 0.0051 & -0.0066 & -0.0079 & -0.0127 & 0.0382 & 0.8787 & 0.1816 & 0.0633 \\ 0.0306 & 0.0052 & -0.0032 & 0.0140 & -0.0164 & -0.0011 & 1.0214 & -0.0189 \\ -0.0061 & 0.0190 & 0.0074 & -0.0200 & 0.0806 & -0.2403 & 0.4113 & 1.1117 \end{bmatrix}$$

$$G_{\mathrm{n}} = \begin{bmatrix} 0.1638 & 0.2423 & -0.1632 \\ 0.0561 & 0.1078 & -0.0374 \\ -0.0727 & -0.1884 & 0.0121 \\ -0.0141 & 0.0252 & 0.0543 \\ -0.0229 & 0.0124 & 0.0594 \\ 0.0153 & 0.0051 & -0.0283 \\ 0.0007 & 0.0000 & -0.0055 \\ 0.0342 & 0.0164 & -0.0582 \end{bmatrix}$$

$$C_{\mathrm{n}} = \begin{bmatrix} -1.4160 & 6.0827 & 1.0965 & -35.6840 & 41.4290 & -28.7220 & -29.8050 & 25.5580 \\ 1.8808 & -4.3033 & -1.1529 & 0.5651 & -13.5740 & -48.7120 & -47.9160 & 11.7400 \\ 0.0139 & 0.0232 & 0.0224 & -0.0241 & 0.0187 & 0.4850 & -0.1754 & -0.2722 \end{bmatrix}$$

and

$$A_{\mathrm{r}} = \begin{bmatrix} 0.4440 & -0.2463 & 0.0672 & -0.0204 & 0.1304 & 0.0269 \\ 0.0885 & 1.0089 & -0.0216 & 0.0234 & -0.0325 & 0.0080 \\ 0.0655 & -0.0264 & 0.8468 & 0.2198 & -0.0278 & 0.1414 \\ -0.0350 & -0.0349 & 0.0071 & 0.9535 & -0.0146 & 0.0013 \\ 0.0318 & 0.05715 & -0.0190 & 0.0384 & 1.0167 & 0.0104 \\ 0.0597 & -0.0469 & -0.1307 & 0.2197 & -0.0502 & 1.1247 \end{bmatrix}$$

$$G_{\mathrm{r}} = \begin{bmatrix} 0.1367 & 0.2140 & -0.3239 \\ -0.0170 & -0.0346 & 0.0696 \\ 0.0659 & 0.0645 & 0.2648 \\ 0.0049 & 0.0092 & -0.0222 \\ 0.0025 & 0.0068 & 0.0374 \\ 0.0689 & 0.0749 & 0.2652 \end{bmatrix}$$

$$C_{\mathrm{r}} = \begin{bmatrix} 2.4026 & -20.4010 & 88.6780 & -35.3950 & 51.4550 & -91.5610 \\ 0.9882 & -1.3717 & -3.6503 & -30.6670 & -16.6910 & 5.0725 \\ 0.0577 & 0.1782 & -0.0084 & -0.5842 & -0.1237 & -0.0001 \end{bmatrix}.$$

A.2 THE SWITCHED LINEAR MODELS FOR THE BOEING 737 AIRCRAFT SYSTEM IN CLOSED-LOOP WITH AN RCS

The state space representation used to build the stochastic hybrid system for the RCS controlled Boeing 737 closed-loop system is given in this section. $\tilde{\Sigma}_{\mathrm{n}}$: $\left(\tilde{A}_{\mathrm{n}}, \tilde{G}_{\mathrm{n}}, \tilde{C}_{\mathrm{n}}\right)$ is the controller canonical form of Σ_{n} for the nominal mode, and $\tilde{\Sigma}_{\mathrm{r}}$: $\left(\tilde{A}_{\mathrm{r}}, \tilde{G}_{\mathrm{r}}, \tilde{C}_{\mathrm{r}}\right)$ is the controller canonical form of Σ_{r} with two extra states embedded for the recovery mode. Both are eight-dimensional systems.

$$\tilde{A}_{\mathrm{n}} = \begin{bmatrix} 5.5673 & -7.6364 & 3.0654 & 4.7791 & -8.5719 & 3.7877 & -10.0493 & 10.0490 \\ 1.0000 & 0.0000 & -0.0000 & -0.0000 & 0.0000 & -0.0000 & -0.0000 & 0.0000 \\ -0.0000 & 1.0000 & -0.0000 & -0.0000 & 0.0000 & -0.0000 & -0.0000 & 0.0000 \\ -2.4555 & 4.5975 & -2.1429 & -1.3480 & 5.0787 & -2.7333 & 5.9803 & -5.9378 \\ 0.0000 & -0.0000 & 0.0000 & 1.0000 & -0.0000 & 0.0000 & 0.0000 & -0.0000 \\ 0.0000 & -0.0000 & 0.0000 & 0.0000 & 1.0000 & 0.0000 & 0.0000 & -0.0000 \\ -0.0000 & -0.0086 & 0.0087 & -0.0000 & -0.0173 & 0.0175 & 2.1759 & -1.1763 \\ 0.0000 & -0.0000 & 0.0000 & -0.0000 & 0.0 & 0.0000 & 1.0000 & -0.0000 \end{bmatrix}$$

$$\tilde{G}_{\mathrm{n}} = \begin{bmatrix} 1.0000 & -0.0000 & -49.9930 \\ -0.0000 & -0.0000 & 0.0000 \\ -0.0000 & -0.0000 & 0 \\ 0.0000 & 1.0000 & 30.4399 \\ -0.0000 & 0.0000 & 0.0000 \\ 0 & 0.0000 & -0.0000 \\ 0.0000 & 0.0000 & 1.0000 \\ -0.0000 & -0.0000 & -0.0000 \end{bmatrix}$$

$$\tilde{C}_{\mathrm{n}} = \begin{bmatrix} -0.0000 & -0.0256 & 0.0244 & -0.0089 & -0.0282 & 0.0350 & 0.3024 & -0.2723 \\ 0.0779 & -0.3664 & 0.2870 & -0.0029 & -0.3824 & 0.3829 & 4.0076 & -3.9825 \\ -0.0002 & -0.0013 & 0.0013 & -0.0007 & -0.0014 & 0.0018 & 0.0130 & -0.0110 \end{bmatrix}$$

and

$$\tilde{A}_{\mathrm{r}} = \begin{bmatrix} 2.4531 & -1.9279 & 0.4746 & 0.0026 & -0.0002 & -0.0023 & -0.0266 & 0.0185 \\ 1.0000 & 0.0000 & -0.0000 & -0.0000 & 0.0000 & -0.0000 & -0.0000 & 0.0000 \\ -0.0000 & 1.0000 & 0.0000 & -0.0000 & 0.0000 & -0.0000 & -0.0000 & 0.0000 \\ -0.0401 & 0.0753 & -0.0352 & 2.4148 & -1.8465 & 0.4318 & -0.0550 & 0.0642 \\ 0.0000 & -0.0000 & 0.0000 & 1.0000 & -0.0000 & -0.0000 & 0.0000 & -0.0000 \\ -0.0000 & -0.0000 & 0.0000 & -0.0000 & 1.0000 & -0.0000 & -0.0000 & 0.0000 \\ 0.0000 & -0.0051 & 0.0051 & 0.0000 & -0.0088 & 0.0088 & 1.5267 & -0.5260 \\ 0.0000 & -0.0000 & -0.0000 & 0.0000 & -0.0000 & 0.0000 & 1.0000 & -0.0000 \end{bmatrix}$$

$$\tilde{G}_{\mathrm{r}} = \begin{bmatrix} 1.0000 & 0.0000 & -0.4080 \\ -0.0000 & -0.0000 & -0.0000 \\ -0.0000 & 0.0000 & 0 \\ -0.0000 & 1.0000 & -2.8971 \\ 0.0000 & 0.0000 & -0.0000 \\ 0.0000 & -0.0000 & 0.0000 \\ 0.0000 & -0.0000 & 1.0000 \\ 0.0000 & 0.0000 & 0.0000 \end{bmatrix}$$

$$\tilde{C}_{\mathrm{r}} = \begin{bmatrix} 0.1680 & -0.3399 & 0.1666 & 0.1052 & -0.2947 & 0.1861 & 0.0865 & -0.2312 \\ 0.0745 & -0.1058 & 0.0324 & 0.0056 & -0.0012 & -0.0039 & 0.0663 & -0.0241 \\ 0.0011 & -0.0016 & 0.0005 & -0.0006 & 0.0010 & -0.0004 & -0.0015 & 0.0009 \end{bmatrix}.$$

A.3 THE STATE TRANSITION MATRICES FOR THE SFSA AND THE FSM

In this section, the state transition matrices for both the SFSA and the FSM used to model the recovery processes of an RCS are given. Π^0 is for the machine input symbol "0", which means no upset was detected. Π^1 is for the machine input symbol "1", which means at least one upset was detected. For both matrices, the summation for each row is equal to 1. The entries in both matrices for the SFSA can

have any value between 0 and 1:

$$\Pi^0 = \begin{bmatrix} 1 & 0 & 0 & 0 & 0 & 0 & 0 \\ 0 & 0 & 1 & 0 & 0 & 0 & 0 \\ 0 & 0 & 0 & 1 & 0 & 0 & 0 \\ 0 & 0 & 0 & 0 & 1 & 0 & 0 \\ 0 & 0 & 0 & 0 & 0 & 1 & 0 \\ \boxed{0.20} & 0 & 0 & 0 & 0 & 0 & \boxed{0.80} \\ 1 & 0 & 0 & 0 & 0 & 0 & 0 \end{bmatrix}, \quad \Pi^1 = \begin{bmatrix} 0 & 1 & 0 & 0 & 0 & 0 & 0 \\ 0 & 0 & 1 & 0 & 0 & 0 & 0 \\ 0 & 0 & 0 & 1 & 0 & 0 & 0 \\ 0 & 0 & 0 & 0 & 1 & 0 & 0 \\ 0 & 0 & 0 & 0 & 0 & 1 & 0 \\ \boxed{0.20} & 0 & 0 & 0 & 0 & 0 & \boxed{0.80} \\ 1 & 0 & 0 & 0 & 0 & 0 & 0 \end{bmatrix}.$$

For the FSM, the entries in both matrices can only take value of either 0 or 1:

$$\Pi^0 = \begin{bmatrix} 1 & 0 & 0 & 0 & 0 & 0 & 0 \\ 0 & 0 & 1 & 0 & 0 & 0 & 0 \\ 0 & 0 & 0 & 1 & 0 & 0 & 0 \\ 0 & 0 & 0 & 0 & 1 & 0 & 0 \\ 0 & 0 & 0 & 0 & 0 & 1 & 0 \\ \boxed{0} & 0 & 0 & 0 & 0 & 0 & \boxed{1} \\ 1 & 0 & 0 & 0 & 0 & 0 & 0 \end{bmatrix}, \quad \Pi^1 = \begin{bmatrix} 0 & 1 & 0 & 0 & 0 & 0 & 0 \\ 0 & 0 & 1 & 0 & 0 & 0 & 0 \\ 0 & 0 & 0 & 1 & 0 & 0 & 0 \\ 0 & 0 & 0 & 0 & 1 & 0 & 0 \\ 0 & 0 & 0 & 0 & 0 & 1 & 0 \\ \boxed{0} & 0 & 0 & 0 & 0 & 0 & \boxed{1} \\ 1 & 0 & 0 & 0 & 0 & 0 & 0 \end{bmatrix}.$$

The distinguishing entries between these two sets of state transition matrices are boxed for comparison.

APPENDIX B

SUMMARY OF EXPERIMENTAL DATA OBTAINED FROM LANSCE AND NASA LANGLEY

In this appendix, a summary of the experimental data sets obtained from LANSCE and NASA Langley is given. Only those data sets used in this dissertation are described. For additional information on the data sets, see [87].

B.1 EXPERIMENTAL DATA OBTAINED FROM LANSCE

The neutron experimental data sets of interest from LANSCE are listed in Table X. For each run, the test number (which is also the MATLAB data file name), data length, recovery count, estimated upset probability, and beam target are given. For targets T2p and T2pp, at least one RCS processor was struck by the beam. For target T3, the primary target was the instruction memory.

B.2 EXPERIMENTAL DATA OBTAINED FROM NASA LANGLEY

The six one hour repeatability runs (72,000 samples/run) done at NASA are listed in Table XI: three of them were generated with no upsets, and the other three were generated with Markov upsets. All six runs were done using the same random number seed for the wind gust models.

TABLE X
List of Experimental Data Obtained from LANSCE

Test number	Data length	Recovery count	Estimated upset probability	Beam target
RCS_071	71,330	0	0	T3
RCS_072	71,330	1	1.4019×10^{-5}	T3
RCS_073	71,320	1	1.4021×10^{-5}	T3
RCS_106	71,320	14	1.9630×10^{-4}	T2p
RCS_107	44,080	10	2.2686×10^{-4}	T2p
RCS_113	71,230	15	2.1059×10^{-4}	T2p
RCS_114	71,210	10	1.4043×10^{-4}	T2p
RCS_136	52,130	20	3.8366×10^{-4}	T2pp
RCS_141	25,900	9	3.4749×10^{-4}	T2pp
RCS_145	38,330	15	3.9134×10^{-4}	T2pp
RCS_151	50,380	31	6.1532×10^{-4}	T2pp

TABLE XI
Repeatability Test at the NASA Langley

Run file	Test description	Seed

`RCS5_22.mat`
`RCS_Pre2_00.mat`
`rcs_preiid1_2.mat`
	Nominal runs with the upset probability $[\Pi_{\mathrm{I}}]_{01} = \pi_{\mathrm{I}}(1) = 0.$	(-220)

`RCS5_29.mat`
`RCS_Pre2_09.mat`
`rcs_preiid1_3.mat`
	Recovery runs with the upset probability $[\Pi_{\mathrm{I}}]_{01} = \pi_{\mathrm{I}}(1) = 0.0009.$	

In total, sixty one hour Markov runs and sixty one hour i.i.d. runs were performed. For both cases, they were divided into ten groups. A different random number seed was employed for each group. Table XII provides the group ID (*MarkovGr* and

TABLE XII
Group ID and Wind Generating Seed for the Markov and the I.I.D. Tests

MarkovGr	PreACC	pre3	main1	main2	main3
IIDGr	preiid2	mainiid0	mainiid1	mainiid2	mainiid3
Seed	(-220)	(-260)	(-280)	(-300)	(-320)
MarkovGr	main4	main5	main6	main7	main8
IIDGr	mainiid4	mainiid5	mainiid6	mainiid7	mainiid8
Seed	(-340)	(-360)	(-380)	(-400)	(-420)

IIDGr) and the corresponding seed. In each group, six different upset probabilities, $[\Pi_{\mathrm{I}}]_{01}, \pi_{\mathrm{I}}(1) \in \mathbb{U}$, were tested. The corresponding MATLAB data file name, upset probability, spectral radius of $\mathscr{A}_2$ and expected recovery count are in Table XIII.

Other tests related to this dissertation are given in Table XIV.

TABLE XIII
Six Runs in Each Group of the Markov and I.I.D. Tests

Markov run file	I.I.D. run file	Upset probability	$r_\sigma(\mathscr{A}_2)$	Expected recovery count
RCS_MarkovGr_00.mat	rcs_IIDGr_00.mat	0	0.9802	0
RCS_MarkovGr_01.mat	rcs_IIDGr_01.mat	0.0001	0.9833	7
RCS_MarkovGr_04.mat	rcs_IIDGr_04.mat	0.0004	0.9902	29
RCS_MarkovGr_06.mat	rcs_IIDGr_06.mat	0.0006	0.9930	43
RCS_MarkovGr_09.mat	rcs_IIDGr_09.mat	0.0009	0.9960	65
RCS_MarkovGr_12.mat	rcs_IIDGr_12.mat	0.0012	0.9983	86

TABLE XIV
Other Runs Cited in This Dissertation

Run file	Data length	Recovery count	Description
upsets_test_0629.mat	6,000	n/a	Trigger signal for RCS5_1.mat
RCS5_1.mat	6,000	24	Upset trigger type test
RCS5_11.mat	36,000	2,421	MSS test

VITA

Hong Zhang
Department of Electrical and Computer Engineering
Old Dominion University
Norfolk, VA 23529

EDUCATION

- M.S. in Systems Engineering, July 2002, Tsinghua University, Beijing, P. R. China
  Thesis Title: *Fuzzy Sets Theory and Its Application in Modeling the Economic Systems* (in Chinese)
  Thesis Advisor: Prof. Deyun Xiao
- B.S. in Automatic Control, July 1997, Northeastern University, Shenyang, Liaoning, P. R. China

ACADEMIC AWARDS AND HONORS

- Best Paper Presentation Award of American Control Conference, 2005
- Student Travel Grant Award for American Control Conference, 2005
- The Honor Society of Phi Kappa Phi, 2005
- The Engineering Honor Society of Tau Beta Pi, 2005
- Supplemental Dissertation Stipend Award, Old Dominion University, 2005

PUBLICATIONS

CONFERENCE PUBLICATIONS:

1. Anushka V. Lakdawala, **Hong Zhang**, Oscar R. González and W. Steven Gray, "Markovian statistical data analysis of single-event upsets triggered by high intensity neutrons," in *Proc. 38th IEEE Southeastern Symposium on System Theory*, Cookeville, Tennessee, Mar. 5–7, 2006, pp. 349–353.

2. **Hong Zhang**, W. Steven Gray and Oscar R. González, "Performance analysis and validation of a recoverable flight control system in a simulated neutron environment," in *Proc. 2005 AIAA Guidance, Navigation, and Control Conference and Exhibit*, San Francisco, California, Aug. 15–18, 2005, paper no. 6430 (invited).

3. **Hong Zhang**, W. Steven Gray and Oscar R. González, "Performance analysis of recoverable flight control systems using hybrid dynamical models," in *Proc. 2005 American Control Conference*, Portland, Oregon, June 8–10, 2005, pp. 2787–2792.

4. **Hong Zhang**, W. Steven Gray and Oscar R. González, "Markov jump-linear performance models for recoverable flight control computers," in *Proc. 36th IEEE Southeastern Symposium on System Theory*, Atlanta, Georgia, Mar. 14–16, 2004, pp. 408–412.

5. W. Steven Gray, **Hong Zhang** and Oscar R. González, "Closed-loop performance measures for flight controllers subject to neutron-induced upsets," in *Proc. 42nd IEEE Conference on Decision and Control*, Maui, Hawaii, USA, Dec. 9–12, 2003, pp. 2465–2470.

JOURNAL PUBLICATIONS:

6. **Hong Zhang**, W. Steven Gray and Oscar R. González, "Performance analysis of digital flight control systems with rollback error recovery subject to simulated neutron-induced upsets," *IEEE Transactions on Control Systems Technology*, 2005, under review.

7. **Hong Zhang**, Deyun Xiao and Zhentao Liu, "A local auto-regressive fuzzy model and its application in modeling of small samples data systems," (in Chinese) *Systems Engineering*, vol. 20, no. 4, Aug. 2002, pp. 91–96.

8. **Hong Zhang**, Deyun Xiao and Zhentao Liu, "FLAR fuzzy forecasting model and its application," (in Chinese) *Science of Science and Management of Science & Technology*, July 2002, pp. 16–19.

Typeset using LaTeX.